

Special Issue: *Australopithecus sediba*

The Skull of *Australopithecus sediba*

DARRYL J. DE RUITER

Department of Anthropology, Texas A&M University, College Station, TX 77843, USA; and, Evolutionary Studies Institute, University of the Witwatersrand, Private Bag 3, WITS 2050, Johannesburg, SOUTH AFRICA; deruiter@tamu.edu

KEELY B. CARLSON

Department of Anthropology, Texas A&M University, College Station, TX 77843, USA; keelyc@tamu.edu

JULIET K. BROPHY

Department of Geography and Anthropology, Louisiana State University, Baton Rouge, LA 70803, USA; and, Evolutionary Studies Institute, University of the Witwatersrand, Private Bag 3, WITS 2050, Johannesburg, SOUTH AFRICA; jbrophy@lsu.edu

STEVEN E. CHURCHILL

Department of Evolutionary Anthropology, Duke University, Durham, NC 27708, USA; and, Evolutionary Studies Institute, University of the Witwatersrand, Private Bag 3, WITS 2050, Johannesburg, SOUTH AFRICA; churchy@duke.edu

KRISTIAN J. CARLSON

Department of Integrative Anatomical Sciences, Keck School of Medicine of USC, University of Southern California, CA 90033, USA; kristian.carlson@usc.edu

LEE R. BERGER

Evolutionary Studies Institute, University of the Witwatersrand, Private Bag 3, WITS 2050, Johannesburg, SOUTH AFRICA; profleberger@yahoo.com

submitted: 26 July 2017; accepted 22 June 2018

ABSTRACT

Australopithecus sediba presents a mosaic of both australopith-like and *Homo*-like characters. The preliminary account of the skull of *Au. sediba* provided in Berger et al. (2010) is augmented here to include a comprehensive descriptive and comparative analysis of both qualitative and quantitative characters of the craniodental remains of the holotype and paratype specimens, Malapa Hominins 1 and 2 (MH1 and MH2). Newly recovered mandibular material attributable to the holotype specimen (MH1), including two unworn premolars, is also presented here. *Australopithecus sediba* shares several cranial characters with other australopiths, most prominent of which include its small brain size, marked glabellar block, robust zygomatics with steeply inclined zygomaticoalveolar crest, degree of prognathism, patent premaxillary suture, topography of the entrance to the nasal cavity and the insertion of vomer, and narrow palate. Combined with postcranial evidence, these confirm that the Malapa skeletons reflect an australopith adaptive grade. At the same time, *Au. sediba* shares numerous characters with specimens of early *Homo*, most prominent of which include its limited postorbital constriction, widely spaced temporal lines, medially positioned mandibular fossa, moderately-defined supraorbital torus and supratoral sulcus with expanded supraorbital trigon, unflared zygomatics, anterolaterally oriented lateral orbital margins, anteriorly positioned anterior nasal tubercle, raised intermaxillary suture, small mandibular symphysis and corpus, well excavated subalveolar fossa, steeply inclined lingual alveolar plane, and weak superior transverse torus with absent inferior transverse torus. The potential for homoplasy in adaptively significant features in late australopiths and basal members of the *Homo* clade, combined with probable reticulate evolution, renders the identification of the ancestor of *Homo* difficult. In addition, the transition from australopith to *Homo* likely took place piecemeal over hundreds or perhaps thousands of generations, thus the combination of traits that characterize early *Homo* are recognizable largely as a result of the imperfect nature of our available fossil record. Notwithstanding this, given the similarities shared between *Au. sediba* and *Homo*, on present evidence we favor the hypothesis that the *Au. sediba* lineage represents the most likely ancestor of the genus *Homo*, or a close sister group to that ancestor.

This special issue is guest-edited by Scott A. Williams (Department of Anthropology, New York University) and Jeremy M. DeSilva (Department of Anthropology, Dartmouth College). This is article #2 of 9.

TABLE 1. CRANIAL MATERIAL ATTRIBUTED TO *AUSTRALOPITHECUS SEDIBA*.

Specimen Number	Element
MH1	
U.W. 88-2	anterior mandible fragment with Lc
U.W. 88-8	right hemi-mandible with M ₁ -M ₃
U.W. 88-29	RI ¹
U.W. 88-30	RC
U.W. 88-31	cranial fragment
U.W. 88-32	cranial fragment
U.W. 88-50	cranium with LI ² , LP ³ -LM ³ , RP ³ -RM ³
UW 88-244	LP ₄
UW 88-245	left mandibular fragment with roots of P ₃ -M ₁
UW 88-246	LP ₃
MH2	
U.W. 88-19	LM ²
U.W. 88-20	LM ³
U.W. 88-54	right mandible fragment with M ₁ -M ₃
U.W. 88-55	left mandible fragment with M ₂ -M ₃
U.W. 88-128	right mandible fragment with P ₄
U.W. 88-129	right mandible fragment with I ₁ -P ₃

INTRODUCTION

Australopithecus sediba represents the first novel australopithecine species named in South Africa since 1949. To date two partial skeletons have been reported (MH1, MH2), while an additional three or four individuals await excavation/preparation (de Ruiter et al. 2013a). In the initial announcement of *Au. sediba* it was recognized that this species shared features across the skull and postcranial skeleton with both australopithecines and representatives of early *Homo* (Berger et al. 2010). The authors of that announcement favored a grade-based attribution to *Australopithecus*, foregrounded in part on the small brain size and relatively primitive nature of several aspects of the postcranial skeleton. At the same time, based on the numerous similarities shared between *Au. sediba* and early *Homo* across the skull and skeleton, they hypothesized that *Au. sediba* represented the ancestor of the genus *Homo*, or a close sister group to that ancestor. The hypothesis that *Au. sediba* might be closely related to the ancestry of *Homo* (Berger et al. 2010; de Ruiter et al. 2017; Pickering et al. 2011), has been dismissed by several commentators (Balter 2010; Cherry 2010; Kimbel 2013; Kimbel and Rak 2017; Lordkipanidze et al. 2013; Spoor 2011; Wood and Harrison 2011). In contrast, the Bayesian analysis of Dembo et al. (2015) provided support for a proposed link between *Au. sediba* and *Homo*, leading to the hypothesis that *Au. sediba* represents a sister taxon to a clade comprising all *Homo* species. To advance the debate over the origin of the genus *Homo*, and the role that *Au. sediba* might have played in that ancestry, we present a comprehensive comparative / descriptive analysis of quantitative and qualitative characters of the craniodental

remains of the holotype (MH1) and paratype (MH2) individuals of *Au. sediba*.

MATERIALS AND METHODS

Malapa Hominin 1 is a sub-adult, probable male individual, and MH2 is an adult, probable female individual. Cranial remains referred to MH1 include a relatively complete and well preserved cranium and partial mandible, while MH2 includes a partial mandible and two maxillary teeth (Table 1). Aspects of these craniodental remains have been discussed elsewhere (Berger et al. 2010; Carlson et al. 2011; Daegling et al. 2016; de Ruiter et al. 2013a,b; Irish et al. 2013), but this study provides the first comprehensive, detailed descriptions and comparative context for the *Au. sediba* cranial remains. The postcranial skeletons of these individuals are documented elsewhere (Churchill et al. 2013, 2018a, b; DeSilva et al. 2013, 2018; Holliday et al. 2018; Kibii et al. 2011; Kivell et al. 2011, 2018; Schmid et al. 2013; Williams et al. 2013, 2018; Zipfel et al. 2011). Laser surface scan generated models of all of the *Au. sediba* cranial material described in this paper are available for download on MorphoSource.org, and we encourage readers to reference these models in conjunction with this paper.

Comparative *Australopithecus* and early *Homo* cranial materials assigned to *Au. anamensis*, *Au. afarensis*, *Au. africanus*, *Homo naledi*, *H. habilis*, *H. rudolfensis*, and *H. erectus* are used throughout this discussion (Table 2; and see de Ruiter et al. 2017 for a more complete discussion of hypodigmis). Clarke (1985, 1988, 2008) has long argued for the existence of a second species in the *Au. africanus* sample, which he attributes to the taxon *Australopithecus prometheus*

TABLE 2. COMPARATIVE EARLY HOMININ CRANIAL AND MANDIBULAR MATERIAL CONSIDERED IN THIS STUDY (refer to de Ruiter et al. (2017) for fuller discussion of hypodigms).

<i>Australopithecus anamensis</i>	
Cranial:	KNM-ER 30745, KNM-KP 29283
Mandibular:	KNM-KP 29281, KNM-KP 29287, KNM-KP 31713, KNM-KP 47956
<i>Australopithecus afarensis</i>	
Cranial:	AL 58-22, AL 199-1, AL 200-1, AL 333-1, AL 333-2, AL 333-45, AL 333-105, AL 444-2, DIK-1-1
Mandibular:	AL 128-23, AL 145-35, AL 188-1, AL 198-1, AL 198-22, AL 207-13, AL, 225-8, AL 228-2, AL 266-1, AL 277-1, AL 288-1, AL 311-1, AL 315-22, AL 330-5, AL 333-108, AL 333-43b, AL 333w-1ab, AL 333w-1e, AL 333w-12, AL 333w-32-60, AL 400-1, AL 417-1, AL 432-1, AL 437-1, AL 437-2, AL 438-1, AL 444-2, AL 582-1, AL 620-1, AL 766-1, DIK-1-1, LH 2, LH 4, LH 10, LH 13, MAK 1/2, MAK 1/12
<i>Australopithecus africanus</i>	
Cranial:	MLD 3, MLD 6/23, MLD 9, MLD 37/38, MLD 45, Sts 5, Sts 17, Sts 52, Sts 53, Sts 63, Sts 71, Sts 3009, Stw 13, Stw 53 ¹ , Stw 73, Stw 151, Stw 183, Stw 252, Stw 265, Stw 272, Stw 370, Stw 391, Stw 498, Stw 505, Stw 579, Taung, TM 1511, TM 1512, TM 1514
Mandibular:	MLD 2, MLD 18, MLD 22, MLD 27, MLD 34, MLD 40, Sts 7, Sts 36, Sts 52, Stw 14, Stw 39, Stw 109, Stw 131, Stw 142, Stw 151 ¹ , Stw 313, Stw 327, Stw 384, Stw 385, Stw 404, Stw 498, Stw 513, Taung
<i>Homo naledi</i>	
Cranial:	DH1, DH2, DH3, DH4, DH5, LES1
Mandibular:	DH1, DH3, LES1, U.W. 101-001, U.W. 101-377, U.W. 101-1142
<i>Homo habilis</i>	
Cranial:	AL 666-1 ² , KNM-ER 1805, KNM-ER 1813, OH 7, OH 13, OH 16, OH 24, OH 65, OMO-L894-1
Mandibular:	KNM-ER 1501, KNM-ER 1502, KNM-ER 1802, KNM-ER 1805, OH 7, OH 13, OH 37, UR 501
<i>Homo rudolfensis</i>	
Cranial:	KNM-ER 1470, KNM-ER 62000, KNM-ER 62003
Mandibular:	KNM-ER 1482, KNM-ER 1483, KNM-ER 1801, KNM-ER 60000
<i>Homo erectus</i>	
Cranial:	BOU-VP-2/66, D 2280, D 2282, D 2700, D 3444, D4500, KNM-ER 730, KNM-ER 3733, KNM-ER 3883, KNM-ER 42700, KNM-WT 15000, OH 9, OH 12, Sangiran 2, Sangiran 4, Sangiran 17, SK 27, SK 847, SK 2635, Trinil 1, Zhoukoudian DI, Zhoukoudian EI, Zhoukoudian HIII, Zhoukoudian LI, Zhoukoudian LII, Zhoukoudian LIII
Mandibular:	D 211, D 2600, D 2735, KGA 10-1, KNM-BK 67, KNM-BK 8518, KNM-ER 730, KNM-ER 731, KNM-ER 820, KNM-ER 992, KNM-ER 1507, KNM-ER 1812, KNM-WT 15000, OH 22, OH 23, Sangiran 1b, Sangiran 5, Sangiran 6, Sangiran 8, Sangiran 9, Sangiran 22, Sangiran Bk7905, Sangiran Bk8606, Sangiran Ng8503, Sangiran Sb8103, SK 15, SK 45, Ternifine I, Ternifine II, Ternifine III, Zhoukoudian AII, Zhoukoudian AN16, Zhoukoudian FI, Zhoukoudian GI, Zhoukoudian HI, Zhoukoudian KI, Zhoukoudian Pa86

¹These specimens are more conventionally placed in early *Homo*.

²We are not convinced this specimen represents *Homo*, but we retain it here following convention.

(Clarke 1994, 2013). However, we agree with the majority of studies that have considered the issue that, for the present, we cannot falsify the hypothesis that *Au. africanus* from

Taung, Sterkfontein, and Makapansgat represents a single, if quite variable, fossil sample (Grine et al. 2013; Lockwood and Tobias 1999, 2002; Moggi-Cecchi et al. 2006). A.L. 666-1

is widely regarded as representing early *Homo* (Kimbel et al. 1996, 1997), though some of us have argued elsewhere that this attribution might not be correct (Pickering et al. 2011; de Ruiter et al. 2013a). Nevertheless, for the purpose of this study we will follow more conventional taxonomy and include this specimen in *H. habilis*. Likewise, many researchers consider StW 53 to represent early *Homo* in South Africa, perhaps even *H. habilis* (Curnoe and Tobias 2006; Hughes and Tobias 1977; Tobias 1991). However, we have suggested in the past (Berger et al. 2010; de Ruiter et al. 2013a; Pickering et al. 2011), as has Clarke (2008, 2013), that there is little reason to consider this specimen to be anything other than a representative of *Au. africanus*, and we regard it as such in this study. Leakey et al. (2012) consider the recently recovered specimens KNM-ER 60000 and KNM-ER 62000 to represent *H. rudolfensis*, to the exclusion of other specimens such as OH 65, KNM-ER 1802, and presumably UR 501. Spoor et al. (2015) followed this up with a geometric morphometric analysis of OH 7 that appears to bear this out. For the purpose of this paper, we will consider OH 65, KNM-ER 1802, and UR 501 to represent *H. habilis*. Given the relative lack of comparative materials available for taxa such as *Kenyanthropus platyops* (Leakey et al. 2001), *Au. bahrelghazali* (Brunet et al. 1995), and *Au. garhi* (Asfaw et al. 1999), specimens attributed to these taxa do not figure prominently in our discussion. The highly derived cranial, facial, mandibular, and dental morphology of the ‘robust’ australopiths, *Australopithecus (Paranthropus) aethiopicus*, *Au. (P.) boisei*, and *Au. (P.) robustus* bear little resemblance to the especially gracile skull of MH1, and are thus largely excluded from consideration.

As part of our analysis, we incorporated a variety of measurements based, in large part, on those outlined by Wood (1991). Data from *Au. africanus*, *Au. sediba*, *H. naledi*, and South African representatives of *H. erectus* were taken by D.J. de R. on original fossils. The remaining data were taken from published sources (Leakey et al. 2012; Lordkipanidze et al. 2013; Kimbel et al. 2004; Rightmire et al. 2006; Tobias 1967, 1991; Ward et al. 2001; Weidenreich 1936, 1937, 1943; Wood 1991). We digitally manipulated some of the larger areas of damage encountered in the cranium of MH1 to correct for measurement errors that might result from displacement (Carlson 2014; Carlson et al. 2016); a small number of measures had to be revised relative to Berger et al. (2010), and are highlighted in the tables below. The raw cranial metrics are presented all together in Table 3, and from this singular, central table we extract the various cranial indices presented in subsequent tables throughout the text below. Mandibular metrics are presented separately in tables below, while dental metrics for *Au. sediba* are presented in Table 4.

Descriptive terminology for cranial remains follows Weidenreich (1943) as modified by Tobias (1967, 1991). Descriptive terminology for mandibular remains follows Weidenreich (1936), as modified by Tobias (1967, 1991) and by White and Johanson (1982). Descriptive terminology for dental remains follows Weidenreich (1937) as modified by Robinson (1956), Tobias (1967), and Grine (1984, 1989).

Wherever possible we anglicize Latin terminology. Fossils viewed firsthand were examined using a series of magnifying hand lenses, as well as a low-power binocular microscope if possible. Where necessary, μ CT and synchrotron scan data were utilized to examine otherwise obscured morphology, and to confirm external visible morphology of the Malapa hominins (see Carlson et al. 2016 for details of synchrotron scanning). Abbreviations: FH, Frankfurt horizontal; EAM, external acoustic meatus; T/N, temporal/nuchal; BL, buccolingual(ly); MD, mesiodistal(ly); ICF, inter-proximal contact facet; C6, tuberculum sextum; CEJ, cervico-enamel junction.

PRESERVATION

MALAPA HOMININ 1 (MH1)

Cranium

U.W. 88-50 comprises the entire face, plus most of the left half and part of the right half of the neurocranium of the sub-adult individual MH1 (Figure 1). The frontal bone is mostly complete, though there is damage on the right side in the area of the temporal foramen. The right parietal is absent from U.W. 88-50, having been dislodged near the coronal and sagittal sutures; portions of the right parietal are represented by the fragments U.W.8 8-31 and U.W. 88-32. The left parietal is mostly complete, being present from the partially fused coronal suture, extending posteriorly along the sagittal suture to a point before the position of lambda, whereafter breakage angles to roughly parallel the projected path of the partially fused lambdoid suture; a small segment of the lambdoid suture is evident near the posterior margin of the preserved parietal, at roughly the posterior extent of the temporal line. The right and left greater wings of the sphenoid are both present and appear well preserved, though both are partially obscured by matrix remaining in the temporal foramina. The right temporal is mostly missing except for a small fragment of the slightly damaged anterior squamous portion adjacent to the sphenosquamosal suture, including a portion of the articular eminence and a short segment of the zygomatic process of the temporal (these latter two portions are still mostly encased in matrix). The left temporal is more complete, in particular the squamous portion which is mostly preserved, though damaged. Posteriorly, a crack has separated a segment of the left temporal squama posterior to the root of the zygomatic, though it remains closely appressed to the remaining part of the squama. The left petrous portion is less well preserved than the squama, having been broken away along an oblique fracture coursing from the entoglenoid process to bisect the postglenoid process; as a result, the articular eminence and mandibular fossa are mostly complete, but the tympanic and mastoid regions are absent. The entire left zygomatic arch is present, though slightly dislocated and separated along the zygomatico-temporal suture. The occipital is missing. The face is well preserved and complete apart from some minor areas of cortical erosion; surface detail of the preserved regions is otherwise excellent.

TABLE 3. CRANIAL METRICS FOR AUSTRALOPITHECUS SEDIBA AND COMPARATIVE HOMININ SPECIMENS.

(W# designations refer to measurement descriptions provided in Wood [1991]. Letters in parentheses indicate the measures used for generating the indices throughout the tables of this paper).

Taxon	Specimen	Cranial height - porion height W6 (a)	Bi- porionic breadth W11 (b)	Bi- parietal breadth W9 (c)	Bi- temporal breadth W10 (d)	Post-orbital constriction breadth (e)	Temporal foramen length W75	Glabella-bregma length W17	Frontal squama angle W129	Temporal lines closest approach (f)
<i>Au. anamensis</i>	Mean									
	KNM-ER 30745									
	KNM-KP 29283									
	Mean	126	91							
	AL 58-22			84						crest
	AL 162-28									
	AL 199-1									
	AL 200-1									
	AL 333-1									
	AL 333-45		120	97			77		93	crest
AL 417-1										
AL 427-1										
AL 442-1										
AL 444-2	86	132							crest	
AL 486-1										
Mean		103	98		106	66	34	77	43	21 ¹
<i>Au. africanus</i>	MLD 1									crest?
	MLD 6/23									
	MLD 9									
	MLD 37/38	70	100	100	105					40
	Sts 5	72	95	98	98	66	39	35	77	45
	Sts 17									
	Sts 19									
	Sts 25									
	Sts 52									
	Sts 53									
Sts 71	67	95	92	96	63	39	35	68	45	

TABLE 3. CRANIAL METRICS FOR AUSTRALOPITHECUS SEDIBA AND COMPARATIVE HOMININ SPECIMENS (continued).

(W# designations refer to measurement descriptions provided in Wood [1991].

Letters in parentheses indicate the measures used for generating the indices throughout the tables of this paper).

Taxon	Specimen	Cranial height - porion height W6 (a)	Bi- parietal breadth W9 (b)	Bi- parietal breadth W11 (c)	Bi- temporal breadth W10 (d)	Post-orbital constriction breadth (e)	Temporal foramen length W75	Temporal foramen breadth W75	Glabella-bregma length W17	Frontal squama angle W129	Temporal lines closest approach (f)	
<i>H. erectus</i>	Mean	86	119	129	131	89	40	33	100	52	73	
	BOU-VP-2/66		123	130	141	95			97	55		
	D2280	87	114	119	126	84			101		60	
	D2282		100	116	115	78			90	45	65	
	D2700	77	106	115	120	77	41	29	84	40	65	
	D4500		123	109	112	75					40	
	KNM-ER 3733	83	126	127	135	90	37	37	95	56	63	
	KNM-ER 3883	78	124	132	134	88	40	39	101	40	75	
	KNM-ER 42700	87	98	110	114	79			95	55	76	
	KNM-WT 15000	93	108	128	132	89	40	32		50	62	
	OH 9	90	132	138	140	101			120	50	81	
	Sangiran 2		114	136	136	83			88	45	67	
	Sangiran 4		120	139	138						78	
	Sangiran 17		130	144	150							
	SK 847					86		30				50
	Trinil I			126		91			98			
	Zhoukoudian DI					106			110	55		
	Zhoukoudian EI		123	131	133	88			100	60		90
	Zhoukoudian HIII											
Zhoukoudian LI		124	135	138	98			112	60		94	
Zhoukoudian LII		120	134	135	93			104	65		86	
Zhoukoudian LIII		128	137	139	95			107	60		104	

¹Non-crested individuals only.

²Digital reconstruction of damage to MH1 using synchrotron data resulted in a value that differs from Berger et al. (2010).

³Position of porion estimated (see text for details).

TABLE 3. CRANIAL METRICS FOR *AUSTRALOPITHECUS SEDIBA*
AND COMPARATIVE HOMININ SPECIMENS (continued).

(W# designations refer to measurement descriptions provided in Wood [1991].

Letters in parentheses indicate the measures used for generating the indices throughout the tables of this paper).

Taxon	Specimen	Zygomatic process sulcus breadth W61	Squamous suture height from FH	Squamous suture length	Mandibular fossa length W80 (g)	Mandibular fossa breadth W82 (h)	Mandibular fossa depth W84 (i)	Total facial height (supra-alveolar plane) (j)	Superior facial height (n-pr) W43 (k)
<i>Au. atamensis</i>	Mean								
	KNM-ER 30745								
	KNM-KP 29283				19	34	5.5	101	87
	Mean								
	AL 58-22								
	AL 162-28								
	AL 199-1								
	AL 200-1								
	AL 333-1				18	32	3.5	88	74
	AL 333-45								
	AL 417-1								
	AL 427-1								
	AL 442-1								
AL 444-2			56	19	35	7.5	113	100	
AL 486-1									
<i>Au. africanus</i>	Mean	19	35	69	16	27	7	92	77
	MLD 1								
	MLD 6/23								
	MLD 9								
	MLD 37/38		33		20	31			
	Sts 5	19	34	70	14	28	10	88	74
	Sts 17							90	
	Sts 19				15	29	7		
	Sts 25				15	22	6		
	Sts 52		35	65					74
	Sts 53								
	Sts 71	19	39	62	15	29	7	88	71

TABLE 3. CRANIAL METRICS FOR AUSTRALOPITHECUS SEDIBA AND COMPARATIVE HOMININ SPECIMENS (continued).

(W# designations refer to measurement descriptions provided in Wood [1991]. Letters in parentheses indicate the measures used for generating the indices throughout the tables of this paper).

Taxon	Specimen	Zygomatic process sulcus breadth W61	Squamous suture height from FH	Squamous suture length	Mandibular fossa length W80 (g)	Mandibular fossa breadth W82 (h)	Mandibular fossa depth W84 (i)	Total facial height (supra-glabellar to alveolar plane) (j)	Superior facial height (n-pr) W43 (k)
<i>H. erectus</i>	Mean	18			20	27	10	98	78
	BOU-VP-2/66	20			20	27	6		
	D2280				17	31	8		
	D2282	18			13	31	6		
	D2700				13	26	5	96	69
	D4500								73
	KNM-ER 3733	17			19	26	5	102	83
	KNM-ER 3883	20			20	28	7		
	KNM-ER 42700				17	20			
	KNM-WT 15000	18			28	27	10		77
	OH 9				19	32	13		
	Sangiran 2				28	23	13		
	Sangiran 4				28	28	18		
	Sangiran 17								82
	SK 847	16			15	26	6	95	84
	Trinil I								
	Zhoukoudian DI								
	Zhoukoudian EI				18	25			12
	Zhoukoudian HIII				21				15
Zhoukoudian LI									
Zhoukoudian LII				21	27	15		15	
Zhoukoudian LIII				18	23	15		15	

TABLE 3. CRANIAL METRICS FOR AUSTRALOPITHECUS SEDIBA AND COMPARATIVE HOMININ SPECIMENS (continued).

(W# designations refer to measurement descriptions provided in Wood [1991]. Letters in parentheses indicate the measures used for generating the indices throughout the tables of this paper).

Taxon	Specimen	Superior facial breadth (fmt-fmt) W49	Bi-orbital breadth (ek-ek) W50	Bi-zygomatic (zy-zy) W52	Bi-maxillary breadth (zm-zm) W53	Orbit breadth (mf-ek) W56	Orbit height W57	Inter-orbital breadth (mf-mf) W55	Nasal bone length (n-rhi) W71	Superior nasal bone breadth W73	Inferior nasal bone breadth W74	Nasal bridge height (nasion subtense)
	(l)	(m)	(n)	(o)	(p)	(q)	(r)	(s)	(t)	(u)		
<i>Au. anamensis</i>	Mean											
	KNM-ER 30745											
	KNM-KP 29283											
	Mean	89		34	38	19						
	AL 58-22											
	AL 162-28											
	AL 199-1											
	AL 200-1											
	AL 333-1	90										
	AL 333-45											
	AL 417-1	83				35	30	16				
	AL 427-1											
	AL 442-1											
AL 444-2	95		167		40	37	19					
AL 486-1	84		122		36	32	18	26	6	10	4	
Mean	94											
MLD 1												
MLD 6/23												
MLD 9												
MLD 37/38												
Sts 5	95	84	126	105	34	29	17	25	3	11	4	
Sts 17	92	75	92									
Sts 19												
Sts 25												
Sts 52	82	82	114	90	35	28	19	28	8	11		
Sts 53												
Sts 71	88	80	116	97	34	31	20	21	5	19	4	
<i>Au. africanus</i>	Mean											
	KNM-ER 30745											
	KNM-KP 29283											
	Mean	89		34	38	19						
	AL 58-22											
	AL 162-28											
	AL 199-1											
	AL 200-1											
	AL 333-1	90										
	AL 333-45											
	AL 417-1	83				35	30	16				
	AL 427-1											
	AL 442-1											
AL 444-2	95		167		40	37	19					
AL 486-1	84		122		36	32	18	26	6	10	4	
Mean	94											
MLD 1												
MLD 6/23												
MLD 9												
MLD 37/38												
Sts 5	95	84	126	105	34	29	17	25	3	11	4	
Sts 17	92	75	92									
Sts 19												
Sts 25												
Sts 52	82	82	114	90	35	28	19	28	8	11		
Sts 53												
Sts 71	88	80	116	97	34	31	20	21	5	19	4	

TABLE 3. CRANIAL METRICS FOR AUSTRALOPITHECUS SEDIBA AND COMPARATIVE HOMININ SPECIMENS (continued).

(W# designations refer to measurement descriptions provided in Wood [1991]. Letters in parentheses indicate the measures used for generating the indices throughout the tables of this paper).

Taxon	Specimen	Superior facial breadth (fmt-fmt) W49	Bi-orbital breadth (ek-ek) W50	Bi-zygomatic (zy-zy) W52	Bi-maxillary breadth (zm-zm) W53	Orbit breadth (mf-ek) W56	Orbit height W57	Inter-orbital breadth (mf-mf) W55	Nasal bone length (n-rhi) W71	Superior nasal bone breadth W73	Inferior nasal bone breadth W74	Nasal bridge height (nasion subtense)
	(l)	(m)	(n)	(o)	(p)	(q)	(r)	(s)	(t)	(u)		
	StW 13			100			18	21	8	11		
	StW 53	91	88	130	92	37	18	24		9		
	StW 73											
	StW 183											
	StW 505	106	97		108	39	19	40	7	10		
<i>Au. sediba</i>	MH1	86	78	102	84	31	32 ²	24	8	13	9	
	Mean											
<i>H. naledi</i>	DH1											
	DH2											
	DH3	86	78			29	21					
	Mean	99	86	116	93	33	27	18	8	11	8	
<i>H. habilis</i>	AL 666-1											
	KNM-ER 1805						38	18	8	11	10	
	KNM-ER 1813	95	86	117	90	33	20	13	7	9		
	OH 7											
	OH 13	102										
	OH 16											
	OH 24	100	86	115	96	33	24	23	10	12	5	
	OH 65											
	Mean		88			35	20					
<i>H. rudolfensis</i>	KNM-ER 1470	106	101		113	41	23	20	8	10	4	
	KNM-ER 62000		74			29	17					

TABLE 3. CRANIAL METRICS FOR AUSTRALOPITHECUS SEDIBA AND COMPARATIVE HOMININ SPECIMENS (continued).

(W# designations refer to measurement descriptions provided in Wood [1991].

Letters in parentheses indicate the measures used for generating the indices throughout the tables of this paper).

Taxon	Specimen	Total nasal height (n-ns) W69 (v)	Nasal aperture height (rti-ns) W70 (w)	Nasal aperture breadth W68 (x)	Alveolar height (ns-pr) W45 (y)	Subnasale to prosthion horizontal projection W47 (z)	Subnasale to prosthion vertical projection W48 (aa)	Orbitale to zygomatic maxillary (or-zm) W58	Zygomatic breadth - jugale to zygomatic maxillary suture W59	Malar thickness (of zygomatic process of maxilla) W60
<i>Au. anamensis</i>	Mean									
	KNM-ER 30745			22						
	KNM-KP 29283			23	28	16	15		42	14
	Mean	58	30							
	AL 58-22									
	AL 162-28									
	AL 199-1				27	16	14			
	AL 200-1				26	16	15			
	AL 333-1			22					35	10
	AL 333-45									
AL 417-1	49	27	23	30						
AL 427-1										
AL 442-1										
AL 444-2	67	37	25					48	17	
AL 486-1			22							
Mean	51	25	25	26	21	19	29	22	12	
<i>Au. africanus</i>	MLD 1									
	MLD 6/23	45	23	20						
	MLD 9									
	MLD 37/38									
	Sts 5	49	24	27	25	25	23	27	21	8
	Sts 17			23	22					
	Sts 19									
	Sts 25									
	Sts 52	50	23	25	24	19	20	30	21	10
	Sts 53				25	16	15			
Sts 71	47	29	26	23	21	18	27	24	16	

TABLE 3. CRANIAL METRICS FOR AUSTRALOPITHECUS SEDIBA AND COMPARATIVE HOMININ SPECIMENS (continued).

(W# designations refer to measurement descriptions provided in Wood [1991].

Letters in parentheses indicate the measures used for generating the indices throughout the tables of this paper).

Taxon	Specimen	Total nasal height (n-ns) W69 (v)	Nasal aperture height (rhi-ns) W70 (w)	Nasal aperture breadth W68 (x)	Alveolar height (ns-pr) W45 (y)	Subnasale to prosthion horizontal projection W47 (z)	Subnasale to prosthion vertical projection W48 (aa)	Orbitale to zygomatic maxillary (or-zm) W58	Zygomatic breadth - jugale to zygomatic maxillary suture W60	Malar thickness (of zygomatic process of maxilla) W60
	StW 13	54	28	24	30	25	24	29		11
	StW 53	46	22	23	25	19	17	26	23	12
	StW 73				27					
	StW 183			25						
	StW 505	64	28	30	29	25	20	35		17
<i>Au. sediba</i>	MH1	49	24	26	22	13	17	25	22	14
<i>H. naledi</i>	Mean									
	DH1					16	20			
	DH2									
	DH3									
<i>H. habilis</i>	Mean	46	28	25	25	19	18	28	23	9
	AL 666-1				32					
	KNM-ER 1805	52	34	28	21	17	13			
	KNM-ER 1813	43	28	23	25	18	22	28	21	9
	OH 7									
	OH 13									
	OH 16									
	OH 24	44	21	25	22	21	20	27	25	9
	OH 65									
<i>H. rudolfensis</i>	Mean	55		24	27					
	KNM-ER 1470	57	39	25	31	17	30	43		15
	KNM-ER 62000	53		23	23					

TABLE 3. CRANIAL METRICS FOR AUSTRALOPITHECUS SEDIBA AND COMPARATIVE HOMININ SPECIMENS (continued).

(W# designations refer to measurement descriptions provided in Wood [1991]. Letters in parentheses indicate the measures used for generating the indices throughout the tables of this paper).

Taxon	Specimen	Maxillo- alveolar length W87 (ab)	Maxillo- alveolar breadth (ekm- ekm) W88 (ac)	I ¹ -I ² alveolar length W94 (ad)	Canine alveolar length W95 (ae)	P ³ -P ⁴ alveolar length W96 (af)	Palate length (ol-sta) W89 (ag)	Canine inter- alveolar distance W98 (ah)	P ³ inter- alveolar distance W99	P ⁴ inter- alveolar distance W100	M ² inter- alveolar distance (enm- enm) W101 (ai)
<i>Au. anamensis</i>	Mean										
	KNM-ER 30745							33	33	34	33
<i>Au. afarensis</i>	KNM-KP 29283	67	64	16	9	16		31	28	29	30
	Mean	67	68	15	9	16	63	28	38	39	36
	AL 58-22		58						29	31	30
	AL 162-28									31	30
	AL 199-1	59	68	13	8	12	54	27	26	27	32
	AL 200-1	72	68	15	8	15	64	30	32	33	34
	AL 333-1								30	32	
	AL 333-45										
	AL 417-1	61	61				58	23			29
	AL 427-1							30			29
<i>Au. africanus</i>	AL 442-1							24			25
	AL 444-2	76	82				75	35			
	AL 486-1	70	64					29			33
	Mean	70	66	13	7	15	63	30	30	32	36
	MLD 1										
	MLD 6/23		56		7	15					
	MLD 9		68	10	7	15		30	30	29	40
	MLD 37/38		63								
	Sts 5	76	68	12	5	14	67	29	29	30	35
	Sts 17	66	63	13	6	15		27	29	31	33
Sts 19											
Sts 25											
Sts 52	71	71	15	7	18		31	30	34	40	
Sts 53	68	64	13	7	13	57	29	30	32	34	
Sts 71	74	70	13	8	15		29	33	36	38	

TABLE 3. CRANIAL METRICS FOR AUSTRALOPITHECUS SEDIBA AND COMPARATIVE HOMININ SPECIMENS (continued).

(W# designations refer to measurement descriptions provided in Wood [1991]. Letters in parentheses indicate the measures used for generating the indices throughout the tables of this paper).

Taxon	Specimen	Maxillo-alveolar length W87 (ab)	Maxillo-alveolar breadth (ekm-ekm) W88 (ac)	I-1 ² alveolar length W94 (ad)	Canine alveolus length W95 (ae)	P ³ -P ⁴ alveolar length W96 (af)	Palate length (ol-sta) W89 (ag)	Canine inter-alveolar distance W98 (ah)	P ³ inter-alveolar distance W99	P ⁴ inter-alveolar distance W100	M ² inter-alveolar distance (enm-enm) W101 (ai)
	StW 13	77	68	15	7	17	64	34	33	35	38
	StW 53	67	70	14	7	16		26	31	33	32
	StW 73	64	60	15	7	16		28	27	29	30
	StW 183										
	StW 505		70		8	14			27		
<i>Au. sediba</i>	MH1	63	63	16	8	18	55	28	30	32	29
	Mean										
<i>H. naledi</i>	DH1	57	71	13	7	14		24	28	32	34
	DH2										
	DH3										
	Mean										
<i>H. habilis</i>	AL 666-1	67	69	15	7	16	58	31	34	37	40
	KNM-ER 1805	71	72	15	7	16	63	30	33	36	39
	KNM-ER 1813	61	65	16	7	16	60	36	41	43	48
	OH 7							28	32	35	37
	OH 13		66			15	60	30	32	34	37
	OH 16										
	OH 24	61	67	13	7	16	55	27	29	33	36
	OH 65	73	76	16	8	15	54	33	37	40	44
	Mean		72	14	7	16		33	37	39	38
<i>H. rudolfensis</i>	KNM-ER 1470		78	14	6	16		33	39	42	38
	KNM-ER 62000	63	66	14	8	16	56	33	34	35	37

TABLE 3. CRANIAL METRICS FOR AUSTRALOPITHECUS SEDIBA AND COMPARATIVE HOMININ SPECIMENS (continued).

(W# designations refer to measurement descriptions provided in Wood [1991].

Letters in parentheses indicate the measures used for generating the indices throughout the tables of this paper).

Taxon	Specimen	(aj)	Inter-canine to inter-M2 length	Palate depth at canines	Palate depth at incisive fossa	Palate depth at M ¹	(ak)
<i>Au. anamensis</i>	Mean	32					
	KNM-ER 30745	29					
<i>Au. afarensis</i>	KNM-KP 29283	35			6	11	
	Mean	34			8	11	
	AL 58-22	34					
	AL 162-28						
	AL 199-1	33				12	
	AL 200-1	38				9	
	AL 333-1						
	AL 333-45			2	5		
	AL 417-1	30				14	
	AL 427-1					11	
<i>Au. africanus</i>	AL 442-1						
	AL 444-2				10	12	
	AL 486-1					11	
	Mean	39		6	9	13	
	MLD 1						
	MLD 6/23						
	MLD 9						
	MLD 37/38						
	Sts 5	37		8	13	15	
	Sts 17	47		5	9	16	
Sts 19							
Sts 25							
Sts 52	42		7	9	17		
Sts 53	35		10	10	12		
Sts 71	40		7	9	10		

TABLE 3. CRANIAL METRICS FOR AUSTRALOPITHECUS SEDIBA AND COMPARATIVE HOMININ SPECIMENS (continued).

(W# designations refer to measurement descriptions provided in Wood [1991].

Letters in parentheses indicate the measures used for generating the indices throughout the tables of this paper).

Taxon	Specimen	(aj)	Inter-canine to inter-M2 length	Palate depth at canines	Palate depth at incisive fossa	Palate depth at M ¹	W103 (ak)
	StW 13	38	5	5	12		
	StW 53	36	6	9	9		
	StW 73	34	3	8	11		
	StW 183						
	StW 505						
<i>Au. sediba</i>	MH1	38	5	10	10		
<i>H. naledi</i>	Mean						
	DH1	29	3	5	10		
	DH2						
	DH3						
<i>H. habilis</i>	Mean	36	7	11	14		
	AL 666-1	30			15		
	KNM-ER 1805	40	9		6		
	KNM-ER 1813	36	8	10	13		
	OH 7						
	OH 13	35			18		
	OH 16						
	OH 24	35	4	10	13		
	OH 65	39	7	12	17		
<i>H. rudolfensis</i>	Mean	39					
	KNM-ER 1470	37	7	14	18		
	KNM-ER 62000	41					

TABLE 3. CRANIAL METRICS FOR AUSTRALOPITHECUS SEDIBA AND COMPARATIVE HOMININ SPECIMENS (continued).

(W# designations refer to measurement descriptions provided in Wood [1991]. Letters in parentheses indicate the measures used for generating the indices throughout the tables of this paper).

Taxon	Specimen	Inter-canine to inter-M2 length (aj)	Palate depth at canines	Palate depth at incisive fossa	Palate depth at M ¹ W103 (ak)
<i>H. erectus</i>	Mean	35	7	11	15
	BOU-VP-2/66				
	D2280				
	D2282	35	10	10	13
	D2700	36	9	9	9
	D4500				
	KNM-ER 3733	36	7	19	20
	KNM-ER 3883				
	KNM-ER 42700				
	KNM-WT 15000				
	OH 9	37	6	7	11
	Sangiran 2				
	Sangiran 4				
	Sangiran 17				
	SK 847				
	Trinil I	33	5	11	12
Zhoukoudian DI					
Zhoukoudian EI					
Zhoukoudian HIII					
Zhoukoudian LI					
Zhoukoudian LII					
Zhoukoudian LIII					

TABLE 4. DENTAL METRICS FOR MH1 AND MH2 OF *AUSTRALOPITHECUS SEDIBA*.

	MH1				MH2			
	Left		Right		Left		Right	
	MD	BL	MD	BL	MD	BL	MD	BL
UI1			10.1	6.9				
UI2	7.2	6.6						
UC			9.0	8.8				
UP3	8.9	11.1	9.0	11.2				
UP4	9.3	12.1	9.2	12.1				
UM1	12.9	12.0	12.7	12.4				
UM2	12.9	13.7	13.0	13.5				
UM3	13.3	14.1	13.1	13.6			12.6	12.9
LI1								5.9
LI2								6.6
LC	8.0	8.6					7.3	7.4
LP3	10.1	10.0					8.1	9.2
LP4	9.8	11.1					8.8	9.7
LM1			13.1	11.5			13.1	11.3
LM2			14.5	13.2			14.4	12.3
LM3			14.9	13.6	14.8	12.5	14.9	12.7

What is preserved of the inferior/internal aspect of the cranium remains encased in matrix, including much of the palate from the incisal region to the preserved pterygoid plates, and the entire remaining neurocranium.

The majority of the cranial sutures are only partially fused, and displacement of several bones along the sutural lines is evident. In addition, the cranium is permeated by several cracks, some small, others more pervasive. In superior view, a large crack is evident near the midline of the frontal squama. The crack begins as a hairline fracture of the supraorbital torus to the left of the glabellar prominence, incising the supero-medial corner of the left internal orbit, and widening posteriorly along the squama to reach a width of ca. 2mm at bregma. The crack has resulted in the lateral displacement of the entire left half of the neurocranium in a ca. 5° arc from a pivot point immediately left lateral to the glabellar prominence. A series of additional hairline cracks are evident across the cranium. The coronal suture shows a slight dislodging of the left parietal from the frontal, narrowing toward the temporal line, thereafter appearing as a hairline separation until reaching the temporal bone, resulting in additional lateral displacement of the left parietal from the point of bregma. The left temporal bone has been slightly laterally displaced along the squamosal suture, with the separation widening slightly toward posterior. The root of the zygomatic process has been slightly medially depressed relative to the temporal bone at its posterior extent. When viewed laterally, the en-

tire, intact left zygomatic bone has been rotated slightly in a clockwise direction from a pivot point that approximates zygomaxillare, dislocating the bone slightly at its temporal, frontal, and maxillary sutures.

When viewed superiorly, relative to the midface the entire neurocranium has been slightly rotated in an oblique clockwise fashion, resulting in a frontal bone that is displaced slightly inferolaterally to the left, such that glabella is positioned some 3mm to the left of the midline of the face. Within the right orbit, the frontal bone has broken away from the frontal process of the maxilla close to, but not coincident with, the frontomaxillary suture. This break continues as an obliquely oriented crack across the nasal bones some 14mm above rhinion, resulting in a left lateral displacement of the superior half of the nasals in conjunction with the frontal and the neurocranium. The rotation of the left zygomatic bone further augments the appearance of the displacement of the neurocranium, such that the upper face, including the supraorbital torus and glabellar area, the upper half of the nasals, the left orbit, and the left zygomatic are shifted slightly inferolaterally in facial view. On the left side, the superior extent of the frontal process of the maxilla has been broken from the rest of the process in two fragments, which are slightly antero-inferiorly displaced from the frontal bone and the nasal bone along the respective suture lines. The left lacrimal has been slightly laterally shifted, while a portion of the orbital plate of the frontal has also been dislodged, though to a lesser

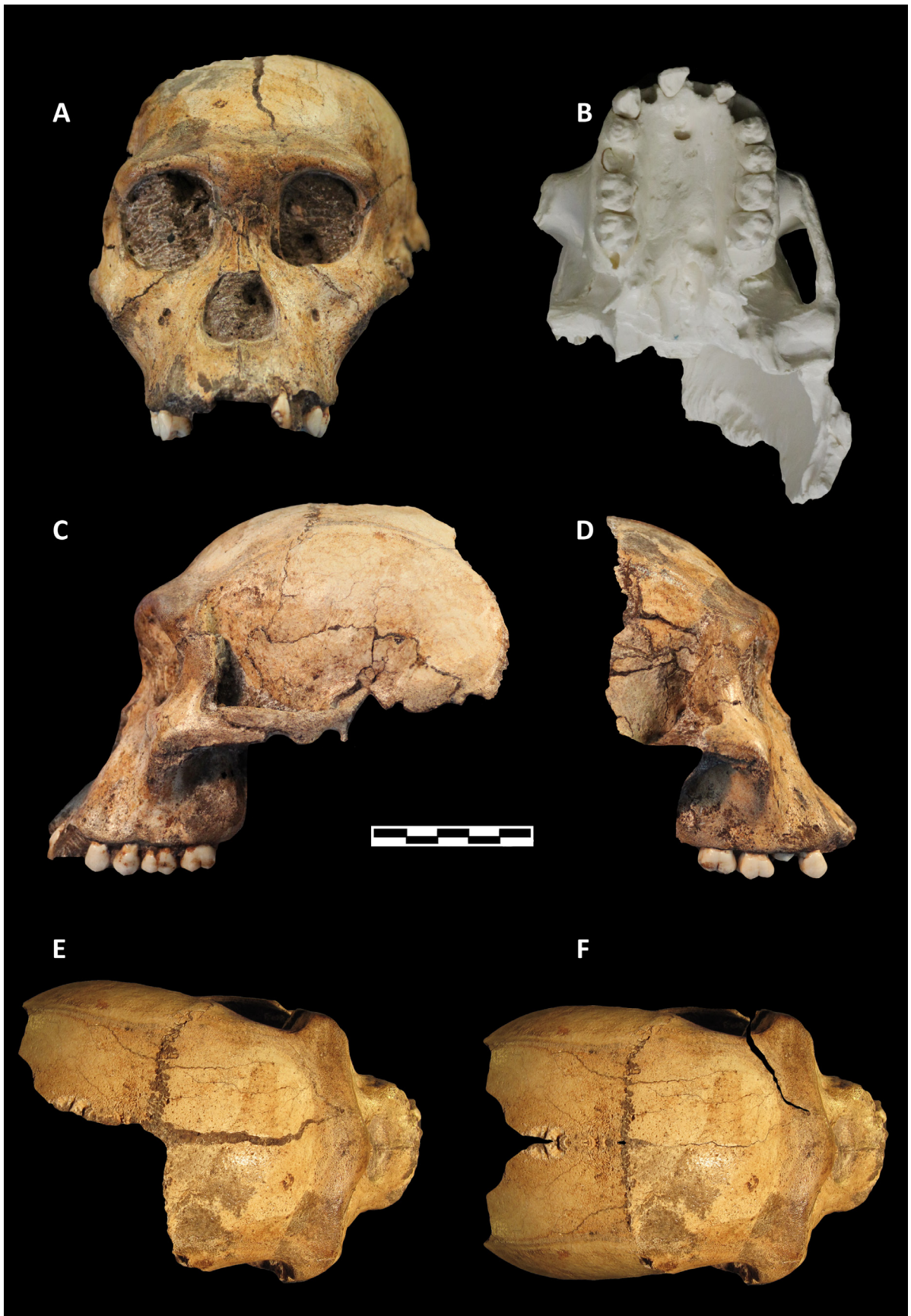


Figure 1. Cranium of *Au. sediba* holotype MH1. U.W. 88-50 in A) anterior view; B) inferior view of 3D printout of cranium to show palate which is otherwise encased in matrix; C) left lateral view; D) right lateral view; E) superior view of original specimen; F) superior view with cracks digitally removed and left parietal mirror imaged onto right side (scale bar=50mm).

extent than the lacrimal. There is a small crack through the right lateral orbital margin from which a small fragment of bone has been removed, and ca. 14mm above this is a slight separation of the right frontozygomatic suture that in turn becomes a crack that traverses posteriorly through the frontal and into the area of the temporal foramen until truncated by more extensive damage. The nasal bones are well preserved, having been broken into superior and inferior segments. The inferior segment of the left nasal has been slightly depressed superiorly, and slightly anteriorly displaced inferiorly. Apart from the breakage to the left frontal process, the maxillae are well preserved and undistorted bilaterally, though there are some small areas of damage evident. The incisural juga all show some abrasion, in particular the LP² jugum, from which a wedge of alveolar bone has been removed, including a flake of the underlying tooth root; a small hole penetrates the root at this point. On the right maxillary alveolar process there are two small points of damage, one above the P⁴, and one above the M². A small wedge of cortical bone has been removed from the maxillary tuber on the right side, while two small pinpoint holes are evident on the left maxillary tuber. The palate is well preserved and appears relatively intact, though it is still partially encased in matrix; as a result, descriptions provided for this region are based upon examination of synchrotron scans of the cranium.

Mandible

The mandible of MH1 is comprised of three main bony parts and two isolated teeth that can be refit (see Table 1). The bony parts include a relatively complete, right hemimandible (U.W. 88-8) preserving most of the corpus distal to the mandibular symphysis and all of the ascending ramus (Figure 2); a cortical fragment of the left anterior corpus with the L_C in place (U.W. 88-2) extending from about the position of the symphysis to immediately distal to the canine alveolus, and from the alveolar margin to 31.5mm inferior to the margin; and most recently a left mandible fragment (U.W. 88-245) was recovered that is mostly present from the area of the mandibular symphysis to an oblique fracture running from the mesial M₁ to a position below the M₂ at the basal corpus. Anteriorly, U.W. 88-8 is broken near the level of the symphysis, obliquely through the alveolus for the RI₂, while on the posterior aspect of the anterior corpus the break transects the corpus at the symphysis. Distally, the matrix filled alveoli for the R_C, RP₃ and RP₄ are preserved, along with the molar teeth distally. A secondary crack runs superoinferiorly between the canine and P₃ alveoli to the basal corpus, and several smaller cracks permeate the basal corpus and ascending ramus, though none are overly pervasive. The medial corpus presents a ca. 15.5mm crack beginning beneath the distal half of the M₂ and traversing anteroinferiorly to about the position of the M₁/M₂ just below mid-corpus height; a small flap of cortical bone is extruded about 1.0mm at the anterior terminus of this crack. Surface preservation of U.W. 88-8 is otherwise good, with slight cortical damage restricted mainly to the antero-

lateral corpus beneath the position of the P₃ and the canine. The cortical surface is notably porous, particularly near the anterior corpus, a result of the juvenile status of the individual. Close examination of the patterns of breakage in the symphyseal areas of U.W. 88-8 and U.W. 88-245 shows that, were the intervening calcified clastic sediment that remains attached to these pieces removed, the two would likely refit, thus the symphysis of the mandible is largely preserved. Anteriorly the cortical surface of U.W. 88-245 was broken away, being represented by U.W. 88-2 which can be clearly refit. The alveolar margins are broken away along the length of the preserved specimen UW88-245 except for a small segment on the posterior alveolar margin between the canine and lateral incisor. The roots of the P₃ and P₄ are preserved, and the two isolated teeth U.W. 88-246 and U.W. 88-244 respectively can be reattached to these broken roots. The mesial roots of the M₁ are also preserved, and along with the posterior crack through the specimen, can be refit to a mandibular fragment that is embedded in a large block of calcified clastic sediment that is currently undergoing preparation; once the fragments are reunited, the mandible of MH1 will be largely complete. The cortical surface of the reunited U.W. 88-2 / U.W. 88-245 appears well preserved and notably porous on the anterior/lateral face, similar to U.W. 88-8. The basal surface of U.W. 88-245 shows some cracking and root etching, and a small wedge of cortical bone has been flaked away from the basal margin taking much of the anterior marginal tubercle with it. U.W. 88-245 has an overall different coloration and patina than U.W. 88-8 that likely results from it being recovered from soft sediment, while U.W. 88-8 was recovered from a block of hard calcified clastic sediment.

Teeth

The cranium of MH1 retains the slightly damaged LP² and all of the premolars and molars bilaterally (Figure 3). The fourth premolar is fully occluded on the left side, but is impacted and only partially erupted on the right. Both of the third molars are forming in the crypt, and neither is visible save by synchrotron scanning. To these *in situ* maxillary teeth, we can add the isolated RI¹ (U.W. 88-29) and R^C (U.W. 88-30). The maxilla of MH1 is still partially encased in matrix, thus the lingual surfaces of the teeth on the left are only partially exposed. The lingual face of the RM¹ was damaged prior to recovery of the specimen. The partially erupted L_C is located in the anterior mandibular fragment U.W. 88-2, and fits in the preserved canine alveolus of U.W. 88-245 (Figure 4). The P₃ (U.W. 88-246) and P₄ (U.W. 88-244) that are refit to the mandible fragment U.W. 88-245 are complete and only very slightly worn. The M₁ and M₂ of the MH1 mandible are fully erupted and in occlusion, while the M₃ is preserved in the crypt. The M₁ and M₂ are in almost their original anatomical position; the M₂ is displaced slightly, as if the tooth were partially extruded from its socket prior to fossilization. The M₃ is visible via synchrotron scans.



Figure 2. Mandible of *Au. sediba* holotype MH1. U.W. 88-8 in A) lateral view; B) medial view; C) occlusal view; D) basal view; E) digital image of M_3 in the crypt; U.W. 88-2 in F) lingual view; G) anterior/labial view; U.W. 88-245 in H) lateral view; I) medial view; J) occlusal view; K) basal view; L) lateral view with U.W. 88-2 refit; M) occlusal view with U.W. 88-2, U.W. 88-244 (P_4), and U.W. 88-246 (P_3) refit (scale bar=50mm).

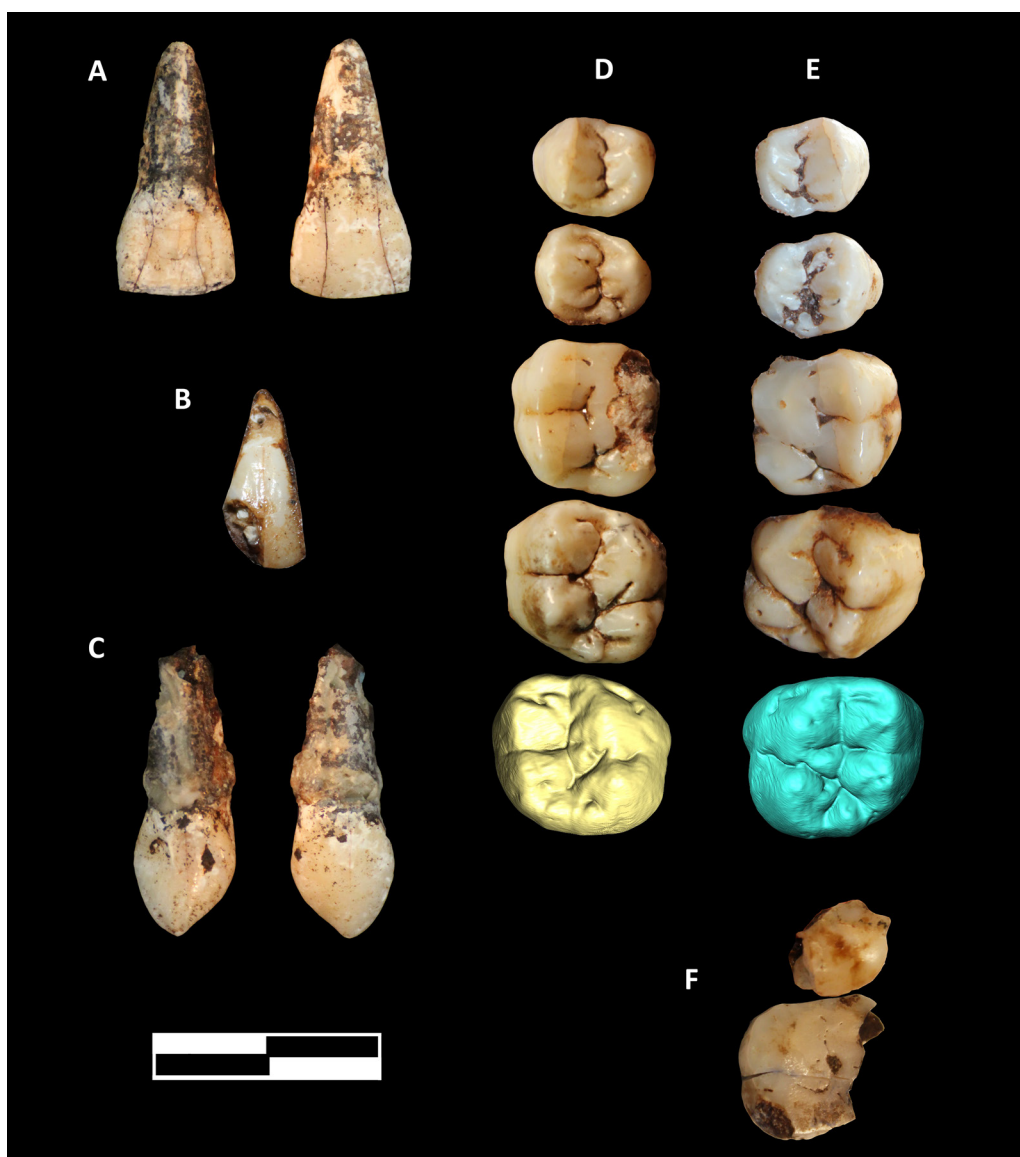


Figure 3. Close up view of maxillary teeth of *Au. sediba* holotype and paratype MH1 and MH2. MH1 includes A) RI^1 (U.W. 88-29) in lingual and labial views; B) RI^2 (U.W. 88-50) in labial view; C) RC (U.W. 88-30) in lingual and labial views; D) right postcanine tooth row (U.W. 88-50) in occlusal view, including digital image of M^3 in the crypt; E) left postcanine tooth row (U.W. 88-50) in occlusal view, including digital image of M^3 in the crypt. MH2 includes F) RM^2 (U.W. 88-19) and RM^3 (U.W. 88-20) in occlusal view. Note that some of the teeth of MH1 are not precisely oriented in occlusal view since U.W. 88-50 remains partially encased in matrix, thus images are difficult to obtain (scale bar=20mm).

MALAPA HOMININ 2 (MH2)

Mandible

The mandible of MH2 is comprised of most of the right ramus and a portion of the corpus (U.W. 88-54), another portion of the right mid-corpus (U.W. 88-128), a portion of the right anterior corpus (U.W. 88-129), and a large portion of the left corpus (U.W. 88-55, two pieces) from the root of the ramus to approximately the level of the P_3 (Figure 5). The right ramus is nearly complete, lacking only the medial half of the condyle and the tip of the coronoid. The lateral surface of the right ramus is pervaded by numerous small cracks, and the gonial region has been displaced

slightly laterally, giving a false impression of an everted gonial angle. The medial surface of the right ramus is more damaged, exhibiting several areas of breakage that appear to be geological in origin. Two principal areas, one posterior to the mandibular foramen and the other posterior to the M_3 and inferior to the pharyngeal crest, display depressed bone tables. The crack in the gonial region is more visible on the medial face, enhancing the false impression of an everted gonial angle. At the anteroinferior extent of this crack, a wedge of bone has been broken away from the basal ramus immediately anterior to the gonial angle. Anterior to this, the basal corpus is nearly intact for a short distance below M_3 before being truncated by a break that

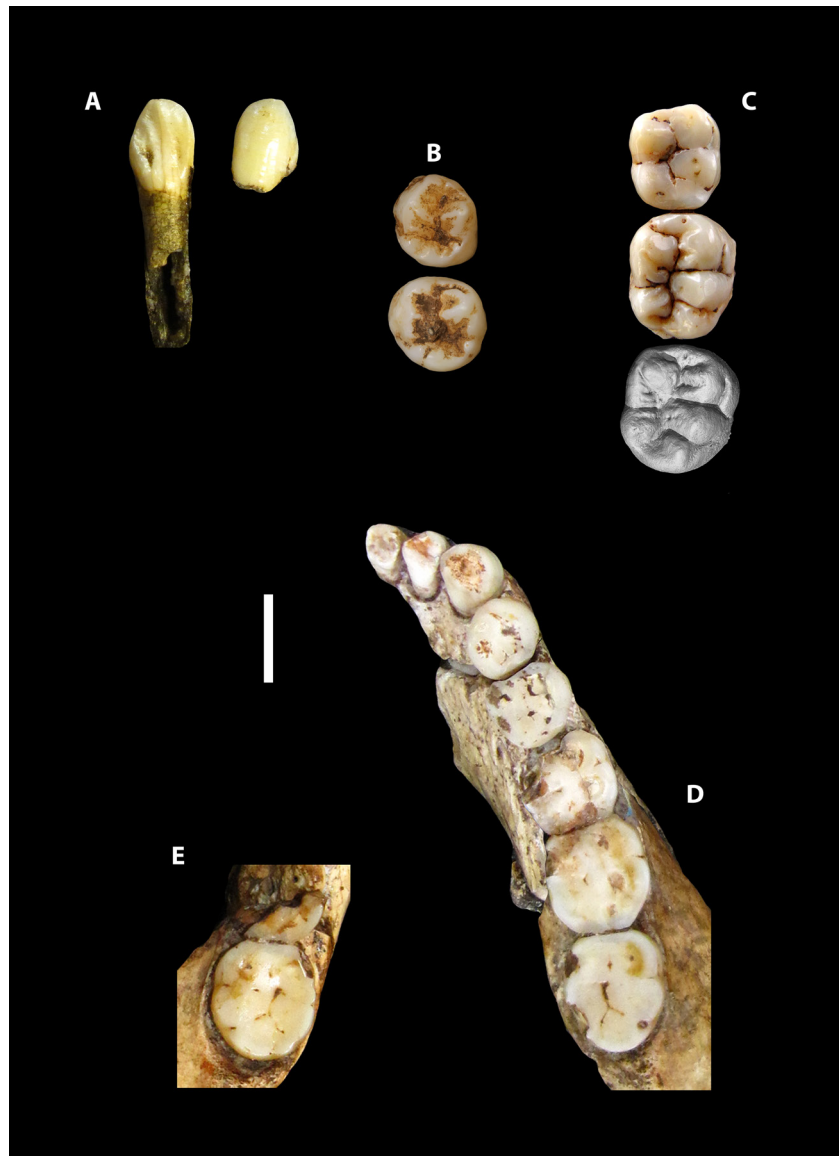


Figure 4. Close up view of mandibular teeth of *Au. sediba* holotype and paratype MH1 and MH2. MH1 includes A) L_c (U.W. 88-2) in lingual and labial views; B) LP_3 (U.W. 88-246) and LP_4 (U.W. 88-244) in occlusal view; C) right molar row (U.W. 88-8) in occlusal view, including digital image of M_3 in the crypt. MH2 includes D) right tooth row (U.W. 88-54, 128, 129) in occlusal view; E) left M_3 (U.W. 88-55) in occlusal view (scale bar=10mm).

runs obliquely upward toward the M_1 on the lateral surface and the M_2 on the medial surface. This break defines the separation between U.W. 88-54 and the more anterior portion, U.W. 88-128. Despite this breakage, the two specimens refit well, lacking only a wedge of basal corpus below M_3 . The remainder of the right corpus (U.W. 88-128) is represented by an approximately triangular-shaped fragment that preserves the RP_4 , to which is refit the smaller anterior fragment U.W. 88-129, the latter which preserves the RP_3 , R_c , RI_2 , and RI_1 . The anterior cortical surface of U.W. 88-129 is well preserved, though a small fragment has been detached, providing a small window to the root of the RI_2 . Mesially U.W. 88-129 is broken from close to the symphysis and partially through the root of the RI_1 , obliquely down to the visible tip of the root of the RI_2 ; this same breakage ex-

tends posteroinferiorly through the corpus fragment U.W. 88-128, thus much of the anterior corpus is not preserved. U.W. 88-128 is pervaded by a series of cracks, and some cortical exfoliation is evident on both the medial and lateral surfaces. At the posterior edge of the medial extent of U.W. 88-128 a small wedge of bone has been extruded some 2.7mm to be truncated by the separation from U.W. 88-54.

The left corpus (U.W. 88-55) is preserved as two conjoined fragments, a larger posterior portion that retains the M_3 , and a smaller anterior portion that is lacking much of the lateral cortical surface, and which lacks the crowns but preserves the partial roots of the M_1 and the M_2 (see Figure 5). Preservation of the medial surface of the anterior portion is good, though a few small cracks are evident. The lateral surface has suffered considerable removal of the cor-

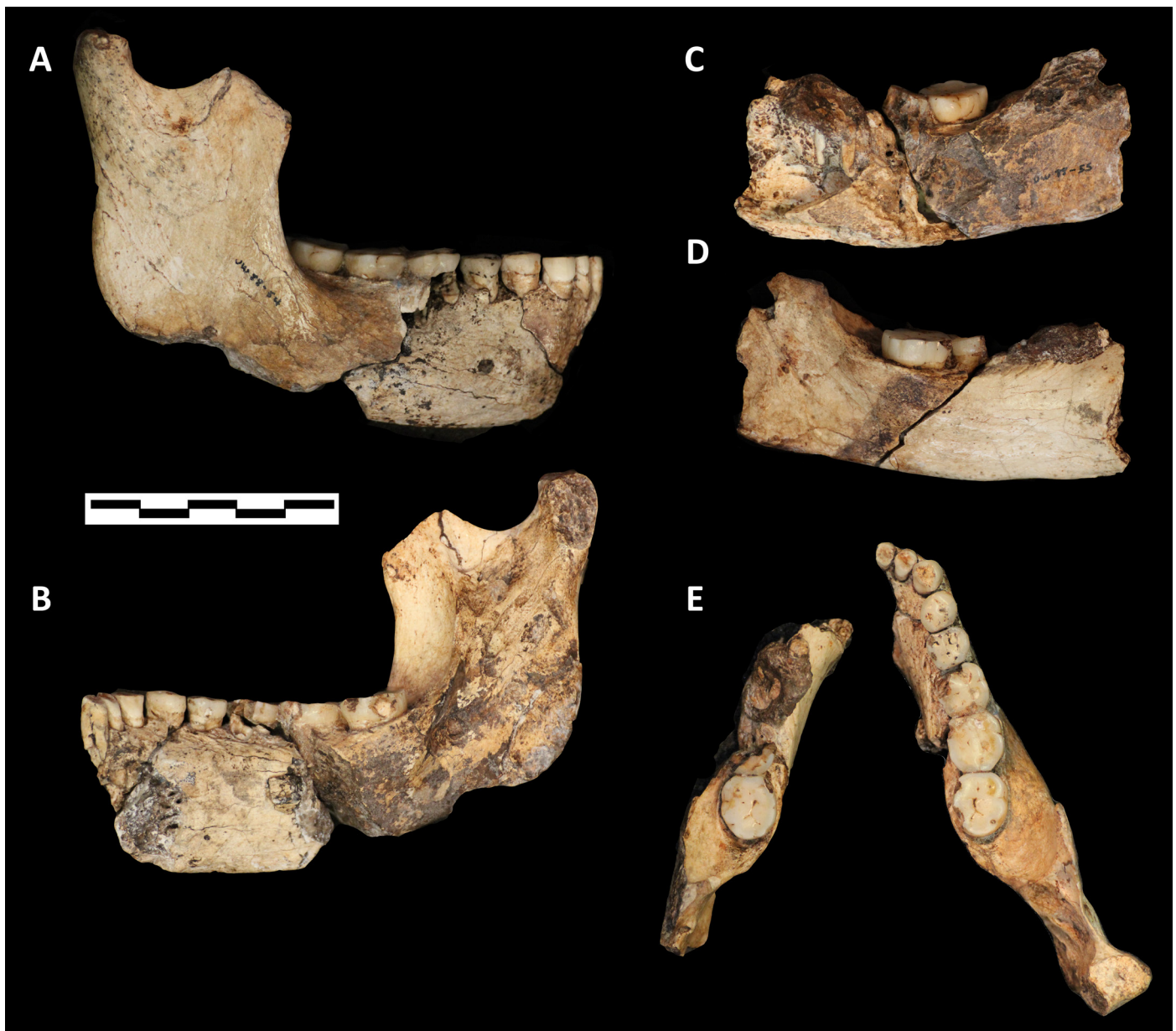


Figure 5. Mandible of *Au. sediba* paratype MH2. Refit specimens U.W.8 8-54, U.W. 88-128, and U.W. 129 in A) lateral view; B) medial view; U.W. 88-55 in C) lateral view; D) medial view; E) reassembled MH2 mandible in occlusal view (scale bar=50mm).

tical bone, amounting to most of the lateral aspect, thereby revealing the roots of the M_1 and M_2 ; only a small triangle of cortical bone remains beneath the roots of the M_1 . Inferiorly, the basal surface is missing an elongated wedge of cortical bone at its anterior extent, while posteriorly the basal corpus is mostly present. The more posterior portion is separated by an oblique crack that runs anterosuperiorly from below the M_3 at the basal margin to the M_2 at the alveolar margin. Posteriorly most of the ramus has been sheared away at about the level of the mandibular foramen. The medial surface of the ramus is fairly well preserved with a few small cracks, while the lateral surface has suffered more extensive removal of cortical bone via abrasion.

Teeth

The maxillary dentition of MH2 is represented by two isolated, fragmented molar crowns (U.W. 88-19, U.W. 88-20) recovered from an area of calcified clastic sediment at Malapa (see Figure 3). The entire right mandibular dentition of MH2 is preserved from the RI_1 - RM_3 , alongside a fragmented LM_1 and LM_2 , and a more complete LM_3 (see Figure 4). Some damage is evident in the mandibular molars, in particular the RM_1 and the LM_2 , and small chips of enamel have been removed from the LI_1 , LI_2 , RM_2 , and RM_3 . Wear is considerably more advanced than in MH1.

ANATOMICAL DESCRIPTIONS

CRANIUM OF MALAPA HOMININ 1 (MH1)

Cranial Vault

Cranial capacity is estimated at approximately 420cc (Bergner et al. 2010; Carlson et al. 2011). Viewed superiorly, the vault appears as an elongated ovoid, with only limited tapering of the vault posteriorly or anteriorly (see Figure 1). The anterior border of the frontal squama is gently rounded in superior view. In lateral view the cranium displays a long, gently rounded profile, with a moderately hollowed post-bregmatic depression near the apex of the cranium; this region is populated by highly porous bone. At the posterior extent of the preserved left parietal, a short, ca. 20mm expanse of the partially fused lambdoid suture is visible, coincident with the posterior curve of the temporal lines. The vertically oriented lateral wall of the left parietal is transversely expanded, with slight parietal bossing evident posterior to the bone's center, thus the greatest lateral expansion of the parietals occurs along a relatively superoinferiorly extended region of the parietals from the parietal bossing to just above the estimated position of the mastoids. As a result, tapering of the parietal breadth superior-ward from the supramastoid region is minimal, presenting instead a more angular transition from the lateral to the superior wall of the parietal just below the level of the temporal lines; this results in a relatively "boxy" appearance of the neurocranium.

The temporal lines are widely spaced, and the superior and inferior temporal lines are readily visible on the left frontal and parietal for most of their duration, with the superior becoming slightly obscured by damage at the posterior extent; they are likewise well-developed where visible on the right frontal bone. The temporal lines begin as well-defined crests at the marginal process, the latter which forms as a clearly marked rugosity on the posterior aspect of the frontal process of the zygomatic. They continue across the frontozygomatic suture and superiorly onto the posterosuperior face of the lateral one-fifth of the supraorbital torus. Turning posterosuperiorly, the temporal lines are restricted mainly to the same vertical plane as the medial wall of the temporal foramen, displaying minimal anteromedial incursion onto the frontal bone. Beginning at the level of the temporal foramen, the superior temporal line appears as a well-defined, striated ridge between 1–2mm wide along its entire extent. The inferior temporal line appears as a well-developed but more diffusely defined, yet still striated, ridge, averaging between 4–5mm in breadth, immediately subadjacent to the superior temporal line. It is especially well delineated superior to the temporal foramen, where its inferior border begins as a discrete ridge that is separated from the superior temporal line by some 2–3mm, though this discrete distinction between superior and inferior lines becomes less well defined posterior to the coronal suture. The temporal lines continue posteriorly across the parietals in a gently convex arc before finally curving around inferiorly and then anteriorly to become continuous with

the low, rounded supramastoid crest. Although the nuchal area is mostly lacking, there is no indication on the preserved parietal or temporal bones that the temporal lines would have contacted the nuchal line. In particular, there is a small flange of bone at the extreme posteroinferior extent of the preserved parietal that extends beyond the superior temporal line, where one would expect to see a trace of the nuchal line had it contacted the temporal line; there is no trace of such a nuchal line, thus a compound temporal/nuchal crest is unlikely.

The squamous suture is elongated and relatively straight edged anteriorly, showing limited overlap of the temporals over the parietals. Posteriorly, the squamous suture tilts inferiorly in a series of jagged bevels toward the (absent via damage) parietomastoid suture. Parietal striae are clearly visible, especially posteriorly, fanning out from the area of the squamosal suture about halfway to the temporal lines. The region of pterion is difficult to define as the temporal bone intrudes between the parietal and the sphenoid as a ca. 10mm wide, diamond-shaped flange of bone. The lateral surface of the temporal curves gently medially toward the sphenosquamosal suture. It is interrupted by a weak ridge of bone that begins at the temporal line on the parietal, follows the coronal suture inferiorly, and continues beyond the squamosal suture across the flange of bone intruding between the parietal and the sphenoid. As can be seen in a digital reconstruction of the cranium, the greater wing of the sphenoid faces predominantly laterally with a slight anterior tilt until it reaches the relatively well-developed infratemporal crest; at this point, the sphenoid angles slightly to take a more inclined course anteromedial to the preglenoid plane. What remains of the supramastoid region shows a weak lateral flaring relative to the temporal squama, the lateral extent of supramastoid indicating only minimal development of the supramastoid crest; the suprameatal region is broken away. Anterior to this, the zygomatic process sulcus appears narrow, grading smoothly into a relatively small temporal foramen. Damage to the mastoid region reveals limited pneumatization of the temporal squama.

Cranial Base

Very little of the cranial base is preserved, restricted mainly to the region of the mandibular fossa on the left side (see Figure 1B). The mandibular fossa is mostly encased in calcified clastic sediment, and is partially observable via visual inspection and via digital reconstruction. It appears relatively shallow, with an estimated depth of at least 6mm, though damage to the postglenoid process prevents more precise measurement. We can estimate the length (ca. 12mm) of the mandibular fossa by measuring from the approximate position of the postglenoid process to the most inferior projection of the articular eminence; this is best considered a minimum estimate (see Table 3). The breadth (ca. 23mm) of the mandibular fossa can be more directly measured. The articular eminence is slightly concave mediolaterally, and more notably convex anteroposteriorly, resulting in a saddle-shaped appearance. The mediolateral

breadth of the articular eminence is ca. 23mm, while the anteroposterior length is approximately 12mm. The mandibular fossa is set almost entirely medial to the parasagittal plane of the lateral wall of the cranium. The medial extent of the articular eminence is angled slightly posteromedially relative to the coronal plane, and the partially obscured entoglenoid process is set posteroinferior to the lateral edge of the articular eminence and faces predominantly inferolaterally. Anterior to the articular eminence, a short but somewhat broad preglenoid plane angles smoothly anterosuperiorly at about 45° to the FH plane. There is a relatively marked infratemporal crest that clearly delineates the infratemporal plane from the preglenoid plane. The horizontal distance between the temporomandibular joint and the distal extent of the M² is short, though eruption of the M³ would likely have influenced this length. The zygomatic arch is relatively gracile, showing a slight lateral convexity along its entire length.

Face

For descriptive purposes, Rak (1983: 9) defines the face as, “the whole section of the skull above the alveolar plane of the upper jaw and in front of the coronal plane that passes through the maximum postorbital constriction.” Rak (1983) also used the term “facial mask” to indicate the part of the face that is visible from the frontal aspect. We follow these definitions here in our description of the face of *Au. sediba* (see Figure 1; Figure 6).

The gently convex frontal squama grades smoothly into a gently concave supratoral sulcus, resulting in the appearance of a slightly elevated, but strongly receding, forehead. The supratoral sulcus is approximately 2.0mm deep as measured by taking a tangent perpendicular to a line drawn from the highest midline point on the frontal squama to the highest midline point on the glabellar prominence. There is a slight degree of frontal bossing. There is no indication of a frontal trigone. Owing to the rounding of the frontal squama in superior view, the supratoral sulcus widens laterally, thus the torus projects anteriorly about 11mm from the depth of the supratoral sulcus at the orbital midline, and widens to about 13mm near the lateral edges. Given the development of the glabellar prominence (see below), the landmark glabella projects some 21mm from the depth of the supratoral sulcus. The supratoral sulcus and the supraorbital torus are populated by relatively porous bone, both superiorly, anteriorly, and laterally, with the porosity continuing onto the frontal processes of the zygomatic bones. Compared to the breadth of the supraorbital torus (i.e., superior facial breadth), relative postorbital constriction is minimal. The face is haftered relatively low on the cranium, with a supraorbital height index value of 56mm.

Considered as a unit, the supraorbital torus is moderately developed and weakly arched overall. The robust glabellar region forms as a prominent block that is moderately convex both superoinferiorly and mediolaterally. In facial view there is a slight midline depression in the glabellar region relative to the supraorbital tori, while this same glabellar region projects considerably when viewed from su-

perior. Near the medial corner of the orbit, the left superior orbital margin displays two shallow supraorbital notches that are separated by a small, bony process, while on the right side a single notch is only weakly palpable. Bilaterally both of these notches are bounded by small bony elevations that correspond to the supraorbital process of Weidenreich (1943). Bilaterally, the supraorbital torus rapidly retreats away from the glabellar prominence in both frontal and superior views, thus contributing only minimally to its development. At its medial extent near the supraorbital notch, the supraorbital torus is 10mm in vertical thickness, gradually tapering to approximately 7.5mm at the orbital midline, before expanding to 8.5mm at the lateral-most corner. The supraorbital torus is weakly arched above the orbits, with the highest point near the orbital midline, and the lowest point at the lateral margins. Traversing laterally, the supraorbital torus angles sharply inferiorly to form the lateral orbital margin; thus, the division between the functional components of the torus occurs farther laterally than most australopiths, near the lateral extent of the torus (see Tobias 1991).

The orbits are relatively square-shaped with rounded corners. The inner aspect of the superior orbital surface slopes evenly inferoposteriorly (not superoposteriorly) away from the superior orbital margin, an occurrence sometimes seen in sub-adult human crania. The lateral half of the infraorbital margin presents as a bluntly rounded, non-projecting keel, transitioning to a somewhat more sharp-edged medial half of the infraorbital margin at the zygomaticomaxillary suture. A relatively well-developed, ca. 4mm diameter lacrimal fossa is visible in the left orbit (the right is obscured by matrix), extending superiorly to almost mid-orbital height. The anterolaterally oriented fossa is bordered by rounded anterior and sharp-edged posterior lacrimal crests, the posterior being slightly laterally displaced as a result of breakage. The frontal processes of the maxillae are gently concave, with a slightly bulbous eminence on the anterior inferomedial orbital corner on the right; the corresponding position on the left side is damaged, though a similar bulbous eminence does not appear indicated. The superior orbital fissures are visible via synchrotron scan, and appear as elongated, comma-shaped channels at the back of the orbit.

The nasal bones are widened superiorly, become narrowest about one-third of the way down, and flare to their widest extent at their inferior margin, taking on an hour-glass-shape. Each of the nasals bears two large and several smaller foramina. At their superior margin, while the nasal bones project superiorly above the frontomaxillary suture, they are not set on a different plane from the suture. Instead, the frontonasal sutures are continuous with the frontomaxillary sutures in a gently superiorly convex arc, with a small denticulation of the frontonasal suture extending superiorly at the midline. The superoinferiorly concave internasal suture forms as a pinched, elevated ridge along its entire extent, this ridge becoming slightly less prominent inferiorly. The inferior extent of the bones marks the anterior-most eversion of the nasals, projecting anteriorly be-



Figure 6. Close up view of the face of *Au. sediba*, U.W. 88-50 (scale bar=50mm).

yond the level of the infraorbital region and the zygomatics. As a result, the sharpened inferior nasal margins are set on an elevated plane relative to the frontal processes of the maxillae. The frontal processes of the maxillae, in turn, face predominantly anteriorly with a slight lateral tilt, and are set on roughly the same plane as the infraorbital region inferolateral to them. Faint traces of a premaxillary suture are evident, especially superiorly, with short, finger-like projections of the premaxilla extending from the inferolateral borders of the nasal bones as slightly everted crests at the superolateral margins of the nasal aperture. The sharpened superolateral edges of the nasal aperture transition to bluntly rounded inferolateral margins at about mid-aperture height.

The frontal process of the zygomatic faces anterolaterally, contributing a gently concavely curved lateral orbital margin. On its posterior face, the frontal process of the zygomatic is broad and flat, continuing as such onto the posterior aspect of the zygomatic process of the frontal. The ca. 15mm long marginal process marking the anterior extent of the origin of the *m. temporalis* occupies the superior half of the posterior aspect of the frontal process of the zygomatic, forming a distinct angle with the root of the frontal process before the latter joins with the main body of the zygomatic. The root of the frontal process of the zygomatic is expanded medially as it forms the smoothly rounded inferolateral orbital margin, while the lateral edge of the root of the process is not expanded, instead being sharply angled (ca. 45°) relative to the temporal process of the zygomatic at jugale. Near the center of the body of the zygomatic is a small zygomaticofacial foramen on the left, while on the right the corresponding foramen is positioned more superiorly. The superior margin of the root of the process of the zygomatic is positioned relatively high, reaching approximately the level of the inferior orbital margin. The root of the zygomatic process of the maxilla is relatively robust (anteroposterior thickness 13mm; minimum vertical depth 22mm), and is positioned above the level of P⁴/M¹. The zygomatic process of the maxilla joins with the maxillary process of the zygomatic and immediately angles almost 90° toward posterior at the weakly developed zygomatic prominence, the latter which shows only limited anterolateral expansion that is congruent inferiorly with the powerful development of the origin of *M. masseter*. As a result, flaring of the zygomatic arches is minimal, and the zygomatic has distinct frontally and laterally oriented faces. The temporal process of the zygomatic rapidly narrows to produce a relatively gracile zygomatic arch. The inferior surface of the temporal process of the zygomatic is particularly rugose for the attachment of *M. masseter*, evincing two distinct muscular scars anteriorly which coalesce into a single ridge posteriorly along the entire length of the temporal process. The zygomaticoalveolar crest is well-developed, coursing superolaterally in a straight, steeply inclined slope to the zygomaticomaxillary suture, resulting in a relatively high masseter origin. Neither a malar notch nor a malar tubercle are present, and the orientation of the zygomaticoalveolar crest relative to the inferior orbital

margin produces a distinctly laterally tapered appearance of the infraorbital region. Despite this development of the zygomaticoalveolar crest, as mentioned above, the zygomatics are only weakly flared laterally. Combined with the sharply inferiorly angled lateral corners of the supraorbital torus, this results in a squared superior facial profile that transitions smoothly into an inferiorly tapered lower facial profile. Viewed from lateral, the zygomatic bone is positioned well posterior to the anterior-most projection of the nasal bones, while the position of the masseter origin is also well posterior to that of sellion.

The bone surface of the maxilla retreats gently away from the superior nasal aperture, resulting in an everted margin of the superolateral portion of the nasal aperture relative to the infraorbital region that is emphasized by the eversion of the premaxillary components. Combined with the sharpened and slightly everted inferomedial orbital margin, this produces a slight concavity of the frontal process of the maxilla between the inferior nasals/superior nasal aperture margin and the inferomedial orbital margin. This results in a topographical arrangement that broadly corresponds to what Rak (1983) termed a nasomaxillary basin in *P. boisei*, though these should not be considered functionally analogous structures. Inferior to this, a broad but weakly defined structure that corresponds to what Rak (1983) referred to as a transverse buttress is evident. Forming as a broad, low, gently rounded eminence just above the midway point of the nasal aperture margin, it traverses laterally for a short distance immediately above the infraorbital foramen before approaching the zygomaticomaxillary suture; a shallow channel separates the transverse buttress from the zygomaticomaxillary suture. Below the transverse buttress, the infraorbital region slopes inferolaterally to the zygomaticoalveolar crest, thus the surfaces above and below the transverse buttress are set on slightly different planes. The infraorbital surface below the transverse buttress is angled at about 90° to the alveolar plane, appearing coplanar with the orbital plane. The canine jugum is relatively prominent, though it does not extend beyond the tip of the root of the canine. It is positioned well lateral to the nasal aperture, being clearly separated from the aperture margin. The canine jugum is also separated from the nasoalveolar clivus by a shallow interalveolar groove between it and the lateral incisor jugum. As a result, there is no indication of an anterior pillar. A well-defined canine fossa is delimited anteriorly by a prominent ridge that takes its origin at the posterolateral edge of the relatively pronounced canine jugum, though the superior extent of this ridge is not part of the jugum itself as it does not appear to house the root of the canine. Instead, the superior extent of this ridge curves slightly posteriorly toward the infraorbital foramen, combining with a very slight bony elevation inferior to the infraorbital foramen to form the ill-defined superior border of the canine fossa. Posteriorly, the canine fossa is delineated by a ridge traversing from the P⁴ jugum to merge superiorly with the root of the zygomatic process of the maxilla. Inferiorly, the fossa is delimited by a slight swelling of bone at the alveolar margin.

Lateral to the transverse buttress is an elevated ridge that coincides with the zygomaticomaxillary suture. In specimens of *P. robustus*, Rak (1983) has termed the difference in facial topography at this point the zygomaticomaxillary step, though *Au. sediba* differs in that the medial infraorbital region is not conspicuously sunken relative to the suture, therefore there is no indication of the depressed maxillary trigon that is so characteristic of *P. robustus*. We suggest that the term *zygomaticomaxillary ridge* is more appropriate for the structure seen in *Au. sediba*, as it is clearly elevated relative to the adjacent inferomedial and superolateral components of the infraorbital region. Near its inferolateral extent, a slight, oval-shaped depression crosses the zygomaticomaxillary ridge in the position of the zygomaticomaxillary fossa of *P. robustus* (Clarke 1977; Rak 1983). However, this structure is not a continuation of the sunken maxillary trigon of the latter taxon as defined by Rak (1983), and thus does not represent a true zygomaticomaxillary fossa. Instead, this depression corresponds more closely to the zygomaticomaxillary fossa of Oschinsky (1962; see also Rak 1983). The infraorbital foramina are positioned relatively high, just under mid-height of the nasal aperture, ca. 15mm below the inferior orbital margin; two foramina are evident on the right side. The foramina all open antero-inferiorly, immediately below the transverse buttress.

The nasoalveolar clivus contour is almost straight in the coronal plane, though a weak convexity is evident in that the alveoli of the incisors protrude slightly beyond the bi-canine line, resulting in a gently curved incisor arc. The root of the I² is positioned slightly lateral to the lateral border of the nasal aperture. Moderate incisor juga are evident, though they are eroded inferiorly. Low, rounded, but clearly defined lateral crests are evident coursing diagonally from the inferolateral nasal aperture margins to contact the lateral incisor juga. Projection of the subnasal region is weak relative to the facial plane. The bluntly rounded inferolateral border of the nasal aperture margin transitions smoothly into the inferior margin of the nasal aperture, the latter of which is marked by a stepped nasal sill grading into the nasal aperture. This nasal sill is weakly defined by a low, rounded, combined turbinal/spinal crest. The small but well-defined anterior nasal tubercle is relatively low and rounded, and is positioned very slightly anterior to the nasal aperture margins. A moderately prominent midline ridge at the intermaxillary suture begins at the base of the anterior nasal tubercle, extending toward the interalveolar septum between the central incisors, though its terminus is partially obscured by abrasion.

Although anterior pillars are lacking in *Au. sediba*, the well-developed canine juga extend forward almost to the plane of the nasoalveolar clivus, the entire clivus being separated from the more lateral portions of the face by the well-developed canine fossae. These combined features are similar to what Rak (1983) referred to as a nasoalveolar triangular frame, the term which Berger et al (2010: Table 1) applied to *Au. sediba* and other hominins in order to distinguish them from the 'guttered' pattern seen in the 'robust' australopiths. However, Rak (1983) applied the term exclu-

sively to the arrangement of the nasoalveolar region seen in *Au. africanus*, in particular relating to the anterior pillars which are absent in MH1, thus we note that our usage does not correspond precisely to Rak's definition. The transition from the mid-facial plane to the plane of the clivus is relatively smooth and straight, thus there is no bi-partite division of the lateral anterior facial contour. The face is mesognathic, showing moderate projection.

Palate

The palate remains encased in matrix, so we are currently limited mainly to morphology visible via synchrotron scans (see Figure 1B). The palate is relatively short and narrow, though the length is undoubtedly influenced by the fact the M³s have not yet erupted. As noted above, the incisor alveoli are arranged in a gently convex arc. The incisors are relatively vertically oriented, with minimal procumbency evident. There is no indication of an I²/C diastema. The size and orientation of the canine jugum, combined with the appearance of the associated canine U.W. 88-30, indicate that the canines were not notably projecting. The incisive foramen appears as a relatively small, circular opening positioned at approximately the level of the P³/P⁴. The palate deepens moderately from the incisor alveoli to the incisive foramen, reaching a depth of around 8mm at the level of the premolars. The palate deepens only slightly more to perhaps 9mm at the level of the M². The internal alveolar margins are steeply inclined, angling sharply into the roof of the palate. The post-canine alveolar processes are roughly parallel, and the teeth are arranged in a gently convex arc, resulting in a weakly parabolic dental arcade. Posteromedial to the maxillary tubers, the greater and lesser pterygoid wings are visible bilaterally, both appearing relatively complete.

MANDIBLE OF MALAPA HOMININ 1 (MH1)

Lateral Corpus

The total length of the right hemi-mandible from the posterior border of the ascending ramus to the point of breakage at the alveolus of RI₂, parallel to the level of the alveolar margin, is ca. 100mm; the length from gonion to the position of the RI₂ alveolus along the basal margin is ca. 80mm. The alveolar and basal margins are effectively parallel from the M₁ to the C alveolus (see Figure 2). There is limited indication of resorption of the alveolar margin on the right, while the area is damaged on the left. There is a single, rounded mental foramen below the P₃/P₄ on the left, and two oval-shaped mental foramina are present below the P₃/P₄ on the right. The mental foramen on the left was probably at about mid-corpus height, while on the right, the larger, upper one sits at about mid-corpus height, with the lower, smaller one ca. 3mm beneath that. The foramina open principally laterally, with the one on the left showing a very slight posterior tilt, and the superior foramen on the right presenting a slightly more posterior tilt; the right superior foramen also exhibits a ca. 8mm channel that extends posteriorly and slightly superiorly from it, likely

conducting a vascular bundle. There is no indication of a lateral mandibular depression of Dart, since the majority of the lateral corpus is convex, except for a slight hollowing superior to the mental foramen and inferior to the position of the P_4 . The juga for the M_1 and the premolars slightly interrupt the lateral contour. The mandibular corpus is relatively gracile at the level of the M_1 , with a small cross-sectional area. The lateral prominence is relatively large, low, and rounded, occupying virtually the entire lateral face in the region of the molars. It reaches its greatest extension at the mesial edge of the M_2 , thereafter revealing a rapid decline in robusticity of the corpus to the level of the P_4/M_1 . It has a predominantly inferior and anterior orientation, notably disrupting the basal contour. The resulting inferiorly convex basal margin, with its pronounced inferior bulge below the M_1 , curves upward slightly beneath the M_3 at the preangular (=pregonial) incisure, traversing posteriorly in a gentle concave arc to a rugosely-defined gonial area. Anteriorly, three distinct structures emanate from the lateral prominence. Superiorly, there is a low, rounded, weakly developed ridge that is a continuation of the margin of the ramus, running anteriorly with a slight superior curve to terminate in the abraded area below the P_4 . This low ridge weakly delineates the extramolar sulcus from the lateral face of the corpus, and corresponds to what Dart (1954) referred to as the supreme lateral torus (see also Tobias, 1991: 322). Inferior to this, below the level of mid-corpus, is the low, rounded superior lateral torus. This torus traverses anteriorly from about the middle of the lateral prominence to the mental foramen, and then turns up to join with the canine jugum. The third structure is the low, rounded, well-developed and clearly defined marginal torus. This latter torus is horizontally extensive, though not notably rugose, taking its origin near the small, weakly defined posterior marginal tubercle at the greatest inferior extent of the lateral prominence on the basal margin, and reaching anteriorly along the basal margin to terminate at a well-developed, rugose anterior marginal tubercle below the P_4 . The marginal torus is clearly delineated from the superior lateral torus by a distinct, moderately deep, intertoral sulcus that shallows only slightly below the canine jugum. The intertoral sulcus continues onto the anterior face, where it curves upward to become continuous with the mandibular incisure. Immediately anterior to the anterior marginal tubercle, and separated from it by a shallow groove, is a well-developed rugosity that corresponds to what Klaatsch and Hauser (1910) termed the posterior mental tubercle, or what was named the submental tubercle by Gorjanovic-Kramberger (1909; see also Tobias, 1991: 325).

Anterior Corpus

The mandible is broken obliquely through the mandibular symphysis, with the posterior edge of the break approximating the symphyseal midline; refitting the left side mandibular fragments U.W. 88-2 and U.W. 88-245 and then aligning them with U.W. 88-8 allows us to examine most of the mandibular symphysis (see Figure 2). As a result, we can estimate the height of the anterior mandible as approx-

imately 34mm, and the anteroposterior depth as 18mm. The lateral profile of the mandibular symphysis appears straight and nearly vertical across its entire extent. Relatively prominent canine juga are apparent, and the anterior mandible fragment U.W. 88-2 preserves moderate incisor juga for LI_1 and LI_2 . Just below the alveolar margin of U.W. 88-2 is a relatively deep hollowing representing a moderate mandibular incisure; the lateral extent of a moderate mandibular incisure is also visible on U.W. 88-8. Considering the mandibular fragments together, the intertoral sulcus of the lateral surface continues onto the anterior face, turning up to approach the mandibular incisure, the latter which is continuous across the symphysis. The mental protuberance is damaged, but appears as a low, rounded, mound of bone. Lateral to the mental protuberance are low, rounded, moderately-developed lateral tubercles (the mental tubercles of Tobias, 1991). Together with the mental protuberance, these structures result in a distinct mental trigon. In turn, the moderate mandibular incisure combines with the mental trigon to weakly indicate a mentum osseum was present. Inferolateral to the lateral tubercles are the slightly rugose posterior mental tubercles.

Posterior Corpus

The lingual alveolar plane is weakly developed and steeply inclined, and is not shelf-like or hollowed (see Figure 2). A low, weakly developed and weakly projecting superior transverse torus is present, while there is no indication of an inferior transverse torus.

Medial Corpus

The alveolar margin is somewhat sharpened at the level of the P_3 and the mesial half of the P_4 , becoming more bluntly rounded to the distal end of the M_1 , then rapidly transitioning to a sharp edge at the mesial extent of the M_2 , and thereafter becoming a more bluntly rounded but still high and slightly sharpened pharyngeal crest (see Figure 2). The mylohyoid line is diffusely defined, coursing antero-inferiorly some 7.0mm below and parallel to the pharyngeal crest on the medial corpus from the mandibular foramen to the mesial extent of the M_2 on the right side. The alveolar prominence is well-developed and moderately deep from the position of P_3 to the position of the developing M_3 , becoming slightly more vertically extensive anteriorly, and with a notable medial projection posteriorly. A moderately large, deep, and elongate subalveolar fossa is present, with continuous anterior and posterior components; it is delineated from the pterygoid region by a low ridge of bone inferior to the developing M_3 .

Basal Corpus

The basal corpus is evenly thick and broadly rounded from the symphysis to the level of the M_2 , tapering gradually from this point to gonion along the preangular incisure (see Figure 2). A weakly concave submental notch is delimited by the combined anterior marginal and posterior mental tubercles at the terminus of the marginal torus. A moderately large, relatively projecting interdigestive spine

is indicated, marking the posterior midline of the symphyseal region. Lateral to this, the digastric fossa is a shallow, slightly rugose, crescent on the basal surface of the corpus.

Occlusal Corpus

The alveoli from the canine to the M_2 are arranged in a gently convex arc, and the anterior fragment U.W. 88-2 indicates that the incisors were arranged in a gentle arc (Figure 7). There is a slightly increasing size gradient from the lateral to anterior corpus. Refitting the mandibular fragments demonstrates that the corpora diverge posteriorly to a greater degree than the tooth rows, though damage inhibits our ability to accurately measure inter-tooth distances. However, comparison with inter-tooth distance of the cranium U.W. 88-50 indicates that the intact mandible must have been quite narrow, with only slightly diverging corpora. There is no indication of a diastema.

Lateral Ramus

The ascending ramus is tall (ca. 76mm along the longitudinal axis of the ramus, from the basal margin to the tip of the coronoid) and relatively broad (ca. 47mm at its greatest width at approximately the alveolar margin). The root of the ramus takes its origin near the mesial half of the M_2 , immediately below the level of the alveolar margin (see Figure 2). The posterior border is concave at the supra-angular (=supragonial) incisure, transitioning to a posteriorly directed convexity toward the gonial angle; the posterior border rises at approximately 75° to the horizontal plane of the corpus. The preangular (=pregonial) incisure is smoothly continuous with the lateral basal contour. The anterior ramal border is thin and sharp-edged at the ramal root, becoming thicker and more bluntly rounded superiorly as it approaches the coronoid; it flares medially as it courses superiorly toward the coronoid, resulting in a distinct, inward flared lip of bone constituting the superior half of the anterior border, and resulting in roughly parallel-oriented ramal borders. The coronoid process is rounded superiorly and relatively flat, with a posteriorly hooked appearance. The low, rounded endocoronoid buttress is positioned near the middle of the process, and does not reach to the tip. The mandibular notch is deep (14.5mm) and relatively narrow (19.0mm), and is relatively posteriorly positioned. The coronoid extends farther cranially than the condyle, and the distance from the tip of the coronoid to the top of the condyle is ca. 23mm. The lateral subcondyloid tubercle presents as a mere roughening of the bone immediately below the condyle. The ectocondyloid buttress is low, rounded, and well-developed, and courses anteroinferiorly to join with the well-developed, robust, clearly defined lateral eminence of the ramus. The extensive lateral eminence occupies much of the ramus, and traverses anteroinferiorly toward the lateral prominence of the corpus, being delineated from the latter structure by a broad, shallow furrow. A shallow, ca. 20mm diameter masseteric fossa is restricted mainly to the gonial region, being delineated superiorly by the lateral eminence, and anteriorly by the posterior extent of the lateral prominence. The gonial angle presents rugose

ectoangular tuberosities, with a slight degree of eversion evident along its inferior margin.

Medial Ramus

The relatively sharp, high, and robust pharyngeal crest curves superolaterally around the posterior aspect of the M_2 and the partially visible crypt for the M_3 , becoming more bluntly rounded and less elevated as it transitions to the low, rounded, triangular torus (see Figure 2). Anterior to the endocoronoid crest, and superior to the developing M_3 , the mandibular recess is broad and deep, measuring 20mm at its greatest width. Just superior to the mandibular foramen, the triangular torus gives rise to a low, rounded endocoronoid buttress, which traverses superiorly and grades out of existence before reaching the tip of the coronoid. There is no indication of an endocondyloid buttress taking origin from the triangular torus, thus the latter structure exists more in name than in form in this specimen. As a consequence, the moderately large triangular planum is not clearly delineated posteroinferiorly, instead continuing inferiorly between the endocoronoid buttress and the condylar neck to terminate near the mandibular foramen. The mandibular foramen is moderate-sized (4.0mm AP, 5.8mm superoinferiorly) with a distinct bony lip preserved on its anterior margin taking the form of a slight lingula. It is flanked superiorly and posteriorly by two small accessory foramina. A shallow but clearly defined mylohyoid groove traverses anteroinferiorly from the mandibular foramen for about 24.0mm before fading out of existence; there is no bridging of the groove. The pterygoid fossa is obliquely anteroposteriorly narrowed and superoinferiorly elongated, being demarcated anteriorly by a slight bony elevation that delimits it from the posterior subalveolar fossa. The area of insertion of the medial pterygoid indicates a strongly developed muscle, as the posterior border of the pterygoid region along the posterior border of the ramus is marked by a series of three clearly defined and rugose inferior pterygoid tubercles. Immediately beneath the condyle is a well-developed, rugose superior pterygoid tubercle. When viewed superiorly, the condyle is relatively straight, mediolaterally elongated (23.0mm), and anteroposteriorly compressed (8.4mm AP). Its axis is posteromedially oriented, close to the coronal plane, with a distinct inferior drop-off along its medial third. The condylar neck is relatively thick and short, with the anterior face presenting a hollowed lateral pterygoid fossa, and the medial face presenting a well-developed superior pterygoid tubercle.

MANDIBLE OF MALAPA HOMININ 2 (MH2)

Lateral Corpus

The reconstructed length of the right hemi-mandible from the posterior border of the ascending ramus to the point of breakage at the alveolus of the RI_1 , parallel to the alveolar margin, is approximately 106mm. The alveolar and basal margins are essentially parallel from the level of M_2 anterior to the incisors (see Figure 5). There is no indication of resorption along the molar row, while the region below the

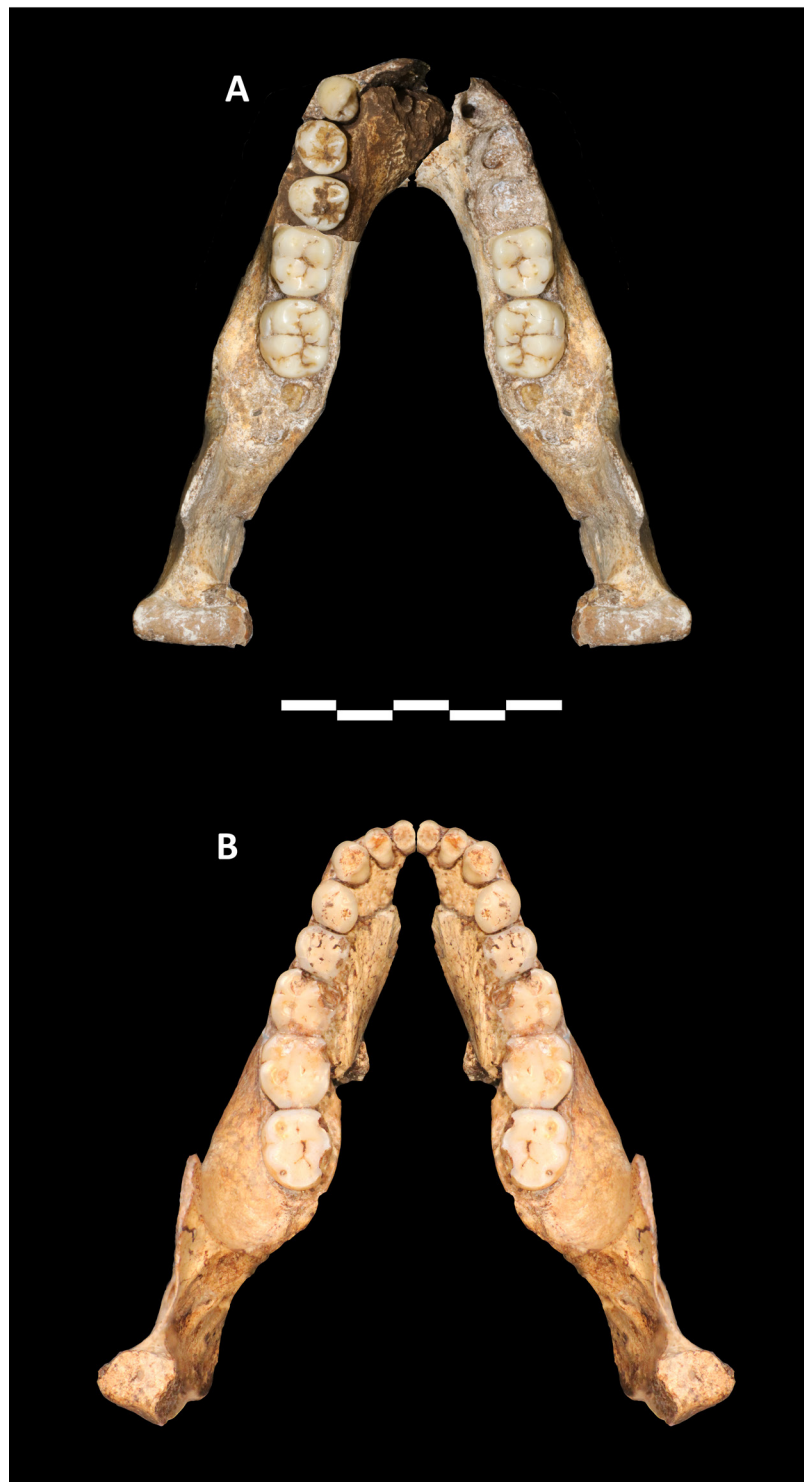


Figure 7. Digitally reconstructed mandibles of A) MH1 and B) MH2. The right hemi-mandible UW88-8 of MH1 was mirror-imaged, then the new mandibular fragment U.W. 88-245 with refit U.W. 88-2, U.W. 88-244, and U.W. 88-246 was overlaid on top of the mirror image to produce a composite virtual reconstruction of the mandible. Since the mandibular symphysis was preserved, the inner contour of the mandible guided the positioning of the tooth rows; the inter- M_2 diameter of the reconstruction is 29mm, which corresponds to the inter- M_2 diameter of the cranium U.W. 88-50. The right hemi-mandible of MH2 was mirror-imaged to produce a virtual reconstruction of the mandible. Since the mandibular symphysis is missing, this reconstruction is more subjective, though we were constrained somewhat by the orientation of the tooth rows and the orientations of the mandibular condyles. These reconstructions should be considered hypotheses until such time as the remainder of the MH1 mandible is extracted from its matrix, and until the cranium of MH2 is recovered (scale bar=50mm).

premolars is damaged; there appears to be some resorption below the P³, and definitely at the canine, thus the occlusal and alveolar margins did diverge, and probably along a slight step-down to the alveolus of the canine. A single, oval-shaped mental foramen is present at about mid-corpus height beneath the P₄, opening laterally with a slight posterosuperior tilt. The lateral mandibular depression of Dart is broad but shallow, and incorporates a slightly deeper area above the mental foramen. The juga for the premolars and molars are generally quite weak, though damage precludes more detailed inspection. The small cross-sectional area at the level of the M₁ indicates an especially gracile corpus. The low, rounded, well-developed lateral prominence is clearly defined, and reaches its greatest lateral extent above mid-corpus height at the mesial edge of M₃, thereafter rapidly tapering to the mesial extent of M₂. The lateral prominence occupies much of the lateral face below the molars, and has a predominantly anteroinferior orientation, though its anteroinferior extent is obscured by damage. The basal margin of the corpus is inferiorly convex, though the extrusion of the lateral prominence onto the basal contour appears less marked than in MH1, grading more gently into the concave preangular (=pregonial) incisure below the M₃. As in MH1, three structures emanate from the lateral prominence. Superiorly, the supreme lateral torus (of Dart 1954) is low, rounded, and moderately well defined, traversing from ramal margin to the distal root of the M₂, and delineating the extramolar sulcus from the lateral face of the corpus. The superior lateral torus is broad and bluntly rounded, traversing from near the middle of the lateral prominence, but below the level of mid-corpus, to anterior to the mental foramen where it turns up to join the canine jugum. Inferiorly, the marginal torus is low, rounded, and weakly developed, evincing a slight rugosity on the basal margin. Anteriorly there are a series of slightly rugose muscular markings corresponding to platysmic striae, and at the anterior extent of the marginal torus, beneath the level of the P₄, a weakly developed anterior marginal tubercle is evident. The marginal torus is weakly delineated from the lateral superior torus by a diffusely defined and shallow intertoral sulcus, that latter which continues onto the anterior aspect of the mandible until it reaches a low, rounded lateral tubercle. The extramolar sulcus is shallow and narrow (ca. 8.2mm). The apex of the canine tooth is worn to the same level as the incisors and the premolars, thus this tooth does not project to any extent.

Anterior Corpus

Much of the anterior corpus is missing, thus we cannot ascertain the verticality of the mandibular symphysis (see Figure 5). The intertoral sulcus of the lateral corpus traverses anteriorly to terminate on a weak lateral tubercle. The area of the mental protuberance is missing, thus a mental trigon cannot be confirmed (nor dismissed). A relatively prominent canine jugum is present, beside slight incisural juga. A moderately deep and well defined mandibular incisure is evident, and appears to have formed an incurvation on the anterior surface.

Posterior Corpus

Although badly damaged, examination of the cross-sectional profile of the corpus posterior to the RI₂ indicates a weakly developed and steeply inclined lingual alveolar plane was likely present, similar to that of MH1 (see Figure 5). There is a slight indication of a low, weakly developed and weakly projecting superior transverse torus, though it is truncated by damage.

Medial Corpus

The alveolar margin is rounded anteriorly, transitioning to a relatively sharpened border at the mesial extent of the M₃, before becoming the well-defined, sharp-edged, and quite prominent pharyngeal crest (see Figure 5). The alveolar prominence is moderately large, becoming slightly more vertically extensive anteriorly. It is moderately deep from the position of P₄ to the position of the M₃, with an increasing medial projection posteriorly. A slightly shallow, ill-defined, continuous subalveolar fossa is present from the position of the P₄ to the position of the M₃, where it is delineated from the pterygoid fossa by a low ridge of bone. The mylohyoid line is diffusely defined and slightly rugose. On the left side, a relatively bulbous, rounded protuberance appears in the form of a strong expression of a mandibular torus; the right side is slightly damaged in this area, though the indication of a similar mandibular torus is much less pronounced.

Basal Corpus

Although broken bilaterally, it is evident that the basal corpus is evenly thick and rounded anteriorly, tapering gradually from the position of the M₃ to the gonial angle (see Figure 5).

Occlusal Corpus

The alveoli of the incisors and canine are arranged in a slightly convex arc, while the alveoli from the canine to the M₃ are also arranged in a gently convex arc (see Figure 7). Mirror imaging of the mandible indicates that the corpora diverge posteriorly to a greater degree than the occlusal rows, an effect that is emphasized by the lateral flaring of the root of the ramus and the lateral prominence. The dental arcade appears tightly curved anteriorly, becoming more divergent posteriorly. There is a slight mesial tilt of the occlusal plane, indicating a weak helicoidal patterning. The corpus is especially small (de Ruiter et al. 2013b), with a slightly increasing gradient of size from the lateral to the anterior corpus. There is no indication of a diastema.

Lateral Ramus

The ascending ramus is relatively tall (ca. 70mm along the longitudinal axis of the ramus, from the basal margin below M₃ to the tip of the broken coronoid) and relatively broad (ca. 43mm at its greatest width at approximately the alveolar margin). The root of the ramus takes its origin at about the mesial extent of the M₃, at approximately the level of the alveolar margin (see Figure 5). The posterior border is concave at the supra-angular (=supragonial) incisure, ris-

ing at approximately 75° to the horizontal plane of the corpus. The anterior border displays a broad concavity along its length, with the narrowest point of the ramus (39mm) at about mid-ramal height. As a result, the ramal borders diverge both superiorly and inferiorly. The anterior border of the ramus is moderately thick and rounded along its entire length. The flat, broad coronoid process is relatively large, though its cranial extent is difficult to gauge as a result of damage. As a result, the size of the mandibular notch must be estimated, appearing relatively deep and broad, in particular compared to the relatively high condyle, and is distinctly posteriorly oriented. We judge that the coronoid would have extended farther cranially than the condyle, and the distance from the tip of the coronoid to the condyle was at least 25mm. Inferior to the condyle there is a small, circular area of damage in the position of the lateral subcondyloid tubercle, the latter of which appears as little more than a slight roughening of bone. The ectocondyloid buttress is a low, rounded, well-developed ridge that grades into the large, prominent, well-developed lateral eminence of the ramus, though the lateral eminence in MH2 is less extensive than the lateral eminence in MH1. There is no indication of an ectocoronoid buttress. The moderately deep masseteric fossa is relatively large, occupying much of the gonial region, delineated by the lateral prominence of the corpus anteriorly and the lateral eminence of the ramus superiorly. A large wedge of the gonial angle has been broken and slightly laterally displaced, resulting in an exaggerated eversion of the gonial angle. The broken gonial angle presents rugose ectoangular tuberosities.

Medial Ramus

The orange, sharp, robust pharyngeal crest curves superolaterally around the distal aspect of the M_3 (see Figure 5). It remains high, sharp, and well-developed until reaching the robust and well-developed triangular torus. Immediately posterior to the M_3 , the pharyngeal crest joins with a weakly developed buccinator crest to form a small but distinct, triangular shaped postmolar trigone. Anterolateral to the triangular torus, the mandibular recess is broad and deep, measuring ca. 15mm at its greatest width, similar to the broad mandibular recess of the sub-adult MH1, despite the absence of an erupted M_3 in the latter specimen. Superior to the level of the mandibular foramen a low but sharply defined endocoronoid buttress traverses superiorly from the triangular torus toward the tip of the coronoid process, becoming lower and less sharply defined on the way. A moderately developed, rounded, but clearly defined endocondyloid buttress originates at the triangular torus and approaches the condyle, though it fines out of existence before making contact. As a result, the triangular planum is only partially interrupted in its inferior extent between the triangular torus and the condylar neck; unlike MH1 it is delineated from the mandibular foramen by the partially complete endocondyloid buttress. Superior to the endocondyloid buttress, residing within the triangular planum, is a secondary buttress paralleling the endocondyloid buttress, reaching almost to the margin of the mandibular notch.

The mandibular foramen is moderate sized and elongated (4.0mm anteroposteriorly, 9.5mm superoinferiorly), being sharply defined superiorly by the partial endocondyloid buttress, and inferiorly by a slight, superoposteriorly oriented crest; there is a faint indication of a lingula on the right, and a slightly more pronounced lingula on the left. A shallow but clearly defined mylohyoid groove courses anteroinferiorly from just posterior of the mandibular foramen for about 19.0mm before terminating rapidly; there is no indication of bridging of the groove. The pterygoid fossa is obliquely oriented, and appears to be anteroposteriorly narrowed and superoinferiorly elongated, being anteriorly delineated from the posterior subalveolar fossa by a slight bony elevation below M_3 . The medial pterygoid insertion is especially well marked by a series of connected, rugose inferior pterygoid tubercles; this rugosity extends superiorly in a slightly concave arc to almost as high as the neck of the condyle. The condyle is missing its approximately medial one-third, though what is preserved is similar to the intact condyle of MH1, the main difference residing in the greater robusticity of the condylar neck of the adult specimen MH2. Viewed superiorly, what remains of the condyle is straight and anteroposteriorly expanded (11.5mm). The axis of the condyle is posteromedially oriented and close to the coronal plane. The condylar neck is relatively short and robust, with the preserved anterior face displaying a sharp attachment for the lateral pterygoid muscle.

TEETH OF MALAPA HOMININ 1 (MH1)

RI¹

This tooth has a complete crown and slight damage to the tip of the root (see Figure 3). Two cracks run the length of the crown from the CEJ to the occlusal margin, closely following the mesial marginal grooves. The crown and root both appear to have been chemically etched, perhaps as a result of contact with roots of plants growing around the tooth. Incisal wear is slight, with a broad strip of dentine exposed along the lingually beveled, distally expanded, wear facet (category 3 of Molnar [1971]). The mesial crown corner is relatively sharp, while the distal crown corner is more rounded. The mesial ICF is flat, and there is no indication of a distal ICF. The slightly curved labial face has a weak mesial marginal ridge that is separated from a secondary ridge on the mesial half of the face by a shallow depression; there is no indication of a distal marginal ridge. The cervical line is slightly convex, and the mesial and distal crown sides taper smoothly from the occlusal margin. The slightly concave lingual face shows a broad and uninflated cervical eminence that is slightly mesially disposed and lacking a tubercle; no shoveling is evident. The median ridge is weakly developed and flat, and the weak mesial marginal ridge joins the cervical prominence closer to the occlusal surface than the moderately developed distal marginal ridge; the distal lingual groove is shallow but more clearly defined than the weak mesial lingual groove. The height of the crown is 11.0mm. The root is ovoid in cross section, with a very slight mesial tilt, and a slight groove

on the distal aspect. The root measures 6.6mm mesiodistally and 6.4mm buccolingually at the CEJ, and is 10.7mm in length.

LI²

This is a near complete tooth missing the mesial corner of the labial surface; a small fragment of the root has been broken away at the CEJ (see Figure 3). The lingual face of the tooth is still obscured by calcified clastic sediment, but visible via CT scans. What is visible of the incisal surface is smoothly rounded, though no dentine is exposed (category 2 of Molnar [1971]). The distal crown corner appears well rounded. The labial face is mostly obscured by damage, but there appears to be a weak mesial marginal ridge bordered by a weak groove. The lingual face is flat mesiodistally, and slightly convex cervico-occlusally. The mesial marginal ridge and probably the distal marginal ridge are moderately developed, and both merge on the cervical prominence to produce a moderately concave lingual face. The mesial and distal crown edges both appear strongly tapered from the occlusal margin to the CEJ. Although partially obscured by damage, the lingual cervical prominence appears weakly expressed to absent, and the cervical enamel line is weakly curved.

RC

This is a complete, unworn crown with a damaged root (see Figure 3). There are no indications of an ICF, as the tooth was likely in the process of eruption at the time of death. Labially the crown presents an irregular pentagonal outline. The apex is positioned slightly mesial to the midcrown transverse axis. The mesial apical edge is slightly longer, and with a slightly steeper slope, than the distal apical edge, resulting in a slight asymmetry of the crown. The mesial crown corner is a moderate swelling at about midcrown height, while the slightly more pronounced distal crown corner is gently rounded and situated slightly closer to the apex. There is no mesial or distal cuspule. The labial surface is weakly convex cervico-occlusally and moderately convex mesiodistally. Shallow grooves demarcate weak mesial marginal ridge and distal marginal ridge. The labial cervical eminence is very weak, and the cervical margin is straight. Lingually, the mesially disposed cervical prominence is weakly developed, and there is a very slight indication of a lingual tubercle. A sharp, narrow crest is evident near the cervical prominence on the otherwise broad, flat, and weakly developed median ridge, the latter which becomes flatter while traversing almost to the apex; parallel to this is a second crest that begins at the apex but does not reach all the way to the cervical prominence. The mesial marginal ridge and distal marginal ridge are well delineated but not strongly developed, blending gently onto the narrow, uninflated lingual cervical prominence. The mesial and distal marginal grooves are present, with the mesial groove broader and deeper than the distal. Perikymata are visible around the circumference of the tooth. The crown is 11.9mm in height. What remains of the root extends almost 13.0mm from the buccal cervical margin,

measuring approximately 6.5mm mesiodistally and 9.2mm buccolingually at the CEJ; it has a lingually tapered, ovoid cross section with a slight distal tilt. Both the mesial and distal root faces present broad, shallow furrows.

L+RP³

These are complete teeth with the roots encased in alveolar bone (see Figure 3). Both teeth are pervaded by a single crack running through each paracone respectively. Wear is minimal, with slight, midline oriented wear facets restricted to the cuspal apices of both teeth (category 2 of Molnar [1971]). On the right, the mesial ICF is obliquely oriented, and restricted to the mesial face of the protocone; it is not deeply impressed. There is no ICF visible on the left, though it is possibly obscured by adherent matrix. The occlusal outline is irregular ovoid. The paracone is larger than the protocone, and is positioned at about the buccolingual mid-crown axis of the tooth. The smaller protocone is positioned mesial to the paracone. The mesial face of the paracone is occupied by three crests, a larger central one and two smaller, flanking ones. The buccal face of the protocone is occupied by two similar-sized, slightly distally deviated crests. The mesial marginal ridge is low, thick, and well-developed, and lacking additional cuspule formation. The anterior fovea is represented by a broad, shallow, buccally directed limb that is in direct contact with the broad, shallow longitudinal fissure. The posterior fovea is broad, and shallow, with both buccally and lingually directed limbs that continue about halfway up the cuspal apices. The distal marginal ridge is low, thick, and well-developed; the left tooth bears a small accessory cuspule. On the buccal face, the cervical prominence is weakly developed, and the cervical margin curves to form a peak of enamel onto the root face. A weak tuberculum premolare is present, being slightly better developed on the left side. Weakly developed mesiobuccal and distobuccal grooves are evident. The lingual cervical prominence is weakly developed, otherwise the lingual face is relatively featureless.

L+RP⁴

These are complete teeth with the roots encased in alveolar bone (see Figure 3). Although the tooth on the left side is fully erupted, the one on the right is impacted and only partially erupted. Occlusal wear is minimal on the left tooth, with only slight polishing of the cuspal apices, while the right tooth is unworn (category 2 of Molnar [1971]). The occlusal outline is irregular ovoid. The paracone is larger than the protocone, and is positioned slightly mesial to the buccolingual mid-crown axis of the tooth. The smaller protocone is positioned mesial to the paracone. The mesial face of the paracone presents three crests, a larger central one flanked by two smaller ones; on the left tooth, the mesial-most crest appears 'waisted', almost forming a distinct cuspule, and the distal-most crest is weakly bifurcated. The buccal face of the protocone is occupied by two crests, a larger mesial and a smaller distal one. The mesial marginal ridge is low, moderately thick, and well-developed, with no additional cuspule formation. The anterior fovea is rep-

resented by a moderately deep, narrow, buccally directed limb that is in direct contact with the broad, shallow, longitudinal fissure. On the right tooth, the posterior fovea is broad and shallow, with both buccally and lingually directed limbs that continue about halfway up the cuspal apices. On the left, the smaller fovea posterior is principally lingually directed, with a reduced buccal limb relative to the right. The distal marginal ridge is low, moderately thick, and well-developed, with a small accessory cuspid on the lingual half. On the buccal face, the cervical prominence is weakly developed, and the cervical margin curves to form a rounded peak of enamel onto the root face. A weak tuberculum premolare is present. Weakly developed mesiobuccal and distobuccal grooves are evident. The lingual cervical prominence is weakly developed, otherwise the lingual face is relatively featureless.

L+RM¹

These teeth have roots encased in alveolar bone (see Figure 3). The left tooth is complete, while the right tooth is missing a large fragment of enamel from the lingual one-third of the crown, including the entire lingual face. Occlusal wear is light, with cusps worn almost to a flat plane, though some relief remains, especially in the buccal cusps; a single pinpoint dentine exposure is visible in the protocone (category 2 or 3 of Molnar [1971]). The occlusal outline is nearly square-shaped, with a slight reduction of the distobuccal corner. All four of the principal cusps are present and well-developed. The protocone is the largest cusp, followed by the metacone, paracone, and hypocone in decreasing order of size. The mesial marginal ridge is thin, high, and well-developed. The short, narrow, shallow anterior fovea is represented by a buccally directed limb that is separated from the longitudinal fissure by a well-developed epicrista. The central fovea is deep and broad, with limbs of approximately equal length; the buccal branch is interrupted at the occlusal margin by a high, thick wall of enamel. The distal trigon crest is well-developed and relatively high. The shallow, narrow posterior fovea is represented by moderate buccally and lingually directed limbs that radiate from the fissure between the protocone and hypocone. The distal marginal ridge is low, thick, and well-developed. Buccally the cervical prominence is weak, and the cervical line projects to form a ca. 1mm peak of enamel between the roots. The buccal groove is a short, shallow fissure that gradually fades out of existence about two-thirds of the way to the CEJ. Lingually, the broad, well-developed lingual groove fades out of existence at about mid-crown height.

L+R M²

These are intact teeth with the roots encased in alveolar bone (see Figure 3). Occlusal wear is slight, with small wear facets visible on the mesial cusp tips (category 2 of Molnar [1971]). The occlusal outline is trapezoidal, with a moderate reduction of the distobuccal corner. All four principal cusps are present and well-developed. The protocone is the largest cusp, followed by the paracone, metacone, and hypocone in decreasing order of size. The midline face of each

of the protocone, paracone, and hypocone is dominated by a single principal crest on the left side, while on the right side, these crests tend to be very weakly bifurcated. The mesial marginal ridge is thin, high, and well-developed, and is slightly thicker on the left side. The short, narrow, shallow anterior fovea is represented by a buccally directed limb that is partially separated from the central fovea by a well-developed, but deeply and narrowly incised, epicrista. The central fovea is deep and broad, with limbs of approximately equal length; the buccal branch is interrupted at the occlusal margin by a high, thick wall of enamel. The distal trigon crest is well-developed and high, though it is deeply and narrowly incised, more so on the right. The shallow, narrow posterior fovea is represented by a short buccally directed, and longer lingually directed, limbs that radiate from the fissure between the protocone and hypocone. The distal marginal ridge is low, thick, and well-developed, and presents a moderately developed cuspule near the midline of the tooth. Buccally the cervical prominence is weak, and the cervical line projects to form a ca. 1mm peak of enamel between the roots. The buccal groove is a short, shallow fissure that gradually fades out of existence about halfway to the CEJ junction. The broad, well-developed lingual groove terminates abruptly at a small, slightly raised shelf of enamel. The mesiolingual face of the protocone displays a small but sharply defined Carabelli's trait on the right, while it is obscured on the left.

L+R M³

These teeth are still forming in the crypt. This description is based on synchrotron scans and on resultant 3D printouts of the teeth (see Figure 3). Crown formation is effectively complete with no indication of root development. The occlusal outline is trapezoidal, with a moderate reduction of the distobuccal corner. All four of the principal cusps are present and well-developed. The protocone is the largest cusp, followed by the paracone, hypocone, and metacone in decreasing order of size. The midline face of the protocone is marked by a shallow groove mesially, and a more deeply incised groove distally that almost delineates a plagioconule; these grooves are more deeply incised on the left than the right tooth, though the plagioconule on the right side is more distinctly segregated from the remainder of the cusp. The midline faces of the paracone and hypocone also display shallow grooves bilaterally. The mesial marginal ridge is thin, high, and well-developed. The anterior fovea is narrow and shallow, traversing as a short, buccally directed limb on the mesial face of the paracone. A weakly developed epicrista is broadly incised by the anterior fovea as it contacts the central fovea. The central fovea is broad and deep, with limbs of unequal length; the buccal branch is the shortest, being interrupted at the occlusal margin by a high, thick wall of enamel. The distal trigon crest is well-developed and high, though it is deeply and narrowly incised. The shallow, narrow posterior fovea is represented by short buccally directed, and longer lingually directed, limbs that radiate from the fissure between the protocone and hypocone; these two limbs are relatively straight on

the right, while on the left they are distinctly angled relative to one another. The distal marginal ridge on the right is almost entirely occupied by a well-developed distostyle, resulting in the angled appearance of the posterior fovea; the distal marginal ridge on the left is low, thick, and well-developed, revealing a slight distostyle and a slight postentoconule. On the buccal face the cervical prominence is weak, and the cervical line projects to form a distinct ca. 1mm peak of enamel between the roots. The buccal groove is a short, shallow fissure that rapidly fines out of existence. Lingually the broad, well-developed lingual groove traverses slightly mesially before terminating abruptly, though without a raised shelf of enamel as in the M². The mesiolingual face of the protocone displays a small, moderately well-defined Carabelli's trait.

L_c

This is a complete crown with approximately half of the root remaining (see Figure 4). This tooth was in the process of eruption at the time of death. There are no ICFs, and the only indication of wear is a slight polish on the apex of the tooth (category 2 of Molnar [1971]). In buccal view the crown presents an irregular pentagonal outline. The labial surface is weakly convex cervico-occlusally and moderately convex mesio-distally. The crown is markedly asymmetrical, with the apex of the tooth positioned distal to the mid-crown axis. The distal apical edge is longer and more steeply vertically angled than the nearly horizontal mesial apical edge; the rounded mesial crown corner is positioned almost at the occlusal margin, while the more gently curved distal crown corner occurs at about mid-crown height. Labially, a weak mesial marginal ridge is evident, alongside a slightly more developed distal marginal ridge; each borders a very shallow groove, the distal groove being more clearly defined than the mesial. There is a faint indication of a nascent distal stylid. On the lingual face the slightly mesially disposed cervical prominence is weakly developed, and there is no tubercle. The lingual mesial marginal ridge and distal marginal ridge are weakly developed, bounding shallow grooves, of which the distal groove is deeper than the mesial. The median ridge is low, broad and minimally pronounced, becoming slightly more prominent near the apex of the tooth. The preserved portion of the root is mesiodistally compressed, with no grooving apparent on the visible distal face. Measuring the alveolus of U.W. 88-245, the root was approximately 16mm long.

LP₃

This is a well preserved crown with the roots retained in the mandibular fragment U.W. 88-245 (see Figure 4). Occlusal wear is slight, with only minimal polishing of cusps and a slight facet on the distal side of the protoconid (category 2 of Molnar [1971]). A small, circular distal ICF is visible, while there is no indication of a mesial ICF. Occlusally the crown has an irregular ovoid outline. The protoconid is larger than the metaconid, and is more mesially positioned. The mesial marginal ridge is low, well-developed, and moderately thick, enclosing a moderately sized,

round-shaped anterior fovea with more expansive buccal and less expansive lingual moieties. The longitudinal fissure is broad and moderately deep. Both the protoconid and metaconid possess a single, large crest coursing from the tip. The low distal marginal ridge is well-developed and thick, with two larger buccal and two smaller lingual accessory cusplids; it is partially incised at the base of the protocone. The posterior fovea is large and elongated, with slightly longer buccal and shorter lingual limbs radiating from the longitudinal fissure. On the buccal face the cervical prominence is weakly developed, with a gently curved cervical line. There is a weak mesial buccal groove, and a more strongly developed distal buccal groove. The lingual cervical prominence is moderately developed with a mostly straight cervical line that dips slightly between the buccal and lingual roots. The root system comprises a larger buccal and a smaller lingual root that are fused together by a well-developed plate. The root neck measures 5.4mm mesiodistally and 8.7mm buccolingually at the cervix.

LP₄

This is a well preserved crown with the roots retained in the mandibular fragment U.W. 88-245 (see Figure 4). Occlusal wear is slight, with only minimal polishing of cusp tips evident (category 2 of Molnar [1971]). A small, circular mesial ICF is visible, while there is no indication of a distal ICF. Occlusally the crown has an irregular ovoid outline. The protoconid is larger than the metaconid, and the metaconid is more mesially positioned. The mesial marginal ridge is low, thin, and weakly developed, enclosing a small anterior fovea that is comprised only of a small, shallow, lingually directed limb. The longitudinal fissure is broad and moderately deep. Both the protoconid and metaconid possess a single, large central crest and two smaller flanking crests coursing from the tip. The low distal marginal ridge is well-developed and thick, with two larger buccal and one smaller lingual accessory cusplids; it is partially incised at the base of the protocone. The posterior fovea is capacious and elongated, with slightly larger lingual and shorter buccal limbs radiating from the longitudinal fissure. On the buccal face the cervical prominence is weakly developed, with a gently curved cervical line. There is a trace of a mesial buccal groove, and a well-developed distal buccal groove. A slight distolingual groove is evident, serving to delineate a large talonid basin. The lingual cervical prominence is weakly developed with a mostly straight cervical line that dips slightly between the buccal and lingual roots. The root neck measures 7.8mm MD and 9.0mm BL at the cervix.

RM₁

This is a complete crown with no cracks or damage (see Figure 4). Occlusal wear is light, and the cusps are worn to nearly a flat plane, though some relief is evident, particularly in the lingual cusps; a pinpoint dentine exposure is visible in the protoconid (category 2 or 3 of Molnar [1971]). The mesial ICF is large and centrally positioned. The occlusal outline of the tooth is ovo-rectangular. All five prin-

cipal cusps are present and well-developed. The metaconid is the largest cusp, followed by the protoconid, hypoconid, hypoconulid and entoconid in descending order of size; there is no C6. The apex of the protoconid is positioned slightly mesial to the apex of the metaconid. The mesial marginal ridge is well-developed and thick buccally, and rapidly thinning lingually. Occlusal attrition has reduced the anterior fovea to a small, lingually directed groove that is continuous distally with the broad, deep central fovea, though a narrowly incised distal trigonid crest is evident. The metaconid contacts the hypoconid, resulting in a slightly asymmetrical Y-pattern. The posterior fovea is represented by a small, lingually situated groove that is bounded mesially by a broad postentocristid between the entoconid and the hypoconulid. It is bounded posteriorly by a low, thick, well-developed distal marginal ridge. Buccally, the cervical prominence is weak, and the cervical line projects to form a ca. 1mm peak of enamel between the roots. The broad, shallow mesiobuccal groove terminates in a moderate sized pit that is enclosed by a moderately developed enamel wall; this wall curves around the buccal face of the protoconid, representing a well delineated protostylid (type 2 of Hlusko 2004). The distobuccal groove is narrow and shallow, ending abruptly just below the occlusal margin. The lingual face presents a narrow, shallow groove that fades out of existence just below the occlusal margin; though a shallow furrow continues to the cervical margin; immediately distal to this furrow is a parallel ridge of enamel on the lingual face of the entoconid. The lingual cervical prominence is weak, and the cervical line projects to form a ca. 1mm peak between the roots.

RM₂

This is a complete, well preserved crown with no damage (see Figure 4). Occlusal wear is slight, with wear facets evident on all cusps except for the entoconid; the wear facets on the mesial three cusps tend to be positioned towards the midline of the tooth, rather than at the cuspal apices, and all of the cusps remain relatively salient (category 2 of Molnar [1971]). The occlusal outline of the tooth is ovo-rectangular. All five principal cusps are present and well-developed. The metaconid is the largest cusp, followed in decreasing size order by the protoconid, hypoconid, hypoconulid and entoconid; as in the M₁, there is no C6. The apex of the protoconid is positioned slightly mesial to the apex of the metaconid. The mesial marginal ridge is well-developed and thick buccally, thinning toward the lingual face. The anterior fovea is a deep, narrow, lingually directed groove that is delineated from the deep, broad longitudinal fissure by a narrow, distal trigonid crest; a very shallow buccal branch of the anterior fovea traverses up the mesial protoconid face toward the apex, but rapidly fades out of existence. The metaconid bears two principal crests: a large, mesially positioned one, and a smaller, distally positioned crest with a short, shallow, distal groove demarcating a weak postmetaconulid. The metaconid contacts the hypoconid in a symmetrical Y-pattern. The posterior fovea is a short, narrow groove that is in direct contact

with the central fovea via a deep, narrow groove between the entoconid and the hypoconulid. It is bounded distally by a moderately thick, well-developed but low distal marginal ridge. Buccally the cervical prominence is moderate, and the cervical line forms a peak between the roots. The mesiobuccal groove reaches a shallow pit approximately one third of the way along the buccal face; a shallow continuation of this groove persists beyond the pit, reaching approximately two thirds of the way along the buccal face before terminating abruptly. The mesiobuccal pit is bounded buccally by a moderately developed enamel wall that courses mesially onto the buccal protoconid face, presenting as a well delineated protostylid (type 5 of Hlusko 2004). The distobuccal groove is broad but shallow, terminating in a small pit about one third of the way along the buccal face; there is a slight buccal thickening of enamel at the point of the pit. The lingual face is occupied by a narrow, shallow groove that fades out of existence just below the occlusal margin. The lingual cervical prominence is weak, and the cervical line projects to form a ca. 1mm peak of enamel between the roots.

RM₃

This is a complete crown that is still forming in the crypt in the right hemi-mandible U.W. 88-8. The following description is based on a synchrotron scan and resultant 3D model of the tooth (see Figure 4). The occlusal outline is ovo-rectangular. All five principal cusps are present and well-developed. The metaconid is the largest cusp, followed by similar-sized protoconid and hypoconid, and the entoconid and hypoconulid in order of decreasing size; there is no C6. The apex of the protoconid is positioned slightly mesial to the apex of the metaconid. The mesial marginal ridge is well-developed and thick buccally, thinning slightly toward the lingual face. The anterior fovea is a moderately deep, narrow channel that is directed both lingually and buccally. The anterior fovea is partially separated from the broad, deep longitudinal fissure by a high, thick distal trigonid crest, though this latter crest is incised by a narrow, deep channel linking the anterior fovea and the central fovea. The metaconid is marked by a broad principal crest on its buccal face, and a second, smaller but well-developed crest on the distal aspect of the cusp; there is no clear indication of a postmetaconulid nor a C7. The metaconid contacts the hypoconid, resulting in a Y-pattern. The posterior fovea is a rounded, poorly-defined groove with a shallow buccal fissure that traverses toward the apex of the hypoconulid; it is in direct contact with the central fovea via a deep, somewhat broad groove between the entoconid and the hypoconulid. It is bounded distally by a low, short, but thick and well-developed distal marginal ridge. Buccally the cervical prominence is moderate, and the cervical line forms a distinct peak of enamel between where the roots would have formed. The mesiobuccal groove traverses approximately one third of the way down the buccal face to a very slight pit; it continues beyond this point as a relatively deep, but shallowing, groove to reach the CEJ. Radiating mesially from the slight pit is another groove that is bounded by a

moderately developed enamel wall that courses onto the buccal face of the protoconid, indicating a well-developed protostylid (type 5 of Hlusko 2004). The distobuccal groove is broad and shallow, terminating in a pit; there is a slight buccal thickening of enamel bounding the pit. The lingual face shows a shallow, weakly defined groove that fades out of existence approximately halfway to the CEJ. The lingual cervical prominence is weak, and the cervical line projects slightly to form a ca. 1mm peak of enamel between where the roots would have formed.

TEETH OF MALAPA HOMININ 2 (MH2)

LM²

This is a fragment of an isolated tooth preserving the metacone and a portion of the distobuccal root (see Figure 3). Occlusal wear is moderate, with the occlusal surface reduced to a flat plane, and no visible dentine exposures (category 2 or 3 of Molnar [1971]). The buccal extent of the distal ICF is visible. A remnant of the central fovea is evident, though the distal branch between the protocone and metacone has been obliterated by attrition. The buccally directed groove branching from the triradiate fissure continues onto the buccal face for a short distance before fading out of existence approximately halfway to the CEJ. A trace of the posterior fovea is visible, joining the distal extent of the groove between the protocone and the hypocone. The development of the posterior fovea suggests a relatively thick distal marginal ridge. The distobuccal root is broken off 10.7mm from the cervical margin. It is mesiodistally compressed, with a moderate buccal flare.

LM³

This is a partial crown preserving the protocone, hypocone, and about the lingual half of the paracone and metacone (see Figure 3). Occlusal wear is moderate, with cusps reduced to a flat plane but no dentine exposures visible (category 2 or 3 of Molnar [1971]). The mesial ICF is large and ovoid. Though the buccal half is missing, it appears that the crown was trapezoidal in outline with a reduced distobuccal corner. All four principal cusps are present and well-developed. Of the visible cusps, the protocone appears the largest, with a smaller hypocone, paracone, and (probably) metacone. A trace of the anterior fovea is evident, and a partially obliterated contact with the central fovea is visible. The mesial marginal ridge appears to have been moderately thick. A small remnant of the posterior fovea is evident, branching from the distal extent of the groove separating the protocone and hypocone. The distal marginal ridge appears to have been thin and weakly developed.

RI₁

This is a slightly damaged tooth missing approximately the infero-mesial half of the root (see Figure 4). The tooth is heavily worn, the occlusal surface being dominated by a large, lingually beveled, ovoid dentine exposure (category 5 of Molnar [1971]). Small chips of enamel are missing from the distal occlusal edge, while the mesial occlusal edge has

been smoothed by wear. Little of the labial face remains, appearing slightly convex mesiodistally. The labial cervical eminence is very slight, and the cervical enamel line is weakly curved. Lingually the cervical eminence is slight and symmetrically disposed; there is no evidence of a tubercle. The root is mesiodistally compressed, measuring approximately 3.6mm mesiodistally and 6.0mm bucco-lingually at the cervix.

RI₂

This is a nearly complete tooth missing a small piece of enamel from the mesiolabial corner of the crown, and lacking the apex of the root (see Figure 4). The tooth is moderately to heavily worn, with a large, distolingually beveled dentine exposure occupying the occlusal surface (category 5 of Molnar [1971]). Damage obscures the labial face, though it was apparently slightly convex mesiodistally. No trace of a labial distal marginal ridge is evident, while the position of the mesial marginal ridge is broken away. Lingually the cervical prominence is slight and symmetrically disposed; there is no tubercle. The root is mesiodistally compressed, measuring approximately 3.7mm MD and 6.9mm BL at the cervix. The preserved length of the root is 13.9mm, while the original length was probably closer to 17.0mm.

R_c

This is a nearly complete tooth missing only the apex of the root (see Figure 4). Occlusal wear is moderate, with the crown reduced to a flat plane with a distolingual bevel and a large, ovoid dentine exposure (category 5 of the Molnar [1991]). The ICF appears small, flat, and minimally impressed by the premolar. Labially the cervical prominence is weak, and the cervical margin is straight. A faint impression of a labial distal groove is evident, bounded distally by a slight distal marginal ridge; there is no indication of a mesial groove or mesial marginal ridge. On the lingual face the slight cervical prominence is distally oriented, and there is no lingual tubercle. A weak medial marginal ridge and distal marginal ridge are evident, bounding shallow grooves. These grooves, in turn, border a weak, apparently flat, median ridge. The root is encased in alveolar bone. It measures approximately 5.7mm mesiodistally and 7.3mm bucco-lingually at the cervix; the preserved length is about 16.0mm.

RP₃

This nearly complete tooth reveals a complete but fractured root system (see Figure 4). Occlusal wear is moderate, with a small, circular dentine exposure in the position of the metaconid, and a larger, crescent shaped dentine exposure in the position of the protoconid (category 3 of Molnar [1971]). The crown has been worn to a relatively flat plane, though the metaconid possesses a slight distolingual bevel, and the protoconid a slight distobuccal bevel. The mesial ICF is small and elongate, and the distal ICF is larger and more deeply impressed by its contact with the P₄. Superior to the distal ICF on the distal marginal ridge, a small chip of enamel is missing, and subsequent smoothing indicates

this damage occurred in life. Occlusally the crown has an irregular ovoid outline. The protoconid is larger than the metaconid, and is more mesially positioned. The mesial marginal ridge is well-developed and moderately thick, enclosing a small, crescent shaped dentine exposure in the position of the anterior fovea. The longitudinal fissure has been largely obliterated by attrition, though the posterior branch leading into a narrow, elongate, posterior fovea is present. The distal marginal ridge is well-developed and thick. The cervical prominence is weakly developed buccally, and the cervical line is straight horizontal. The lingual cervical prominence is moderately developed with a straight cervical line. The root system comprises a larger buccal and a smaller lingual root that are fused together by an obliquely oriented, well-developed plate. The root neck measures 5.3mm mesiodistally and 8.8mm buccolingually at the cervix.

RP₄

This is a complete tooth with the roots encased in alveolar bone (see Figure 4). Occlusal wear is moderate, with a small, circular dentine exposure on the metaconid, and a larger, oval dentine exposure in the position of the protoconid; there is an additional pinpoint dentine exposure on the distal marginal ridge (category 4 of Molnar [1971]). The crown has been worn to an approximately flat plane, with the more heavily worn protoconid set slightly inferior relative to the metaconid. The centrally positioned mesial ICF facet is large and elongate, and relatively deeply impressed by its contact with the P₃. The centrally positioned distal ICF is relatively large and flat. Occlusally the crown has an ovo-rectangular outline, with a slight reduction of the distobuccal corner. The protoconid is larger than the metaconid, and both appear to be approximately equally mesially positioned. The anterior fovea has been obliterated by wear, obscuring the mesial marginal ridge. The longitudinal fissure between the cusps is largely obliterated, though a posterior branch connects with a small, circular pit marking the posterior fovea, the latter which is bounded distally by a thick and well-developed distal marginal ridge. On the buccal face the cervical prominence is weakly developed, and the cervical line is slightly curved. The lingual cervical prominence is weak, and the cervical line projects to form a ca. 1mm peak that corresponds with a longitudinal furrow on the lingual root face. The root neck measures 7.3mm mesiodistally and 7.5mm buccolingually at the cervix.

RM₁

This is a partially complete crown missing the mesiolingual corner (principally the metaconid); the broken roots are preserved in the associated specimen U.W. 88-128 (see Figure 4). Occlusal wear is moderate, and the crown has been worn to a flat plane with a slight distal bevel. Of the preserved cusps, the protoconid is the most heavily worn, with a moderate-sized, circular dentine exposure; the hypoconid and hypoconulid display smaller, circular dentine exposures, while a pinpoint dentine exposure is visible in the entoconid (category 4 of Molnar [1971]). Occlusally the

crown appears ovo-rectangular in outline, with reduction of the mesiodistal length resulting from inter-proximal attrition. All five principal cusps are present and well-developed, including the broken metaconid. There is no indication of a C6. The metaconid was likely the largest cusp, followed by the protoconid, hypoconid, entoconid, and hypoconulid in descending order of size. The mesial marginal ridge is broken away, and the distal marginal ridge has been obliterated by attrition; neither the anterior fovea nor posterior fovea are visible. The metaconid contacts the hypoconid, resulting in a Y-shaped pattern. Only faint traces remain of grooves on the lingual and buccal faces, including a pit-like terminus of the mesiobuccal groove.

LM₂ + RM₂

The right tooth is missing a small wedge of enamel from the lingual face of the mesiolingual corner (see Figure 4). The left tooth is represented by a small wedge of enamel comprised principally of a fragment of the entoconid and the distal marginal ridge; the following description applies mainly to the right tooth. Occlusal wear is moderate, and the crown has been worn to a flat plane with a slight distal bevel. The hypoconid is the most heavily worn cusp, with a moderate-sized exposure of dentine visible; the protoconid presents a smaller, crescent-shaped dentine exposure, and the hypoconulid shows a very small, circular dentine exposure (category 4 of Molnar [1971]). Neither of the lingual cusps exhibit dentine exposures. Occlusally the crown is rectangular with a notable reduction of the distobuccal crown corner. All five principal cusps are present and well-developed. There is no C6. The metaconid is the largest cusp, followed by the protoconid, hypoconid, entoconid, and hypoconulid in descending order of size. Wear has obliterated the mesial marginal ridge, distal marginal ridge, and foveae anterior and posterior. The metaconid contacts the hypoconid, resulting in a Y-shaped pattern. Only faint traces remain of both the lingual and the buccal grooves. The mesiolingual portion of the mesial root plate is partially visible, and appears to have been relatively straight and round, with a slight distal tilt.

LM₃ + RM₃

The right tooth is near complete crown missing two small wedges of enamel from the lingual face, the smaller adjacent to the metaconid, and the larger adjacent to the entoconid (see Figure 4). The left tooth is missing a small fragment of enamel from the mesiolingual corner. Occlusal wear is light, and the crowns have been worn to a near flat plane with a slight lingual bevel, though some cuspal relief is still evident. A pinpoint of dentine is exposed in the position of the protoconid of both teeth (category 3 of Molnar [1971]). Occlusally the crown is ovo-rectangular, with a notable reduction of the distobuccal crown corner. All five principal cusps are present and well-developed. On the left tooth a small C6 is clearly visible, and while this area is damaged in the right tooth, we judge that a small C6 would have been present. In addition, the presence of distinct grooves on the lingual face of the left tooth strongly suggests that

a tuberculum intermedium was initially present; damage obscures this region on the right. The metaconid is the largest cusp, followed by the protoconid, hypoconid, and by similar-sized entoconid and hypoconulid, the latter which appears better developed than in the more anterior molars. Wear has obliterated the mesial marginal ridge and anterior fovea. The metaconid contacts the hypoconid, resulting in a Y-shaped occlusal pattern. The distal branch of the longitudinal fissure of the central fovea traverses toward the position of the C6, resulting in a posterior fovea that curves around the C6; the C6 occupies the position of the distal marginal ridge. The mesiobuccal groove is a small cleft that traverses from the occlusal margin to terminate in a small protostylid that extends a small way onto the metaconid (Type 2 of Hlusko 2004). Only a faint trace of the distobuccal groove remains. The buccal cervical prominence is weakly developed, and the cervical line appears straight. Lingually, the lingual grooves that delineate the tuberculum intermedium (at least on the left) extend from the occlusal margin to almost halfway to the cervical line before fading out of existence. The cervical line is slightly curved, and projects to form a ca. 1mm peak of enamel between the lingual roots.

COMPARATIVE MORPHOLOGY

The Malapa hominins MH1 and MH2 possess a unique combination of characters that is not encountered in any other hominin, thus we recognize them as the holotype and paratype specimens, respectively, of the novel taxon *Australopithecus sediba* (Berger et al. 2010). In the discussion below we include both qualitative and quantitative aspects of morphology, focusing in particular on those characters that are taxonomically informative relative to *Au. sediba*. In Tables 6 to 17 we present numerous indices describing the quantitative aspects of cranial and palatal morphology, drawing on raw data presented in Table 3. Mandibular measures and indices are combined in Tables 19 to 22.

CRANIAL VAULT

Cranial Capacity

Australopiths such as *Au. afarensis*, *Au. garhi*, and *Au. africanus* all have similar estimated cranial capacities (Table 5). It is with specimens attributed to *H. habilis*, *H. rudolfensis*, and *H. erectus* that we begin to see some level of brain expansion, and indeed the relatively enlarged brains of several key specimens (e.g., OH 7, KNM-ER-1470) attributed to these taxa, in particular *H. habilis* and *H. rudolfensis*, have played a role in their taxonomic allocations (Leakey et al. 1964; Holloway et al. 2004; Stringer 1986; Wood 1985). However, with cranial capacity estimates of between 465–600 ml, specimens of *H. naledi* fall within the range of australopiths (Berger et al. 2015), thus small cranial capacity does not necessarily distinguish *Homo* from australopiths. We have estimated the cranial capacity of MH1 as 420ml (Berger et al. 2010; Carlson et al. 2011), and although MH1 is a juvenile individual, it is at an ontogenetic age where brain growth is virtually complete (Tobias 1971). The rela-

tively small brain of *Au. sediba* aligns it most closely with australopiths, falling within the ranges of *Au. afarensis*, and *Au. africanus*. However, even among this group of australopiths, MH1 appears small, falling roughly 1SD below the mean for *Au. africanus*. At the same time, MH1 falls slightly below values for *H. naledi*, roughly 3SD below the mean for crania referred to *H. habilis*, and even farther below the means for crania referred to *H. rudolfensis* and *H. erectus* respectively.

Despite the small size of the brain of MH1, and its generally australopith-like convolutional patterns on the frontal lobes, posterior positioning of the olfactory bulb relative to the temporal poles and the orbitofrontal surface, together with an orbitofrontal shape and organization (e.g., broadening of the anterior frontal region and medial movement of the temporal poles), combine to foreshadow certain aspects of human endocasts that are collectively less apparent in other australopith casts (Carlson et al. 2011). As a result, it appears that neural reorganization was decoupled from brain expansion in the lineage to which *Au. sediba* belongs, at least in the orbitofrontal region. This interpretation supports the conclusions of previous researchers that cortical reorganization in the frontal lobes began with *Australopithecus*, prior to the appearance of early *Homo*, and that it did so in the absence of a substantial increase in brain size (Falk et al. 2000; Holloway 1988).

Height And Breadth Of The Cranial Vault

Although damage prevents direct identification of the position of porion in MH1, using the alveolar plane as a guideline to orienting the cranium relative to the FH plane we can estimate the vertical position of porion relative to orbitale, and using Sts 5 as a guideline we can estimate the sagittal position of porion some 15.0mm posterior to the preserved post-glenoid process, thereby fixing the point porion with a reasonable degree of reliability. In absolute terms, the low cranial vault of MH1 is most similar in height to Sts 71 of *Au. africanus*, falling short of values encountered in early *Homo* (see Table 3). Cranial indices such as height relative to bi-porionic breadth or bi-temporal breadth or relative cranial vault breadth do not reliably distinguish between australopiths or early *Homo*, and MH1 intersects with values for both groups (Table 6).

Despite the overlap in relative cranial breadth across australopiths and early *Homo*, the notably vertical parietal walls of MH1 present a relatively “boxy” appearance (see Figure 1). This appearance is not clearly captured by relative cranial breadth, since bi-parietal and bi-temporal measures are taken at the point of maximum breadth, which tends to be lower down on the cranium in fossil hominins. This leaves no measure to capture the relative breadth nearer the top of the cranium where the lateral parietal wall transitions to the superior parietal wall in MH1, and indeed it is not possible to fix a consistent point at which to take such a measure. Qualitatively speaking, vertically oriented lateral parietal walls appear more common among early *Homo* (e.g. KNM-ER 1470, KNM-ER 1805, OH 24) than australopith specimens, though not all early *Homo* crania have

TABLE 5. CRANIAL CAPACITY ESTIMATES IN HOMININS.

Taxon	Specimen	Cranial capacity ¹
<i>Au. afarensis</i>	Mean	444
	AL 162-28	400
	AL 288-1	387
	AL 333-45	485
	AL 333-105	400
	AL 444-2	550
<i>Au. africanus</i>	Mean	455
	MLD 1	510
	MLD 37/38	425
	Sts 5	485
	Sts 19	436
	Sts 60	400
	Sts 71	428
	StW 505	505
<i>Au. sediba</i>	MH1	420
<i>H. naledi</i>	Mean	542
	DH1	560
	DH3	465
	LES1	600
<i>H. habilis</i>	Mean	609
	KNM-ER 1805	582
	KNM-ER 1813	509
	OH 7	729
	OH 13	650
	OH 16	638
	OH 24	590
<i>H. rudolfensis</i>	KNM-ER 1470	752
<i>H. erectus</i>	Mean	846
	BOU-VP-2/66	995
	D2280	730
	D2282	650
	D2700	601
	D4500	546
	KNM-ER 3733	848
	KNM-ER 3883	804
	KNM-ER 42700	691
	KNM-WT 15000	900
	OH 9	1067
	OH 12	727
	Sangiran 2	813
	Sangiran 4	908
	Sangiran 17	1004
	Zhoukoudian DI	915
	Zhoukoudian LI	1025
Zhoukoudian LII	1015	
Zhoukoudian LIII	1030	

¹Cranial capacity estimates for hominin fossils from Holloway et al. (2004), Berger et al. (2010, 2015), Lordkipanidze et al. (2013), and Spoor et al. (2015).

TABLE 6. CRANIAL VAULT INDICES FOR AUSTRALOPITHECUS SEDIBA AND COMPARATIVE HOMININ SPECIMENS (W# indications refer to indices provided in Wood [1991]; letters in parentheses refer to values presented in Table 3).

Taxon	Specimen	Cranial height / bi-porionic breadth	Cranial height / bi-temporal breadth	Relative cranial breadth
		W vii (a)/(b)	W iv (a)/(d)	(c)/(b)
<i>Au. afarensis</i>	AL 333-45			81
	AL 444-2	65		
<i>Au. africanus</i>	Mean	72	70	98
	MLD 37/38	70	67	100
	Sts 5	76	73	103
	Sts 71	71	70	97
	StW 53	71	70	91
<i>Au. sediba</i>	MH1	67	66	100
<i>H. naledi</i>	Mean	79	76	101
	DH1	77	74	103
	DH2	76	74	96
	DH3	85	81	104
<i>H. habilis</i>	Mean	73	69	99
	KNM-ER 1805	75	73	101
	KNM-ER 1813	73	72	95
	OH 24	70	62	101
<i>H. rudolfensis</i>	KNM-ER 1470	74	71	99
<i>H. erectus</i>	Mean	74	66	109
	BOU-VP-2/66			106
	D2280	76	69	104
	D2282/211			116
	D2700/2735	73	64	108
	D4500/2600			89
	KNM-ER 3733	66	61	101
	KNM-ER 3883	63	58	106
	KNM-ER 42700	89	76	112
	KNM-WT 15000	86	70	119
	OH 9	68	64	105
	Sangiran 2			119
	Sangiran 4			116
Sangiran 17			111	
Zhoukoudian EI			108	
Zhoukoudian LI			111	
Zhoukoudian LII			113	
Zhoukoudian LIII			109	

them (e.g., KNM-ER 1813), while some australopiths do (e.g., MLD 37/38). In this regard, MH1 appears generally more *Homo*-like in the appearance of the lateral parietal walls, though there is overlap between the australopiths and early *Homo*.

Recently, Kimbel and Rak (2017) suggested that the growth that would have occurred had MH1 survived into full adulthood would have been substantial in some regions of the cranium, and would obviate the similarities shared

between *Au. sediba* and *Homo*. Metrically, they focused on levels of postorbital constriction, spacing of the temporal lines, and flaring of the zygomatics, using ratios of various cranial breadths to suggest that an adult version of MH1 would no longer look especially *Homo*-like. However, their conclusions are contradicted by those of Carlson et al. (2016), who conducted a developmental simulation of the MH1 cranium using geometric morphometric techniques to extrapolate adult morphology. In this study, Carlson et

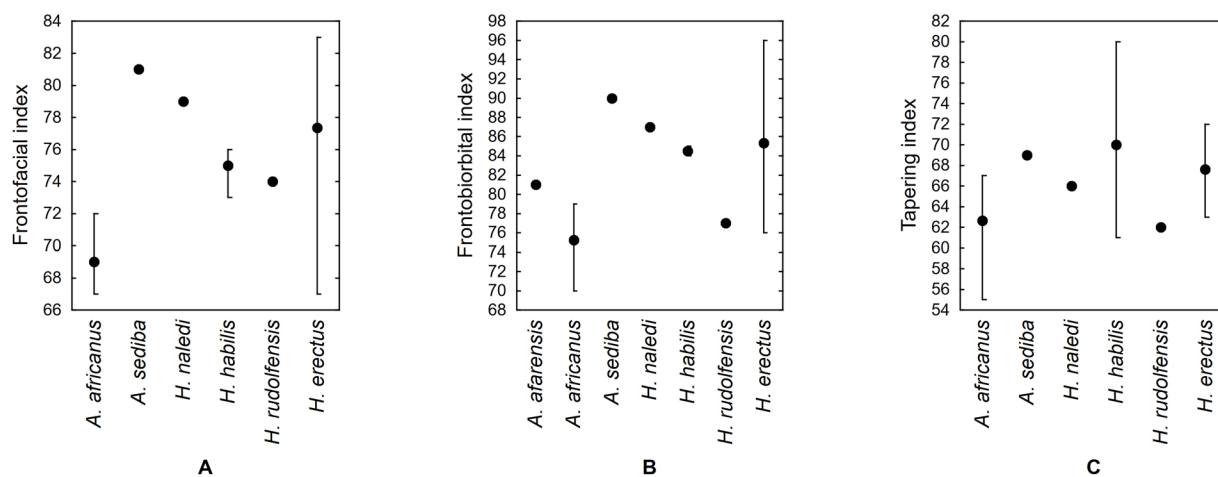


Figure 8. Postorbital constriction indices: A) frontofacial index; B) frontobiorbital index; C) tapering index. Points represent single values or means, whiskers represent min/max values. Data from Table 7.

al. (2016) applied developmental trajectories derived from sub-adult versus adult males and females of extant humans, chimpanzees, and gorillas to the cranium of MH1 in order to assess how much change might be expected had MH1 lived to full maturity. They determined that subsequent cranial growth was principally a reflection of secondary sexual development, and would not likely be sufficient to alter the suggested morphological affinities of *Au. sediba*. In particular, of the six different scenarios generated (male vs. female human, chimpanzee, or gorilla) the most significant changes were associated with male gorillas: glabella became more pronounced, the supraorbital torus thickened, the zygomatic increased in its superior-inferior dimension, the midface became more flexed, and lower facial prognathism became more prominent. In contrast to Kimbel and Rak (2017), no significant changes in levels of postorbital constriction, spacing of temporal lines, or flaring of zygomatics were detected. Similar transformations were also observed in male chimpanzees, though to a lesser extent than was observed in male gorillas. The magnitude of morphological change observed using female gorilla and chimpanzee developmental vectors was comparatively much less than for the males. Changes associated with male and female humans were minimal, producing no notable deviations from the juvenile form of MH1. Carlson et al. (2016) suggested that either chimpanzee or human developmental patterns provided the best estimates of developmental patterning in *Au. sediba*, though neither pattern resulted in a significant change in estimated adult form relative to MH1. They considered the gorilla development pattern, in particular that of the male gorilla, to be the least suitable model for growth in *Au. sediba*; nonetheless, even the most extreme variation that was noted with a male gorilla trajectory still did not result in an estimated adult form that differed significantly from MH1. Indeed, principal components analysis indicated that all six simulated *Au. sediba* adult crania—regardless of sex or species used—clustered with the original MH1 cranium in a discrete group relative

to other fossil taxa. As a result, in order to achieve the *Au. africanus*-like morphology proposed by Kimbel and Rak (2017), the developmental trajectory for *Au. sediba* would have to be unrealistic for primates. Carlson et al. (2016) therefore concluded that additional growth into adulthood would not likely have substantially altered the morphology of MH1, thus an adult version of MH1 would not look very different from its preserved sub-adult morphology.

Additionally, a recent study has demonstrated that MH1 shared a (post-cranial) maturation schedule with KNM-WT 15000, which itself is of similar ontogenetic development to MH1 (Cameron et al. 2017). The skull of KNM-WT 15000 is comparable in morphology to adult *H. erectus* specimens. Thus, if these similarly ontogenetically-aged specimens—KNM-WT 15000 and MH1—followed a similar maturation schedule, and if KNM-WT 15000 would have undergone only limited morphological change had it survived into adulthood; this suggests that MH1 would likewise only have undergone limited morphological change had it survived into adulthood.

Postorbital Constriction And The Temporal Foramen

We measure postorbital breadth as the narrowest chord across the deepest part of the cranial constriction posterior to the orbits (see Table 3). On its own, postorbital constriction is difficult to assess, but there are a number of ways that we can examine its relative size. We can scale it to superior facial breadth, referred to as frontofacial breadth (Kimbel et al. 1984); we can scale it to inner bi-orbital breadth, referred to as frontobiorbital breadth (Kimbel et al. 1984); or we can scale it to the maximum cranial breadth, sometimes referred to as the transverse-frontoparietal index, though perhaps this would be better termed the tapering index, since maximum cranial breadth typically falls on the temporals in australopiths and early *Homo* (see Tobias 1967: 100). In all three indices MH1 stands out as being only minimally constricted (Table 7, Figure 8), thus it is clearly distinguished from other australopiths, to the extent that

TABLE 7. POSTORBITAL CONSTRICTION INDICES
(letters in parentheses refer to values presented in Table 3).

Taxon	Specimen	Fronto-facial breadth index	Fronto- biorbital breadth index	Tapering index	Temporal foramen
		Kimbel et al. 1984 (e)/(l)	Kimbel et al. 1984 (e)/(m)	Tobias 1967 (e)/(d)	(e)/(n)
<i>Au. afarensis</i>	AL 444-2		81		46
<i>Au. africanus</i>	Mean	69	75	63	51
	Sts 5	69	79	67	52
	Sts 71	72	79	66	54
	StW 53	68	70	55	48
	StW 505	67	73		
<i>Au. sediba</i>	MH1	81	90	69	69
<i>H. naledi</i>	DH3	79	87	66	
<i>H. habilis</i>	Mean	75	84	70	63
	KNM-ER 1805			80	
	KNM-ER 1813	76	84	69	62
	OH 16	76		70	
	OH 24	73	85	61	63
<i>H. rudolfensis</i>	KNM-ER 1470	74	77	62	
<i>H. erectus</i>	Mean	77	85	68	65
	BOU-VP-2/66	77		67	76
	D2280	80	83	67	
	D2282/211	76	82	67	61
	D2700/2735	80	86	64	66
	D4500/2600	67	76	67	50
	KNM-ER 3733	76	85	67	66
	KNM-ER 3883	73	83	66	59
	KNM-ER 42700	82		69	
	KNM-WT 15000	82	89	67	71
	OH 9	75	88	72	
	Sangiran 2			63	
	SK 847	83	96		73
	Trinil I			72	
	Zhoukoudian EI			66	
	Zhoukoudian LI			71	
	Zhoukoudian LII			69	
	Zhoukoudian LIII			68	

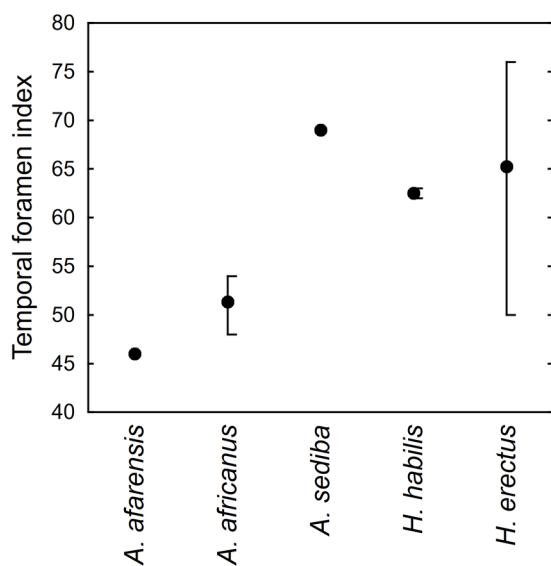


Figure 9. Temporal foramen index. Points represent single values or means, whiskers represent min/max values. Data from Table 7.

it appears even less constricted than many specimens attributed to early *Homo*. Taking the frontobiorbital index in particular, for example, MH1 is less constricted than any individual specimen of *H. erectus*, highlighting the limited degree of postorbital constriction that is apparent in *Au. sediba*. In contrast, Spoor (2011) and Kimbel and Rak (2017) suggested that because MH1 was not fully adult, the degree of postorbital constriction would have changed significantly had it grown to maturity, thus postorbital constriction in *Au. sediba* might have been more marked than is evident in MH1. However, as noted above, developmental simulations that estimated adult form in *Au. sediba* using male and female human, chimpanzee, gorilla developmental trajectories demonstrated that relative postorbital constriction would likely not have changed substantively had it lived to adulthood (Carlson 2014; Carlson et al. 2016). In addition, Lockwood and Tobias (1999) suggested that postorbital constriction was more effective at discriminating between sexes than between taxa. This relates to the relatively greater expansion of the supraorbital torus in males, which results in the appearance of greater postorbital constriction compared to females. As a result, if MH1 is indeed a male (Berger et al. 2010), this implies that a female should show even less relative constriction, thus favoring the argument that postorbital constriction is indeed limited in *Au. sediba*. This relative lack of postorbital constriction is perhaps not surprising given the orbitofrontal expansion documented in this taxon (Carlson et al. 2011).

The degree of postorbital constriction, in conjunction with the degree of lateral flaring of the zygomatic arches, can be used to describe the relative breadth of the temporal foramen (Figure 9). In *Au. afarensis* and *Au. africanus* postorbital breadth usually reflects some 40%–50% of bi-zygomatic breadth, while in specimens assigned to *H. habilis* and *H. erectus* the temporal foramen tends to be small,

with postorbital breadth hovering around 60% to 70+% of bi-zygomatic breadth; among this early *Homo* group, two specimens stand out as having temporal foramina that are larger than the rest, KNM-ER 3883 at 59%, and D4500 at 50% (see Table 7). Notwithstanding, MH1 exhibits an especially small temporal foramen, with postorbital breadth accounting for 69% of bi-zygomatic breadth, a value exceeding that seen in specimens of *H. habilis* and overlapping with values in specimens of *H. erectus*, appearing closest to KNM-WT 15000. The small size of the foramen is also evident in its length and breadth (see Table 3). In addition, MH1 stands out for having an unusual shape of the temporal foramen, being considerably longer than it is broad.

Frontal Bone

The frontal squama in MH1 is broadly rounded and convex, and arises from the supratoral sulcus at the same angle as specimens such as Sts 5, Sts 71, D2282, D4500, and Sangiran 2 (see Table 3). Sagittal length of the frontal overlaps with several australopiths, while appearing shorter than any specimen attributed to *Homo*. The overall appearance of the frontal squama of *Au. sediba* is thus similar to both australopiths and *Homo*, though the bone is generally shorter than specimens of the latter.

Temporal Lines and Cranial Cresting Patterns

From their origin on the marginal process, the temporal lines in australopiths traverse upward and then curve medially onto the supraorbital arch/bar, typically continuing along the superior summit of the arch/bar for half or more of its length. In contrast, in specimens attributed to early *Homo* the temporal lines do not encroach on the supraorbital torus for more than about one-fifth of its length, instead curving rapidly posterosuperiorly onto the cranial vault. This results in a lateral extent of the supraorbital torus that takes on a distinctly triangular appearance from the superior aspect, what Rak (1983; after Schwalbe 1906) refers to as a supraorbital trigon. In addition, the temporal lines in early *Homo* typically do not occupy the highest point on the supraorbital torus, being instead positioned on its posterior face. *H. erectus* generally matches this early *Homo* pattern, though the development of the supratoral sulcus is so extensive that the temporal lines are typically restricted to the far lateral margin of the supraorbital torus, and the supraorbital trigon takes on a decidedly expanded triangular shape. In MH1 we see minimal encroachment of the temporal lines on the supraorbital torus (\leq one-fifth), and these lines are positioned below the summit of the torus, on its posterior aspect (see Figure 1). Combined with the limited convergence of the temporal lines, this results in a distinctly broadened supraorbital trigon at the lateral extent of the supraorbital torus. This pattern is not witnessed in any other australopith, and thus aligns *Au. sediba* most closely with the early *Homo* sample.

As the temporal lines continue along their posterosuperior course, they begin to converge to varying degrees in the area of the postorbital constriction. In australopiths, the temporal lines converge markedly, traversing medial to the

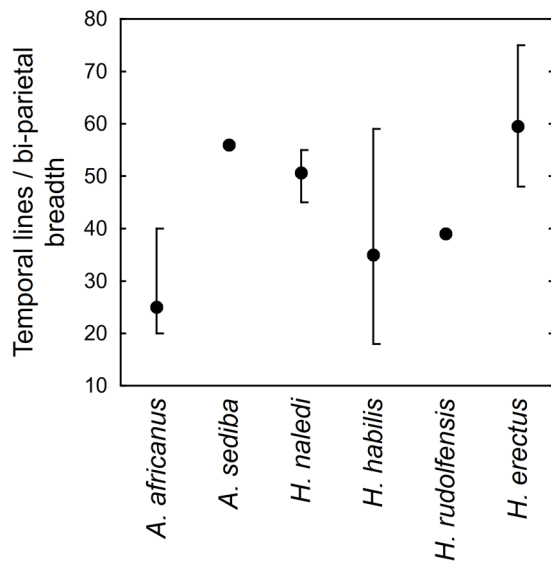


Figure 10. Temporal lines index. Points represent single values or means, whiskers represent min/max values. Data from Table 8.

medial wall of the temporal fossa, sometimes converging to form a sagittal crest (see Table 3, Figure 10). Specimens attributed to *H. habilis* show considerable variability in the arrangement of the temporal lines. In KNM-ER 1813, the convergence of the temporal lines is weak, and they are coplanar with the medial wall of the temporal fossa. In OH 16 and OH 24, the convergence of the temporal lines is more marked, and while the lines begin coplanar with the medial wall of the temporal fossa, they converge to such a degree that posteriorly they are located medial to the medial wall of the temporal fossa. KNM-ER 1805 is even more extreme in that the temporal lines converge anterior to bregma to form a sagittal crest. *H. rudolfensis*, *H. erectus*, and *H. naledi* all show weak convergence of the temporal lines, which are all either coplanar with the medial wall of the temporal fossa, or only slightly medially inset. MH1 matches this pattern, with temporal lines that show limited convergence and which are coplanar with the medial wall of the temporal fossa, appearing most similar to the majority of specimens assigned to early *Homo*.

After the convergence of the temporal lines, they either continue as separate bilateral entities, or in some specimens as a distinct sagittal crest. Most specimens of *Au. afarensis* preserving the relevant areas show a posteriorly disposed sagittal crest, and where a sagittal crest occurs, a compound T/N crest is also present. Only a single specimen of *Au. africanus* has revealed a definite sagittal crest, StW 505 (Lockwood and Tobias 1999), though it has been suggested that MLD 1 (Dart 1948; Robinson 1958), Sts 17 (Wolpoff 1974; Tobias 1991), and perhaps StW 13 (Tobias 1991) would have presented sagittal crests; Lockwood and Tobias (1999) later discounted the likelihood of a crest in MLD 1. A compound T/N crest is not indicated in any specimen of *Au. africanus*. In those *Au. africanus* specimens without a sagittal crest, the temporal lines nonetheless tend to be absolutely

and relatively closely spaced (see Table 3; Table 8). Among specimens attributed to *H. habilis*, KNM-ER 1805 is alone in presenting sagittal and compound T/N crests. The remaining *H. habilis* individuals show relatively broadly spaced temporal lines, though there is some indication of variability among them. While in KNM-ER 1813 they are relatively far apart compared to bi-parietal breadth, some Olduvai specimens such as OH 13, OH 16, and probably OH 24 reveal more closely spaced temporal lines. In contrast, in *H. rudolfensis*, *H. erectus*, and *H. naledi* specimens the temporal lines are absolutely and relatively widely spaced. MH1 is broken posteriorly, though the temporal lines can be traced as they course inferiorly over the parietals and curve anteriorly onto the temporals. They are absolutely and relatively widely spaced and show no indication of a compound T/N crest, similar to most specimens of early *Homo*.

Kimbel and Rak (2017) suggested that had MH1 reached adulthood, the convergence of the temporal lines would likely have become more marked. However, the developmental simulation of MH1 conducted by Carlson et al. (2016), and discussed in more detail above, indicated that relative temporal line convergence would likely not have changed substantively had it lived to adulthood.

Supramastoid Crest And The Root Of The Zygoma

Although australopiths exhibit well-developed, laterally extensive supramastoid crests, there are sufficient examples of early *Homo* specimens with equally well-developed supramastoid crests to limit the utility of this character in separating the two groups. Of more importance is the pattern recognized by Tobias (1991: 93) regarding the point at which the supramastoid crest transitions to the posterior root of the zygoma. In australopiths, the supramastoid crest retreats medially above the EAM, and then immediately swells out laterally above the EAM as the posterior root of the zygoma; StW 53 matches other *Au. africanus* specimens in this arrangement. In contrast, in specimens of early *Homo* the supramastoid retreats medially above the EAM, but then swells out laterally in a more anterior position, above the level of the mandibular fossa. Although there is extensive damage in the supramastoid area of MH1, sufficient bone is preserved, including what we interpret to be the lateral-most extent of the supramastoid crest, to document the pattern in this region. In MH1 the supramastoid crest retreats medially above the area of the (missing) meatus, but then it swells laterally in a more anterior position, above the level of the mandibular fossa, in common with specimens of early *Homo* (Figure 11).

The zygomatic process sulcus (Weidenreich 1943) is moderately wide in *Au. afarensis* and *Au. africanus* (see Table 3), and both reveal a relatively parallel orientation of the root of the zygomatic process of the temporal relative to the FH. Specimens attributed to *H. habilis* have a somewhat narrow zygomatic process sulcus, while *H. erectus* has a broader sulcus, owing to the overall larger size of the specimens. Of note is the fact that in specimens such as KNM-ER 1813 and OH 24, the root of the zygomatic process of the temporal is angled roughly 30° downward relative to FH.

TABLE 8. TEMPORAL LINE WIDTH RELATIVE TO BI-PARIETAL BREADTH
(letters in parentheses refer to values presented in Table 3).

Taxon	Specimen	Temporal lines¹ / bi-parietal breadth
<i>Au. africanus</i>	Mean	25
	MLD 37/38	40
	Sts 5	20
	Sts 71	20
	StW 53	20
<i>Au. sediba</i>	MH1	56
<i>H. naledi</i>	Mean	53
	DH1	52
	DH2	45
	DH3	55
<i>H. habilis</i>	Mean	33
	KNM-ER 1813	59
	OH 7	39
	OH 13	24
	OH 16	18
<i>H. rudolfensis</i>	KNM-ER 1470	39
<i>H. erectus</i>	Mean	57
	D2280	50
	D2282/211	56
	D2700/2735	59
	D4500/2600	57
	KNM-ER 3733	50
	KNM-ER 3883	57
	KNM-ER 42700	69
	KNM-WT 15000	48
	OH 9	59
	Sangiran 2	51
	Sangiran 4	62
	Zhoukoudian EI	68
Zhoukoudian LI	68	
Zhoukoudian LII	64	
Zhoukoudian LIII	75	

¹Non-crested individuals only.

This condition is also seen in most, but not all, *H. erectus* specimens (Weidenreich 1943), and in all specimens of the novel taxon, *H. naledi* (Berger et al. 2015; Laird et al., 2017). The zygomatic process sulcus of MH1 is especially narrow and the zygomatic root parallels the FH plane (see Figure 1C). As a result, although the closest comparison for MH1 in terms of breadth of the sulcus lies with OH 24, these two differ in the relative orientation of the root of the zygomatic, the latter which aligns *Au. sediba* with other australopiths.

Squamosal Suture And Pterion

There is a great deal of variability evident in the arrangement of the squamosal suture, and *Au. sediba* overlaps in appearance and size with specimens of *Au. africanus* as well as early *Homo* (see Table 3). The most common arrangement of cranial sutures in the region of pterion in humans, bonobos, and orangutans is to have the greater wing of the sphenoid and the parietal intrude between the frontal and the temporal (Aiello and Dean 1990). The pattern is reversed in chimpanzees and gorillas, with the frontal and tempo-

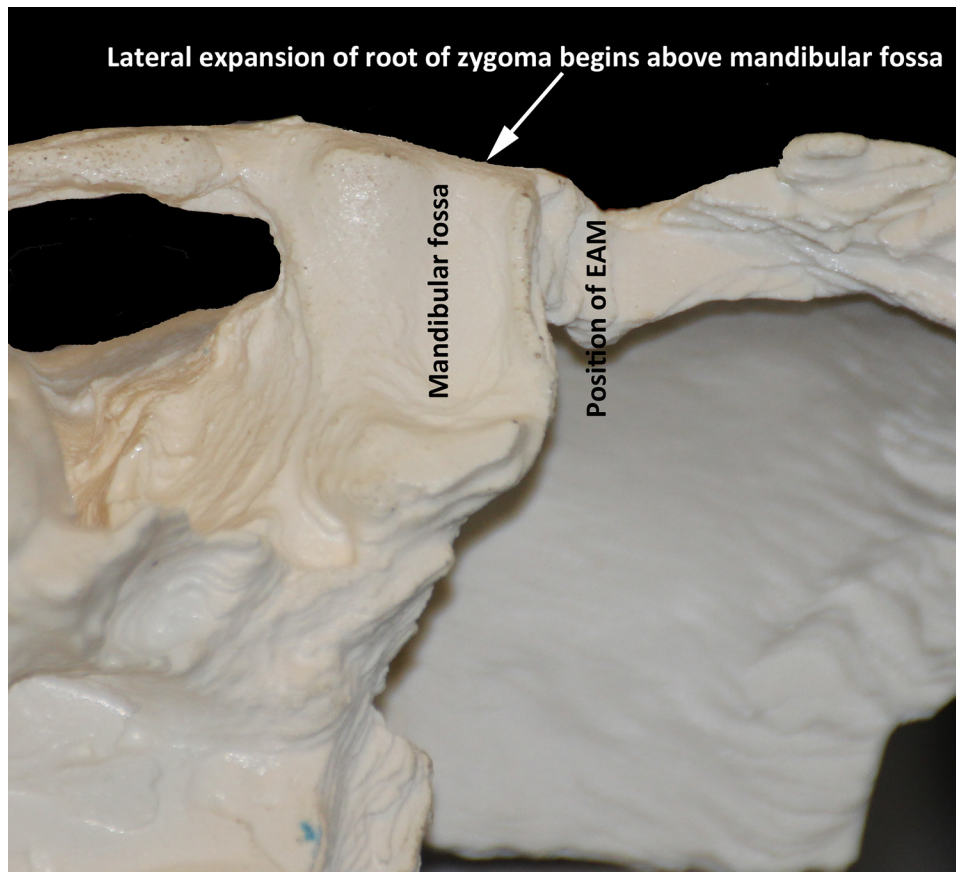


Figure 11. Close up view of mandibular fossa region of a 3D printout of U.W. 88-50, generated from synchrotron scans.

ral bones contacting each other, preventing the sphenoid and parietal from articulating. In all early hominin fossils preserving the area in sufficient detail, the more human arrangement is visible. However, in MH1 the chimpanzee/ gorilla pattern is evident, as the temporal is in direct contact with the frontal (see Figure 1C). In and of itself, such a sutural arrangement is of interest, though little phylogenetic importance can be placed on this distinction as both patterns are variably represented in all groups of humans and apes (Aiello and Dean 1990).

CRANIAL BASE

Mandibular Fossa And The Articular Eminence

This region is preserved only on the left side in MH1, and shows considerable damage, though some detail is preserved. Since this area remains partially encased in calcified clastic sediment, synchrotron scans were used to augment the visible morphology and to allow measurements to be taken (see Figure 11). In terms of absolute and relative size, there is a wide range of variability seen in the hominins, though what sets MH1 apart is its overall small size, falling as it does at the lower end of the range for hominins (see Table 3). There is variability across hominins in fossa shape, with fossae ranging from about as long as they are broad to roughly half as long as they are broad (Table 9, Figure 12). Within this variability, a pattern emerges wherein the fos-

sae in australopiths tend to be about half as long as they are broad, while in early *Homo* they range widely but overall length tends to be greater than half of fossa breadth, sometimes being longer than they are broad. MH1 aligns most closely with the australopith pattern, though again there is overlap between australopiths and early *Homo*. If we scale mandibular fossa breadth to bi-porionic breadth, we see again that there is a great deal of overlap in our samples (see Table 9). *Au. afarensis* shows relatively large fossae, even taking into account the relatively broad bi-porionic width. However, *Au. africanus*, *H. habilis*, *H. naledi*, and *H. erectus* all overlap with *Au. sediba*, while KNM-ER 1470 reveals a somewhat smaller relative fossa size. Considered in terms of either absolute depth or in depth relative to length and to breadth, the mandibular fossa in *Au. afarensis* is especially shallow (see Table 9), while there is considerable overlap in fossa depth among the other hominins considered here. MH1 reveals a relatively shallow mandibular fossa that overlaps with numerous specimens of both australopiths and early *Homo*, thus the clearest distinction appears to be from the notably shallow fossa of *Au. afarensis*.

The articular eminence in MH1 is low and rounded, with a distinct saddle shape that is oriented roughly parallel to the coronal plane (see Figure 11). The entoglenoid process is difficult to examine, though from what is visible we can say that it is moderately well-developed and projecting, with an inferolateral orientation. In overall configu-

TABLE 9. MANDIBULAR FOSSA INDICES (W# indications refer to indices provided in Wood [1991]; letters in parentheses refer to values presented in Table 3).

Taxon	Specimen	Mandibular fossa shape	Mandibular fossa breadth / bi-porionic breadth	Relative depth I	Relative depth II
		W xlvi	(g)/(h)	W xlviii	W xlix
<i>Au. afarensis</i>	Mean	54	27	30	16
	AL 333-45	55	27	20	11
	AL 444-2	54	27	39	21
<i>Au. africanus</i>	Mean	59	28	47	27
	MLD 37/38	65	31		
	Sts 5	50	29	71	36
	Sts 19	52	26	47	24
	Sts 25	68		40	27
	Sts 71	52	31	47	24
	StW 53	50	21	42	21
	StW 505	80		35	28
<i>Au. sediba</i>	MH1	52	23	50	26
<i>H. naledi</i>	DH3	96	26	21	20
<i>H. habilis</i>	Mean	60	23	55	26
	KNM-ER 1805	79	23	53	42
	KNM-ER 1813	58	25	40	23
	OH 24	44	26	83	37
<i>H. rudolfensis</i>	KNM-ER 1470	79	20	32	25
<i>H. erectus</i>	Mean	75	23	51	37
	BOU-VP-2/66	74	22	28	20
	D2280	55	27	47	26
	D2282/211	42	31	42	18
	D2700/2735	50	25	38	19
	KNM-ER 3733	73	21	26	19
	KNM-ER 3883	71	23	35	25
	KNM-ER 42700	85	20		
	KNM-WT 15000	104	25	36	37
	OH 9	59	24	68	41
	Sangiran 2	122	20	46	57
	Sangiran 4	100		64	64
	SK 847	58		40	23
	Zhoukoudian EI	72	20	67	48
	Zhoukoudian HIII			71	
	Zhoukoudian LII	78	23	71	56
	Zhoukoudian LIII	78	18	83	65

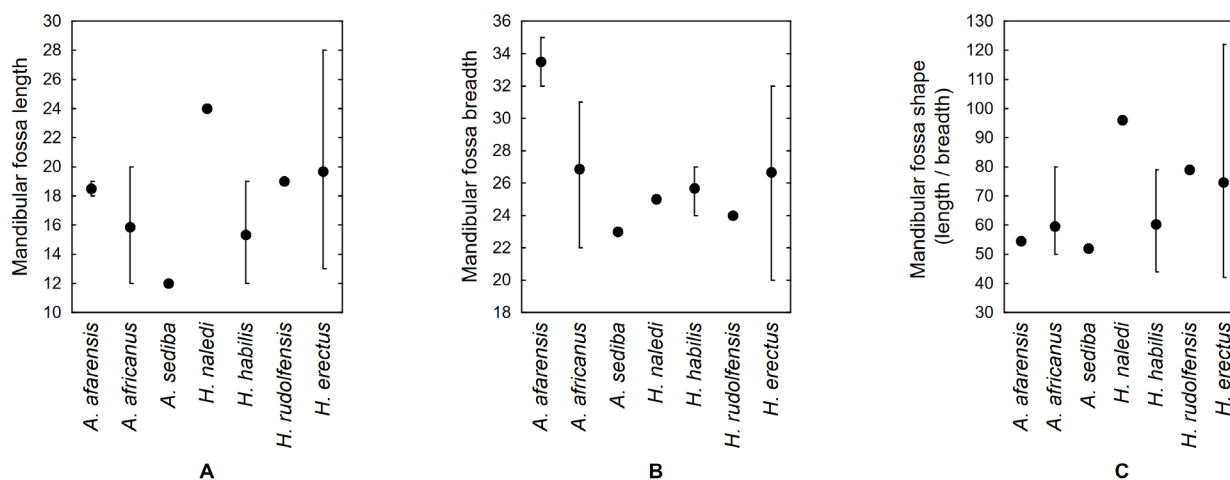


Figure 12. Mandibular fossa size and shape: A) length; B) breadth; C) shape. Points represent single values or means, whiskers represent min/max values. Data from Tables 3 and 9.

ration, it looks similar to specimens of *Au. africanus* such as Sts 5, as well as specimens attributed to *H. habilis* such as KNM-ER 1813 and OH 24, and *H. erectus* specimens such as KNM-ER 3733 and KNM-WT 15000. The arrangement of the articular eminence does not distinguish between *Au. africanus*, *Au. sediba*, and early *Homo*, but can separate these taxa from *Au. afarensis*, the latter which reveals a weakly developed and flat articular eminence, with a massive, projecting entoglenoid process.

Position Of The Mandibular Fossa

The position of the mandibular fossa relative to the lateral wall of the cranium has long been recognized as an important diagnostic character in hominins (Tobias, 1991; Weidenreich 1943). In *Au. afarensis*, half or less of the mandibular fossa is positioned medial to the parasagittal plane of the lateral cranial wall. The pattern appears to change slightly with *Au. africanus*, where in all specimens two-thirds to three-quarters of the mandibular fossa is positioned medial to the parasagittal plane of the lateral wall of the temporal squama; StW 53 matches this pattern. With specimens attributed to *H. habilis*, *H. rudolfensis*, and *H. naledi*, a more medial position of the mandibular fossa is apparent. Allowing for some displacement, in KNM-ER 1813 between two-thirds to three-quarters of the mandibular fossa is positioned medial to the parasagittal plane of the lateral wall of the cranium, while in KNM-ER 1805, OH 24, KNM-ER 1470, and DH3 almost the entire mandibular fossa is more medially positioned than the parasagittal plane of the lateral cranial walls. *H. erectus* carries this trend farthest among the fossil hominins, with a mandibular fossa that is positioned almost entirely medial to the parasagittal plane of the lateral wall of the temporal squama. In MH1, the mandibular fossa is positioned almost entirely medial to the parasagittal plane of the lateral wall of the cranium, similar to specimens of early *Homo*, and unlike australopith fossils. Lockwood and Tobias (1999) suggested that the relative positioning of the mandibular fossa was impacted

more by the masticatory apparatus than by cranial expansion, and with its small cranial capacity, MH1 provides further substantiation of this hypothesis.

FACE

Outline Of The Facial Mask

In absolute size, facial height in MH1 intersects with specimens of *Au. africanus*, *H. habilis*, and *H. erectus* (see Table 3). The facial breadth of MH1 is particularly narrow, appearing narrower than almost all australopith and early *Homo* specimens, except for DH3 of *H. naledi*. Turning to relative facial proportions we see some overlap between the australopiths, including *Au. sediba*, and early *Homo*, though in several measures the two groups can be distinguished (Table 10, Figure 13). In australopiths, superior facial height tends to account for a greater proportion of total facial height than in most early *Homo* specimens. MH1 falls within the range of values seen in early *Homo*, and outside the range seen in the australopiths, though there is some overlap between these latter groups. Comparing total facial height to bi-orbital breadth, MH1 aligns more closely with the australopiths than early *Homo*, reflecting the relatively narrow upper face in *Au. sediba*. Contrasting bi-zygomatic breadth in MH1 against superior facial height again highlights the narrow face of MH1, whose value is exceeded only by SK 847, though once again there is considerable overlap between the australopiths and early *Homo* specimens, and MH1 does not align closely with either group. Dividing superior facial breadth by bi-maxillary breadth, we see that MH1 has an upper face that is wider than its mid-face. This arrangement is more typical of early *Homo*, though as is seen elsewhere in the face, there is overlap between australopith and early *Homo* values, with some early *Homo* specimens revealing mid-faces that are slightly wider than the upper face (e.g., KNM-ER 1470, KNM-ER 3883, D2700). The greatest distinction between australopiths and early *Homo* is encountered when comparing superior facial

TABLE 10. FACIAL INDICES (W# indications refer to indices provided in Wood [1991]; letters in parentheses refer to values presented in Table 3).

Taxon	Specimen	Superior facial height / total facial height	Total facial height / bi-orbital breadth	Superior facial height / bi-zygomatic breadth	Superior facial breadth / bi-maxillary breadth	Superior facial breadth / bi-zygomatic breadth
		(k)/(j)	(j)/(m)	W xxix (k)/(n)	(l)/(o)	W xxxiv (l)/(n)
<i>Au. afarensis</i>	Mean	86	112			
	AL 417-1	84	106			
	AL 444-2	88	109	60		
<i>Au. africanus</i>	Mean	83	108	60	96	74
	Sts 5	84	105	59	90	75
	Sts 17		120		100	
	Sts 71	81	110	61	91	76
	StW 13	82				
	StW 53	88	91	54	99	70
	StW 505	83	113		98	
	MH1	78	112	67	102	84
<i>H. habilis</i>	Mean	78	99		105	84
	KNM-ER 1813	77	100	56	106	81
	OH 24	80	98		104	87
<i>H. rudolfensis</i>	KNM-ER 1470	83	107		94	
<i>H. erectus</i>	Mean	81	103	61	103	85
	BOU-VP-2/66					99
	D2282/211				110	80
	D2700/2735	72	107	59	99	83
	D4500/2600					75
	KNM-ER 3733	81	96	61	112	87
	KNM-ER 3883				86	80
	KNM-WT 15000			62	109	87
	Sangiran 17			55		83
	SK 847	88	106	71	102	88

breadth to bi-zygomatic breadth. In this index there is a clear separation between *Au. africanus* and early *Homo* that relates to the flaring of the zygomatics that occurs in australopiths, but not in specimens of early *Homo*, with the singular exception of D4500 and its widely flared zygomatics. In this measure, MH1 overlaps closely with early *Homo*, but not with any specimen of *Au. africanus*. The overall pattern is that the facial mask in *Au. africanus* is tapered superiorly and inferiorly from the bi-zygomatic breadth, resulting in a diamond-shaped appearance, while in early *Homo*, the fa-

cial mask is tapered inferiorly but with relatively vertically oriented lateral orbital margins that produce a squared superior facial profile. MH1 shares this pattern with early *Homo* specimens.

Kimbel and Rak (2017) suggested that had MH1 reached adulthood, the relative breadths of various components of the face would have altered considerably, to the point that MH1 would have resembled *Au. africanus*. In particular, they contend that the lack of flared zygomatics in MH1 was the result of its juvenile status. In contrast, as

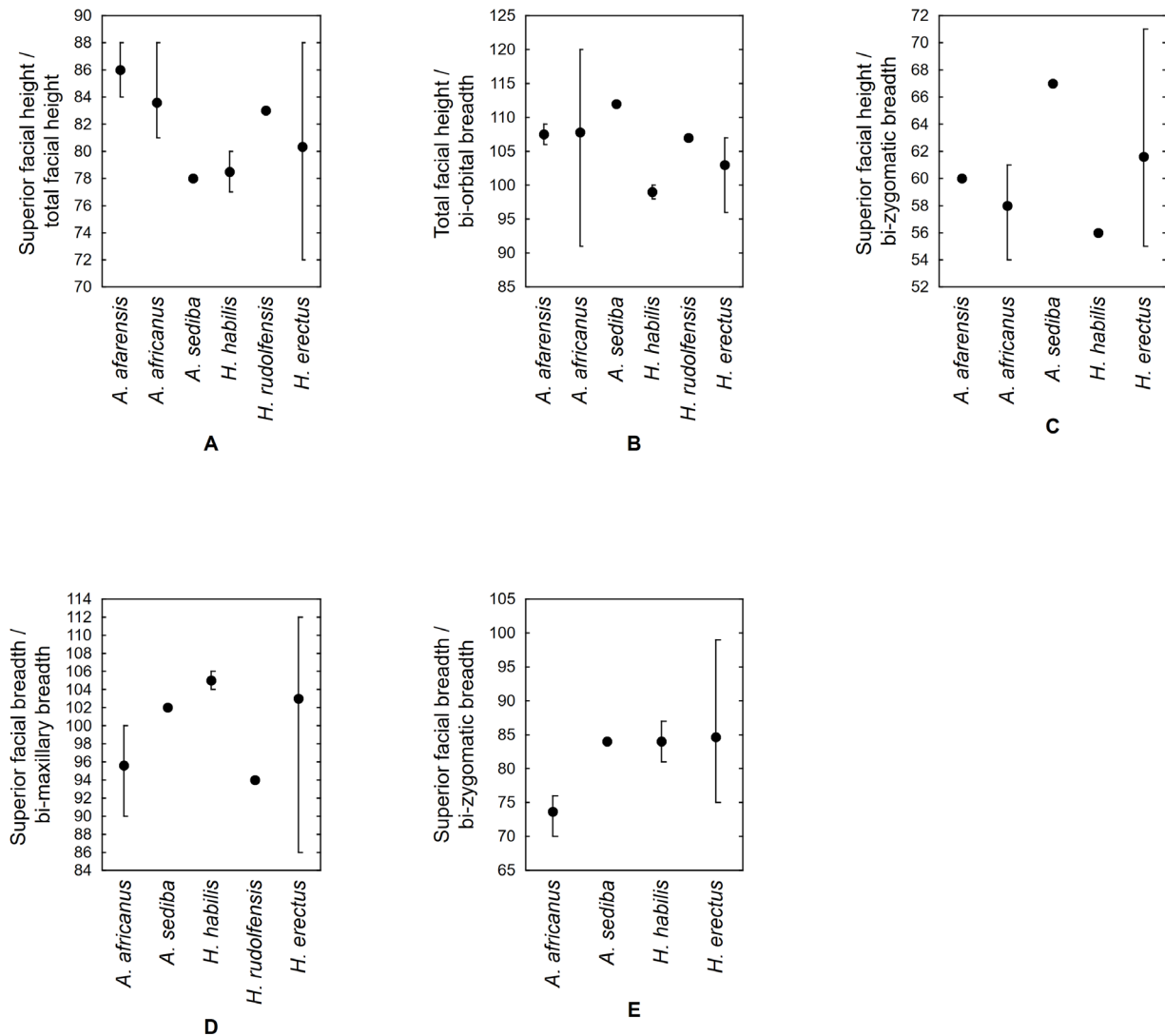


Figure 13. Facial mask indices: A) relative facial height; B) relative facial height / breadth I; C) relative facial height / breadth II; D) relative facial breadth I; E) relative facial breadth II. Points represent single values or means, whiskers represent min/max values. Data from Table 10.

discussed in more detail above, Carlson et al. (2016) demonstrated that relative zygomatic flaring would likely not have changed substantively had it lived to adulthood.

Facial Prognathism

Facial prognathism can be expressed in a series of angular measures (Table 11). Typically nasion is used as the superior point of measurement, though we agree with Kimbel et al. (2004) that because nasion is often difficult to detect, sellion is the preferred point of measurement. Overall facial prognathism is measured as the angle between the sellion-prosthion line and FH. The australopiths (including *Au. sediba*) and *H. habilis* all share overlapping, moderately sloping faces, while KNM-ER 1470 and most specimens of *H. erectus* show much more steeply inclined faces, the exception being the relatively prognathic SK 847. The nasal profile angle is measured between the sellion-nasospinale line and

FH. *Australopithecus afarensis*, *Au. africanus*, and *H. habilis* group together apart from KNM-ER 1470 and *H. erectus*, though once again SK 847 appears relatively prognathic. MH1 intersects with the australopiths and OH 24, and falls alongside SK 847. The alveolar profile angle is measured from the nasospinale-prosthion line to FH, and shows extensive overlap across all hominins. For instance, the difference between Sts 5 (37°) and Sts 52 (57°) encompasses the entirety of variability across all taxa, save only Sangiran 17 (72°). As a result, MH1 overlaps with specimens of both australopiths and early *Homo*. The angle of the nasal bones on the sellion-rhinion line relative to FH likewise shows extensive overlap across taxa. In this case, the difference between SK 847 (59°) and D2700 (81°) encompasses nearly all the variability in the entire hominin sample, minus only A.L. 417-1 (56°) and Sts 5 (58°). As before, MH1 overlaps with both australopith and early *Homo* specimens.

TABLE 11. ANGULAR MEASURES OF FACIAL PROGNATHISM.

Taxon	Specimen	Overall prognathism sellion- prosthion angle	Nasal profile angle sellion- nasospinale	Alveolar profile angle nasospinale -prosthion	Nasal bones angle sellion- rhinion	Nasal aperture angle rhinion- nasospinale
<i>Au. afarensis</i>	Mean	63	72	41	65	80
	AL 417-1	60	68	42	56	74
	AL 444-2	65	76	39	74	85
<i>Au. africanus</i>	Mean	61	67	48	69	66
	MLD 6/23	65				
	Sts 5	53	66	37	58	70
	Sts 52	63	68	57	67	67
	Sts 71	65	72	47	72	72
	StW 53	60	65	47	75	60
	StW 505	58	66	50	74	60
<i>Au. sediba</i>	MH1	61	70	40	66	72
<i>H. habilis</i>	Mean	63	73	42		
	KNM-ER 1813	65	76	47		
	OH 24	61	70	35	68	68
	OH 65			45		
<i>H. rudolfensis</i>	Mean	74		55		
	KNM-ER 1470	79	82	55		
	KNM-ER 62000	69		55		
<i>H. erectus</i>	Mean	70	81	48	70	89
	D2282/211			43		
	D2700/2735	73	83	45	81	84
	D4500/2600			42		
	KNM-ER 3733	81	90	44	69	112
	KNM-WT 15000	75	81	42		
	Sangiran 17			72		
	SK 847	63	73	46	59	78

Finally, considering the angle of the nasal aperture from the rhinion-nasospinale line to FH, we see some distinction between *Au. afarensis*, *Au. africanus*, and *H. habilis* relative to KNM-ER 1470 and *H. erectus*, though SK 847, and to a lesser extent D2700, appear relatively prognathic, falling near the mean for *Au. afarensis*. MH1 falls closest to the australopiths, though it does appear less prognathic than OH 24. In sum, though there is a great deal of overlap in angular measures of prognathism across the hominins, MH1 tends to correspond slightly more closely to *Au. africanus*, in particular in those measures where there is some indication of separation between the australopiths and early *Homo*, the sellion-prosthion angle and the rhinion nasospinale angle.

Infraorbital Plane Angle

Lordkipanidze et al. (2013) suggested that the angle that the infraorbital plane forms with the alveolar plane was diagnostic of early *Homo*. In *Au. afarensis*, the infraorbital plane is oriented at an obtuse angle relative to the alveolar plane, i.e., the infraorbital region is not coplanar with the orbital plane. In most specimens of *Au. africanus*, the infraorbital plane is oriented at an obtuse angle to the alveolar plane, though in specimens such as Sts 5, Sts 17, and StW 183 the two planes approach (but do not reach) a right angle. The infraorbital plane in KNM-ER 1470, KNM-ER 1813, OH 24, and probably KNM-ER 1805 and KNM-ER 62000, is set at an approximately right angle to the alveolar plane, a pat-

tern matched in all *H. erectus* specimens, and in all of these specimens the infraorbital plane is coplanar with the orbital plane. Likewise, the infraorbital plane in MH1 is set at an approximately right angle to the alveolar plane, appearing coplanar with the orbital plane (see Figure 1C). MH1 thus mirrors the condition seen in early *Homo*, eroding the utility of this character in diagnosing *Homo*.

Glabellar Region

In MH1, the glabellar region forms as a moderately prominent, square-shaped block, with a weakly palpable midline depression between the right and left halves of the supraorbital torus (see Figure 6). Wood (1991) hypothesized that a midline glabellar depression represented the derived condition in the hominid clade. However, given the high degree of variability in the development of this area across all of the hominins, it does not appear to be strongly taxonomically diagnostic. StW 505, for example, exhibits a clear midline depression, while other *Au. africanus* specimens do not. Lockwood and Tobias (1999) suggested that a midline glabellar depression was part of a pattern of variation relating to sex, as male humans showed the pattern of glabellar morphology similar to that of StW 505 more often than females. Thus the slight midline glabellar depression of MH1 likely relates more to its status as a male than to any particular taxonomic affinity. Notwithstanding this, the form of the glabellar block in MH1 is most similar to that of Sts 71 in overall appearance.

Supraorbital Torus And The Supratoral Sulcus

The moderately-developed supraorbital torus of MH1 is weakly but distinctly defined by a shallow supratoral sulcus (see Figures 1C and 6). This differs from the supraorbital bars encountered in A.L. 444-2, which are flat with no indication of a supratoral sulcus. Likewise, the supraorbital arch of *Au. africanus* is thin, does not project anteriorly, and is not delineated by a supratoral sulcus, thus it does not form as a supraorbital torus proper. The moderately thickened and anteriorly projecting torus of MH1 is bordered posteriorly by a distinct supratoral sulcus. As such, MH1 appears similar to specimens attributed to *H. habilis*, *H. erectus*, and *H. naledi*, all of which possess a distinct supratoral sulcus and therefore supraorbital torus proper. Although the supraorbital torus is sometimes only weakly defined (e.g., OH 16, OH 24, D2280, D2700, KNM-ER 3883, KNM-ER 42700), it is nonetheless comparable to the development we see in MH1. The only outlier among the early *Homo* sample is KNM-ER 1470, which lacks a supratoral sulcus, and thus a supraorbital torus proper. Setting this specimen aside, the morphology of the supraorbital torus and supratoral sulcus of *Au. sediba* corresponds most closely to that of early *Homo*.

Kimbel and Rak (2017) argue that because the supraorbital torus of *H. habilis* protrudes above the supratoral sulcus as a topographically discrete entity, while in MH1 it does not, the latter does not actually present a genuine supraorbital torus. We disagree with the notion that because the supraorbital morphology of MH1 is not identi-

cal to that of *H. habilis* it does not represent a supraorbital torus. Supraorbital development in MH1 is comparable to several early *Homo* specimens, and in specimens such as OH16, D2280, D2700, KNM-ER 3883, and KNM-ER 42700 in particular, the supraorbital torus does not protrude above the supratoral sulcus as a topographically discrete entity in a substantively different manner from MH1. We also disagree with their contention that the supraorbital morphology of MH1 is comparable to that of Sts 17 or TM 1511, neither of which are complete enough to fully assess. We therefore maintain that the supraorbital torus and supratoral sulcus of MH1 correspond most closely with that of early *Homo*.

Orbits And The Interorbital Region

The orbits in MH1 are roughly square-shaped (see Figure 6). In overall appearance they are closest to specimens of *Au. africanus*, though there is a similarity to *H. erectus* specimens such as D2700. The lateral orbital margin of MH1 (i.e., the frontal process of the zygomatic) faces anterolaterally in a gently curved arc. This arrangement is unlike the anterior orientation seen in *Au. afarensis*, and unlike the anteriorly oriented and ‘folded’ appearance of *Au. africanus* (Rak 1983). Instead, *Au. sediba* appears most similar to specimens of early *Homo* in the anterolateral orientation of the lateral orbital margin.

In absolute breadth and height of the orbits, there is a great deal of overlap among hominins (see Table 3). The orbits of MH1 stand out as being rather small, especially in orbital breadth, though orbital height intersects values in australopiths and early *Homo*. Likewise, in orbital shape there is considerable overlap in hominins, though MH1 again stands out as an exception in that the orbit is slightly taller than it is broad (Table 12, Figure 14). This is an unusual situation only recorded elsewhere in KNM-WT 15000 and in KNM-WT 17000. Absolute interorbital breadth tends to be smaller in australopiths and larger in early *Homo*, though there is overlap between specimens in the two groups (see Table 3). MH1 aligns with early *Homo* with an interorbital breadth that is wider than in australopiths. When we scale interorbital breadth to a series of cranial breadths, the distinction between australopiths and early *Homo* becomes slightly clearer (see Table 12). Though there continues to be overlap between groups, compared to bi-orbital breadth, superior facial breadth, or orbital breadth, australopiths once again appear relatively smaller than early *Homo*. Of greater importance is the fact that MH1 appears even more similar to specimens of early *Homo* in relative interorbital breadth. In particular, relative to bi-orbital breadth and to orbital breadth, MH1 is clearly delineated from the australopiths, while relative to superior facial breadth, the interorbital breadth of MH1 overlaps with Sts 71 alone among the australopiths, but otherwise aligns with *H. habilis*, *H. erectus* and *H. naledi*.

Rak et al. (1996) describe the morphology of the superior orbital fissure in apes and humans, noting that in the former it appears as a circular foramen, while in the latter it forms more of an elongated comma shape. They also noted

TABLE 12. ORBITAL REGION INDICES (W# indications refer to indices provided in Wood [1991]; letters in parentheses refer to values presented in Table 3).

Taxon	Specimen	Orbit shape	Interorbital breadth / biorbital breadth	Interorbital breadth / superior facial breadth	Interorbital breadth / orbit breadth
		W xxxii (p)/(q)	W xxxiii (r)/(m)	(r)/(l)	(r)/(p)
<i>Au. afarensis</i>	Mean	112	20		
	AL 417-1	117	19		
	AL 444-2	108	20		48
<i>Au. africanus</i>	Mean	113	21	19	50
	Sts 5	117	20	18	50
	Sts 52		23		54
	Sts 71	110	25	23	59
	StW 53	119	17	16	41
	StW 505	105	20	18	49
	MH1	97	26	23	65
<i>H. naledi</i>	DH3		27	24	72
<i>H. habilis</i>	Mean	107	26	23	67
	KNM-ER 1813	110	23	21	61
	OH 24	103	28	24	73
	Mean	117	23		58
<i>H. rudolfensis</i>	KNM-ER 1470	117	23	22	56
	KNM-ER 62000		23		59
	Mean	109	25	23	62
<i>H. erectus</i>	BOU-VP-2/66			26	
	D2280		26	25	
	D2700/2735	113	21	20	54
	KNM-ER 3733	117	22	19	55
	KNM-ER 3883	114	21	18	54
	KNM-WT 15000	93	31	28	79
	OH 9		27	23	
	SK 847	109	28	24	69

that all specimens of *Au. afarensis* and *Au. africanus* that preserve the region show the ape-like pattern, while 'robust' australopiths present the human-like pattern. Unfortunately no specimens of early *Homo* are well enough preserved or have the area visible to determine their arrangement. However, we would note that based on synchrotron scans of MH1, the superior orbital fissure appears as an elongated comma as in humans, and unlike other non-robust australopiths.

Arrangement, Shape, And Projection Of The Nasal Bones

In most hominins, including *Au. sediba*, the nasal bones present an hourglass shape, but with a superiorly convergent taper such that the widest part of the nasal bones occurs at their inferior extent (see Figure 6); KNM-ER 1470, on the other hand, presents nasal bones that are superiorly tapered, but not hourglass shaped. Overall, the hourglass shape of the nasal bones should not be considered overly diagnostic (Lockwood and Tobias 1999). The superior pro-

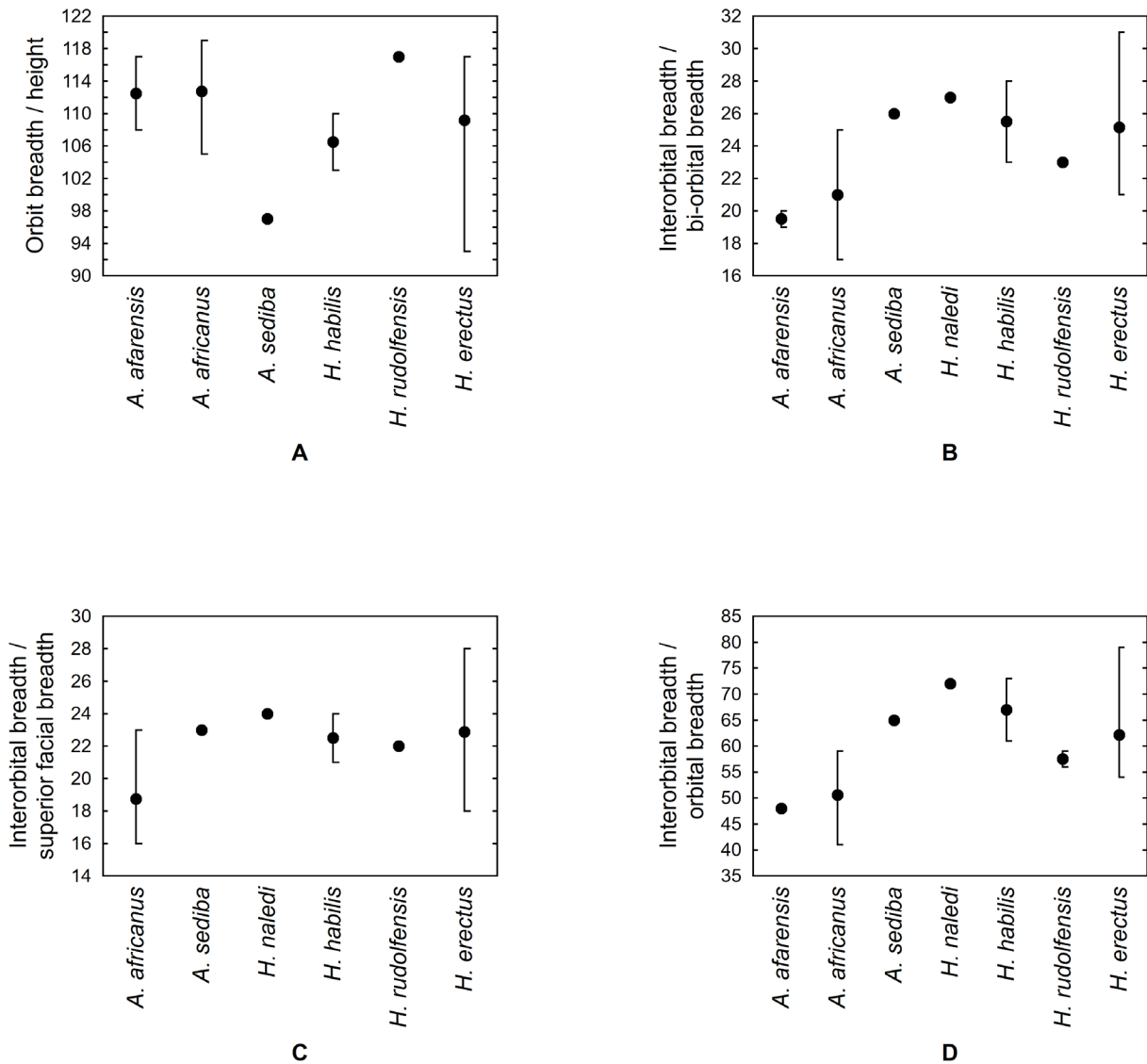


Figure 14. Orbital and interorbital indices: A) orbit shape; B) relative interorbital breadth I; C) relative interorbital breadth II; D) relative interorbital breadth III. Points represent single values or means, whiskers represent min/max values. Data from Table 12.

jection of the nasal bones in early hominins has been the matter of some debate over the years (Eckhardt 1987; Olson 1978, 1985; Strait et al. 1997). MH1 overlaps with specimens of both australopiths and early *Homo*, with a frontonasal suture that is continuous with the frontomaxillary suture in a superiorly concave arc. Indeed, Eckhardt (1987) has demonstrated that the frontonasal suture is highly variable in apes, and thus of little phylogenetic significance. The pinched-up internasal suture of MH1 corresponds to the arrangement seen in some, but not all, specimens of *Au. africanus* and early *Homo*. Looking at the height of the nasal bridge, it is notable that the nasion subtense of *Au. sediba* is similar to that of most specimens of early *Homo*, and unlike that of other australopiths (see Table 3). In other words, the nasal bridge of *Au. sediba* is relatively prominent. There is overlap between australopiths and early *Homo*, with speci-

mens such as OH 24 (possibly as a result of damage) and KNM-ER 1470 intersecting with the australopiths.

Turning to the size of the nasal bones, if we divide inferior nasal breadth by superior nasal breadth, we see a great deal of variability that nonetheless highlights the slightly narrower average breadth of the superior nasals in some specimens of *Au. africanus* (Table 13). However, when we scale the inferior breadth of the nasals to their length, there is a clearer distinction between *Au. africanus* and early *Homo* (Figure 15). In *Au. africanus*, the nasals tend to be relatively longer compared to their inferior breadth, resulting in lower index values, while in early *Homo*, the nasals tend to be relatively shorter. MH1 aligns most closely with early *Homo* in having relatively short nasals compared to inferior breadth, though there again is overlap between the australopiths and early *Homo*.

TABLE 13. NASAL BONE INDICES (letters in parentheses refer to values presented in Table 3).

Taxon	Specimen	Superior nasal bone breadth / inferior nasal bone breadth (t)/(u)	Inferior nasal bone breadth / nasal bone length (u)/(s)
<i>Au. africanus</i>	Mean	202	41
	MLD 6/23	367	46
	Sts 5	367	44
	Sts 52	138	39
	Sts 71	180	43
	StW 13	138	52
	StW 53		38
	StW 505	143	25
	MH1	163	54
<i>H. habilis</i>	Mean	129	61
	KNM-ER 1805	138	61
	KNM-ER 1813	219	69
	OH 24	120	52
<i>H. rudolfensis</i>	KNM-ER 1470	125	50
<i>H. erectus</i>	Mean	179	64
	D2700/2735	120	50
	KNM-ER 3733	238	73
	KNM-ER 3883	167	83
	KNM-WT 15000	129	
	SK 847	240	48

Premaxillary Suture

Contributing to the prominence of the nasals in MH1 is the remnant premaxillary suture at the superior lateral margins of the nasal aperture (Figure 16). Patent premaxillary sutures are known only in the australopiths among African early hominins (Clarke 1985, 2008; Maureille and Braga 2002). Such sutures have been recognized in A.L. 333-86, A.L. 333-105, LH 21a, the Taung Child, MLD 6, MLD 45, Sts 17, StW 53, and KNM-WT 17000 (Maureille and Braga 2002). The presence of a premaxillary suture is a character that appears to align *Au. sediba* with the australopiths.

Nasal Aperture, Canine Juga, And The Anterior Pillars

There is considerable overlap among hominins in absolute nasal aperture height and breadth, with *H. erectus* displaying somewhat broader apertures than the others (see Table 3). In relative terms, the nasal aperture of *Au. afarensis* stands out as comparatively tall and narrow, while *Au. africanus*, *Au. sediba*, and early *Homo* overlap with each other

and less so with *Au. afarensis* (Table 14). In most australopiths, the height of the nasal aperture accounts for roughly half of the total nasal height, while in early *Homo*, the nasal aperture tends to account for more than half of the total nasal height, though again there is overlap between the groups (Figure 17). MH1 is aligned more closely with the australopiths in relative nasal aperture height, approaching only OH 24 among early *Homo* specimens, though damage to the nasal regions in the latter is likely influencing this result. When we consider nasal aperture breadth relative to orbit breadth, *H. habilis* and *H. rudolfensis* overlap with the australopiths, while in *H. erectus* the relatively broad nasal aperture sets it apart from other hominins, the one exception to this being SK 847 and its relatively narrow aperture which intersects with australopiths. The narrow orbit in MH1 results in an aperture breadth index value that overlaps exclusively with *H. erectus*, and differentiates it from the australopiths as well as *H. habilis* and *H. rudolfensis*.

The lateral nasal aperture margins in MH1 (see Figure

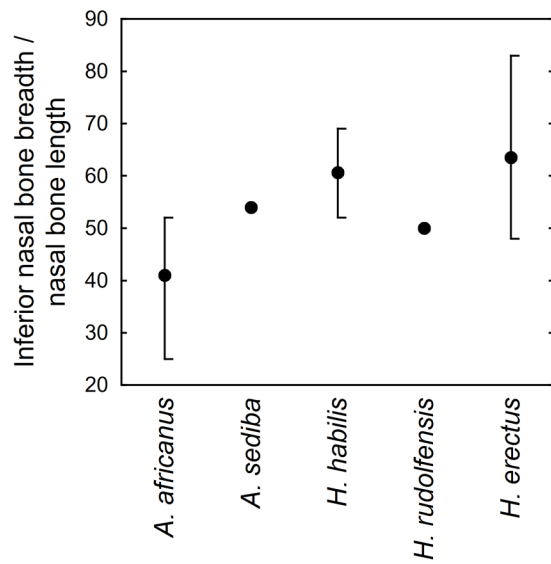


Figure 15. Inferior breadth of the nasal bones relative to nasal bone length. Points represent single values or means, whiskers represent min/max values. Data from Table 13.

6, Figure 18) are sharp superiorly and transition to bluntly rounded at about mid-aperture height as in other hominins with the exception of *Au. afarensis*, the latter which possesses sharpened aperture margins along their entire extent. MH1 does not display the anterior pillars (column-like structures beginning at the canine juga and running along the lateral margins of the nasal aperture that extend farther superiorly than the tip of the canine root, and that often incorporate not only the canine jugum but part of the P³ jugum as well) and attendant maxillary furrows that are variably developed in most, but not all, *Au. africanus* specimens (Sts 52, StW 391, StW 498, and TM 1512, for instance, lack anterior pillars; see Lockwood and Tobias 2002). And, while anterior pillars are absent in *Au. afarensis* and most specimens of early *Homo*, they are present, though weakly developed, in KNM-ER 1805 and OH 24. The canine juga of MH1 are clearly separated from the lateral nasal aperture margins, similar to what we typically, though not exclusively, see in early *Homo*.

Entrance To The Nasal Cavity

McCollum et al. (1993) reported on the topography of

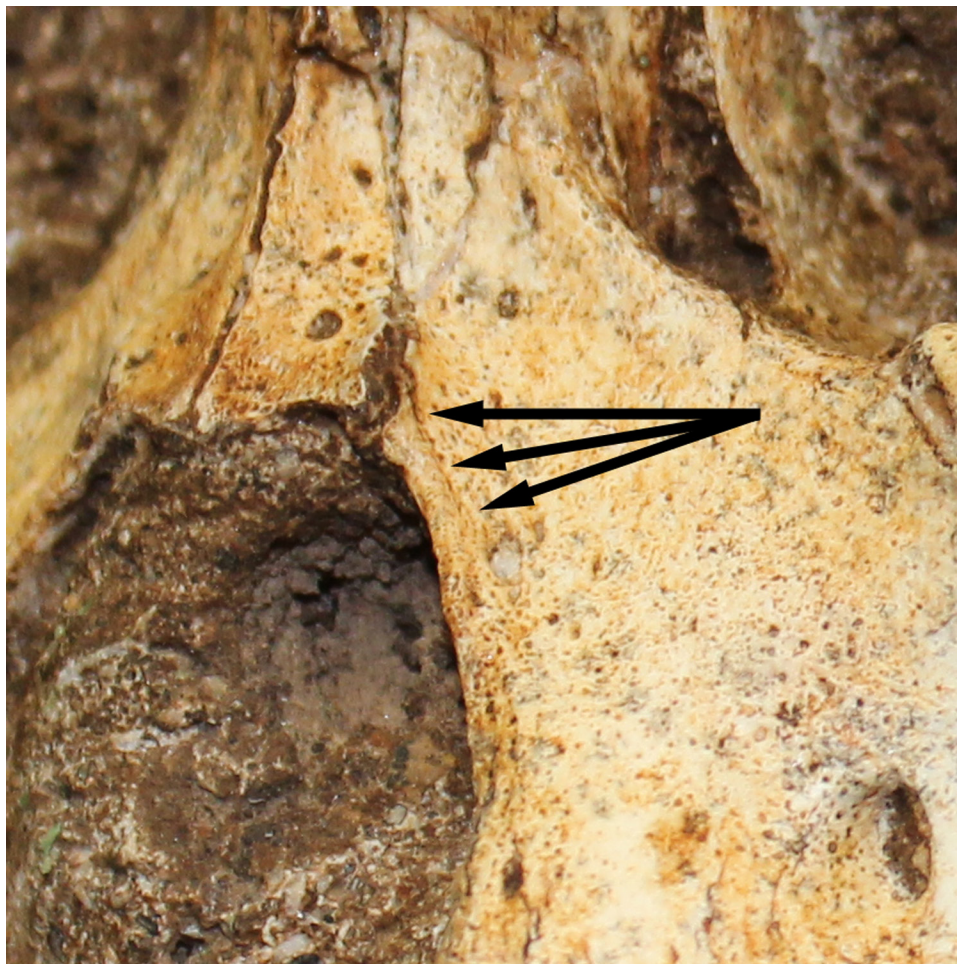


Figure 16. Premaxillary suture in U.W. 88-50. Arrows demarcate the line of the suture, which is bilaterally present.

TABLE 14. NASAL APERTURE INDICES
(letters in parentheses refer to values presented in Table 3).

Taxon	Specimen	Nasal aperture breadth / nasal aperture height (x)/(w)	Nasal aperture height / total nasal height (w)/(v)	Nasal aperture breadth / orbit breadth (x)/(p)
<i>Au. afarensis</i>	Mean	78	55	64
	AL 417-1	85	55	66
	AL 444-2	68	55	63
	AL 486-1	81		
<i>Au. africanus</i>	Mean	99	50	73
	MLD 6/23	87	51	
	Sts 5	113	49	79
	Sts 52	109	46	71
	Sts 71	90	62	76
	StW 13	86	52	
	StW 53	105	48	62
	StW 505	107	44	77
<i>Au. sediba</i>	MH1	108	49	84
<i>H. habilis</i>	Mean	95	59	73
	KNM-ER 1805	82	65	
	KNM-ER 1813	82	65	70
	OH 24	119	48	76
<i>H. rudolfensis</i>	Mean			70
	KNM-ER 1470	64	68	61
	KNM-ER 62000			79
<i>H. erectus</i>	Mean	100	58	81
	D2700/2735	90	62	80
	KNM-ER 3733	120	58	86
	SK 847	89	53	67

the nasal cavity entrance in early hominins, recognizing discrete patterns in the 'robust' australopiths that distinguished them from *Au. afarensis* and *Au. africanus*. They also noted substantial variability in the appearance of this area in early *Homo*. However, subsequent detailed analysis (McCollum 2000) revealed that the two subnasal morphologies that were originally identified were best divided into multiple discrete morphologies. McCollum (2000) noted that *Au. afarensis* and *Au. africanus* shared a subnasal morphology which she described as 'continuous-discrete', while the 'robust' australopiths exhibited what was referred to as a 'continuous-smooth' transition from the entrance of the nasal cavity to the floor of the nasal cavity. McCollum (2000) also noted that the majority of early *Homo* fossils that had been scored in the initial (McCollum et al. 1993) paper were

actually too damaged to provide meaningful information. As a result, only three specimens attributed to *Homo* could be scored with confidence: KNM-WT 15000, OH 62, and A.L. 666-1. In all three of these specimens, the subnasal morphology was reported as being smooth. Although the area in MH1 is obscured by calcified clastic sediment, we used synchrotron scans to determine that the subnasal morphology in this specimen is likely continuous-discrete, similar to that seen in *Au. afarensis* and *Au. africanus*.

McCollum et al. (1993) examined the height of the insertion of the vomer on the anterior nasal tubercle. McCollum (2000) revisited and updated her discussion of this character. In *Au. afarensis*, the vomer inserts high on the posterior face on the nasal sill. In *Au. africanus* the vomer inserts within the incisive fossa, below the nasal sill.

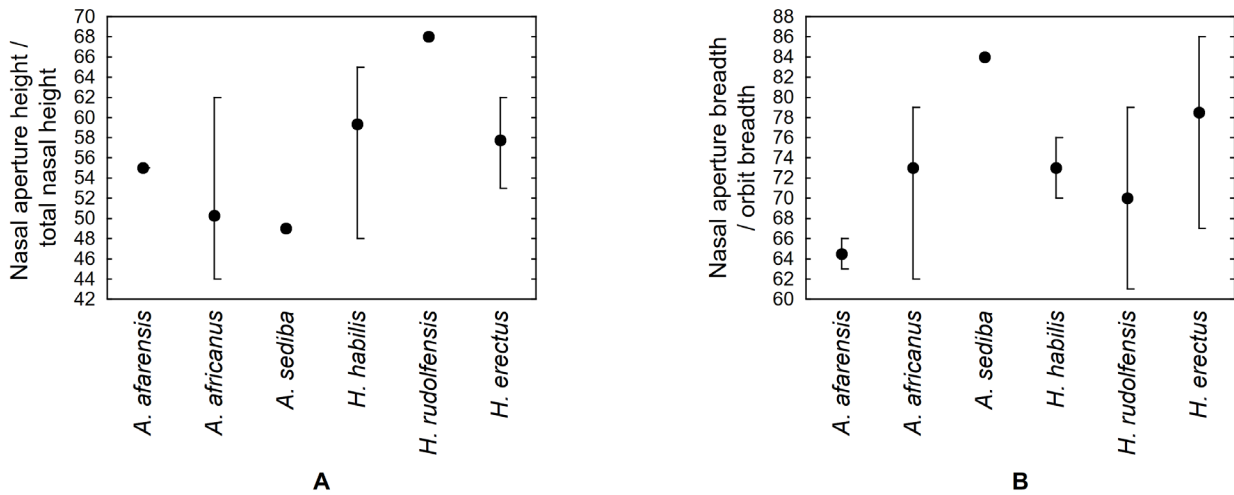


Figure 17. Nasal aperture indices: A) relative nasal aperture height; B) nasal aperture breadth relative to orbit breadth. Points represent single values or means, whiskers represent min/max values. Data from Table 14.

Examination of synchrotron scans of MH1 reveals that the vomer likely inserted within the incisive fossa, below the nasal sill as in *Au. africanus*. Unfortunately, no specimens of early *Homo* were well enough preserved to allow scoring (McCollum 2000).

Nasoalveolar Clivus

The nasoalveolar clivus of MH1 is slightly convex in both coronal and sagittal planes, with a gently convex incisor row (see Figures 1B, 18), similar to some specimens of *Au. africanus* (e.g., Sts 52) as well as to specimens of *H. habilis*

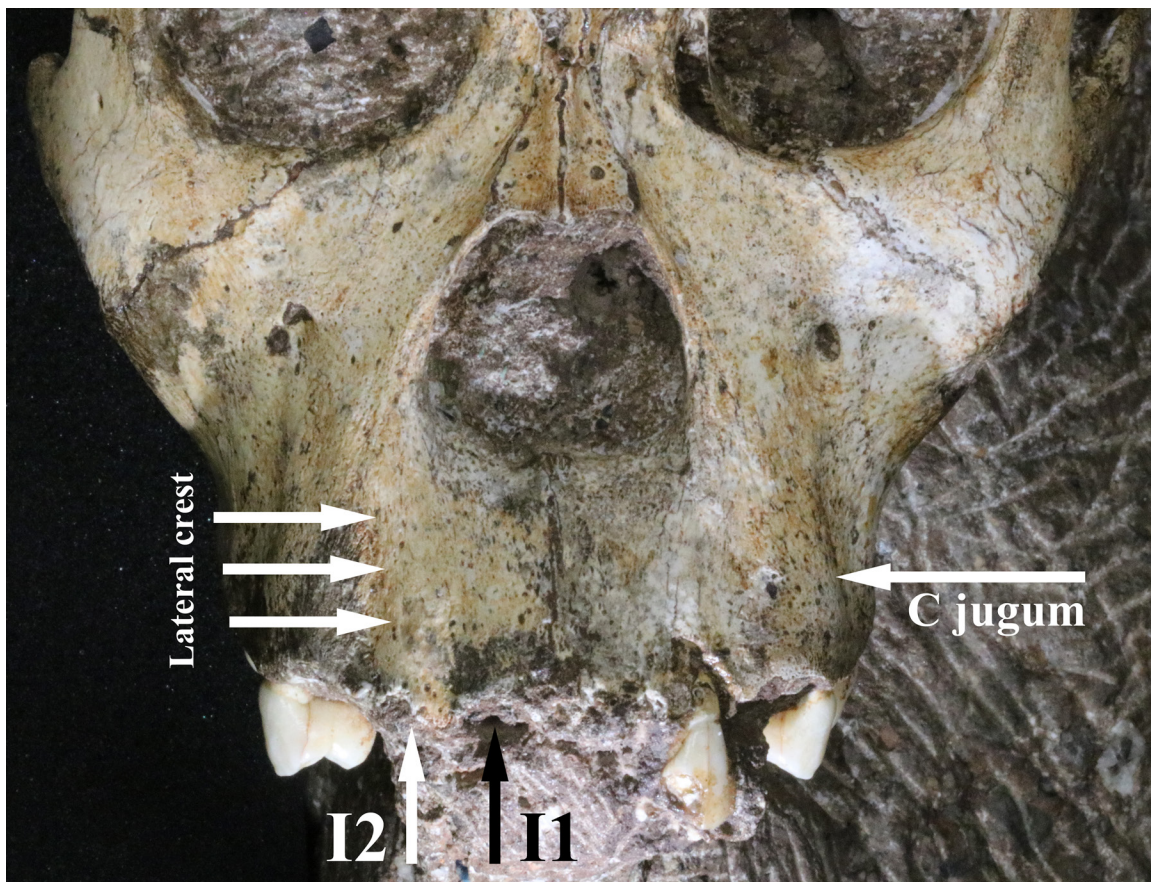


Figure 18. Close up view of nasal aperture and nasoalveolar region showing the canine jugum and the lateral crest. Note the absence of anterior pillars. Note also that the lateral crest does not incorporate the I_1 jugum.

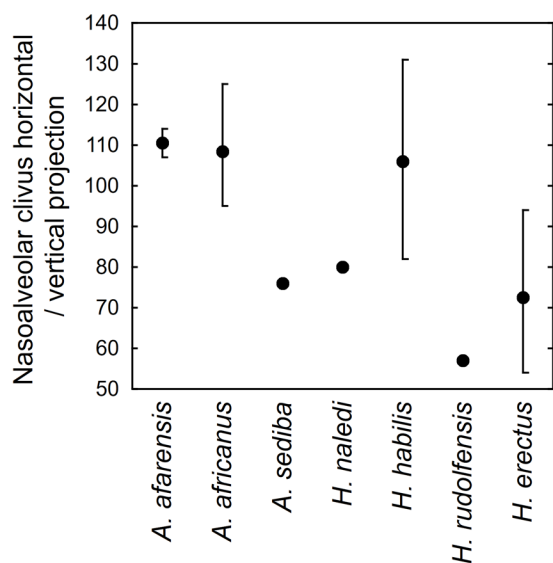


Figure 19. Nasoalveolar clivus projection index. Points represent single values or means, whiskers represent min/max values. Data from Table 15.

and *H. erectus*. In contrast, the clivus in *H. rudolfensis* is relatively flat and straight in coronal and sagittal planes, and the incisors are arranged in a straight line (e.g., KNM-ER 1470, KNM-ER 62000). A similar flatness in both the coronal and sagittal planes of the clivus is seen in *H. naledi*, though the incisors are gently arced beyond the bi-canine line. The lateral incisor root is positioned lateral to the lateral margin of the nasal aperture in *Au. afarensis*, while in *Au. africanus*, *Au. sediba*, and early *Homo* the lateral incisor root is either level with, or medial to, the lateral margins of the nasal aperture. The inter-maxillary suture in *Au. afarensis* and *Au. africanus* is either flat or slightly furrowed, while in early *Homo* it forms as a slightly elevated ridge traversing from the alveolar margin toward the nasal aperture; in OH 24 this ridge is especially well-developed and appears as a sharpened crest. MH1 shares this raised form of the inter-maxillary suture with specimens of early *Homo*, though it does not form as a sharpened crest.

Alveolar height in *Au. afarensis* is substantial owing to the great projection of the nasoalveolar clivus (see Table 3). In *Au. africanus* mean alveolar height is less than that of *Au. afarensis*, though there is overlap between the two groups, and between *Au. africanus*, *Au. sediba*, and specimens of early *Homo* in absolute values. However, comparing alveolar height to superior facial height, *Au. afarensis* stands out as having a notably elongated nasoalveolar clivus compared to all other hominins (Table 15).

When we measure the horizontal projection from subnasale to prosthion versus the vertical projection from subnasale to prosthion, we get a mean value of 111 for *Au. afarensis*, indicating that the horizontal projection is greater than the vertical projection (see Table 15, Figure 19). When we compare the same in *Au. africanus*, most specimens show a longer horizontal projection ($\chi=108$). The only standout

is Sts 52, which has a relatively vertically projecting, but not so much horizontally projecting, clivus (95). StW 53 is close to the other *Au. africanus* specimens in having a relatively greater horizontal projection of the clivus (112). Early *Homo* specimens KNM-ER 1805 (131) and OH 24 (105) have a relatively more horizontally projecting clivus, while DH1 (80), KNM-ER 1813 (82), and, in particular, KNM-ER 1470 (57), have a clivus that is taller than it is long, i.e., more vertically projecting. All specimens of *H. erectus* have a clivus that is taller than it is long; SK 847 (54) stands out as having the greatest vertical over horizontal projection of the clivus in the entire hominin sample. In the relative vertical versus horizontal projection from subnasale to prosthion, MH1 (76) falls within the range of variation of early *Homo*, though in turn there is overlap between australopiths and *H. habilis* owing to KNM-ER 1805 and OH 24. In this case, we can more closely align *Au. sediba* with early *Homo*, as both share a clivus that is more vertically projecting than it is horizontally projecting.

Kimbel and Rak (2017) discuss the level of nasoalveolar prognathism in MH1, arguing that nasospinale would have been a better point to measure than subnasale as Berger et al. (2010) used (Berger et al. [2010] utilized subnasale following Wood [1991]). By using nasospinale, Kimbel and Rak (2017) recorded a horizontal projection of 16mm instead of 13mm as in Berger et al (2010). However, even at 16mm in length, the nasoalveolar clivus is less horizontally projecting in MH1 than it is vertically projecting (17mm), as we recorded above and in Table 15. In addition, even using their preferred method for measuring prognathism, Kimbel and Rak (2017) record a value for MH1 that still falls within the range of variation of *H. habilis*. As a result, MH1 still resembles *Homo*, while we continue to observe that there is overlap between *Homo* and *Australopithecus* in this measure.

Gower (1923) identified three crests near the inferior border of the nasal aperture of humans. The lateral crest arises from the lateral margin of the nasal aperture and continues onto the nasoalveolar clivus; the spinal crest branches laterally from the anterior nasal tubercle/spine and when present forms a boundary between the clivus and the floor of the nasal aperture; the turbinal crest arises from the anterior extent of the inferior turbinal bone, and possibly reaches the midline near the anterior nasal tubercle/spine. These three crests can fuse together and/or become obscured in myriad ways, and thus are difficult to identify with precision. MH1 presents a low, rounded spinal crest demarcating the nasal aperture, as well as a low, rounded lateral crest coursing from the inferolateral margin of the nasal aperture to contact the juga of the lateral incisor (see Figure 18). Lockwood and Tobias (1999) noted that *Au. africanus* was unique among hominins in possessing a lateral crest that incorporated both the lateral and medial incisor juga. The lateral crest that we see in MH1 differs from this pattern in that the central incisor jugum is not incorporated into the lateral crest, a pattern which Lockwood and Tobias (1999) also noted occurred in some chimpanzees and humans, as well as some fossils such as A.L. 200-1 and KNM-

TABLE 15. NASOALVEOLAR CLIVUS INDICES (W# indications refer to indices provided in Wood [1991]; Letters in parentheses refer to values presented in Table 3).

Taxon	Specimen	Alveolar height / superior facial height	Clivus horizontal / vertical projection
		(y)/(k)	W xxxv (z)/(aa)
<i>Au. afarensis</i>	Mean		111
	AL 199-1		114
	AL 200-1		107
	AL 417-1	41	
<i>Au. africanus</i>	Mean	34	108
	Sts 5	34	109
	Sts 52	32	95
	Sts 53		107
	Sts 71	32	107
	StW 13	38	104
	StW 53	36	112
	StW 505		125
<i>Au. sediba</i>	MH1	32	76
<i>H. naledi</i>	DH1		80
<i>H. habilis</i>	Mean	35	106
	KNM-ER 1805	30	131
	KNM-ER 1813	38	82
	OH 24	39	105
<i>H. rudolfensis</i>	Mean	33	
	KNM-ER 1470	34	57
	KNM-ER 62000	32	
<i>H. erectus</i>	Mean	33	72
	D2282/211		80
	D2700/2735	29	69
	KNM-ER 3733	37	66
	KNM-WT 15000	29	94
	SK 847	38	54

ER 1813. As a result, the development of the lateral crest in MH1 is not taxonomically diagnostic.

Anterior Nasal Tubercle

In extant humans the anterior nasal spine tends to be a large, prominent structure, though in fossil hominins it tends to be less well-developed, thus we refer to it as an anterior nasal tubercle. In *Au. afarensis* and *Au. africanus*, the anterior nasal tubercle is small, roughened elevation that is positioned behind the lateral margins of the nasal aperture. Specimens attributed to *H. habilis*, *H. rudolfensis*, and *H. erectus* typically exhibit a weak to moderately devel-

oped tubercle, though in OH 24 and Sangiran 4 it forms a prominent crest. Early *Homo* specimens differ from the australopiths in that the anterior nasal tubercle is positioned either level with, or anterior to, the lateral margins of the nasal aperture in the former, and posterior to the aperture margins in the latter. MH1 is closest to the arrangement in early *Homo*, in that the anterior nasal tubercle is positioned slightly anterior to the lateral nasal aperture margins (see Figures 6 and 18).

Relation Of The Zygomatics To The Face

The root of the frontal process of the zygomatic in *Au. afa-*

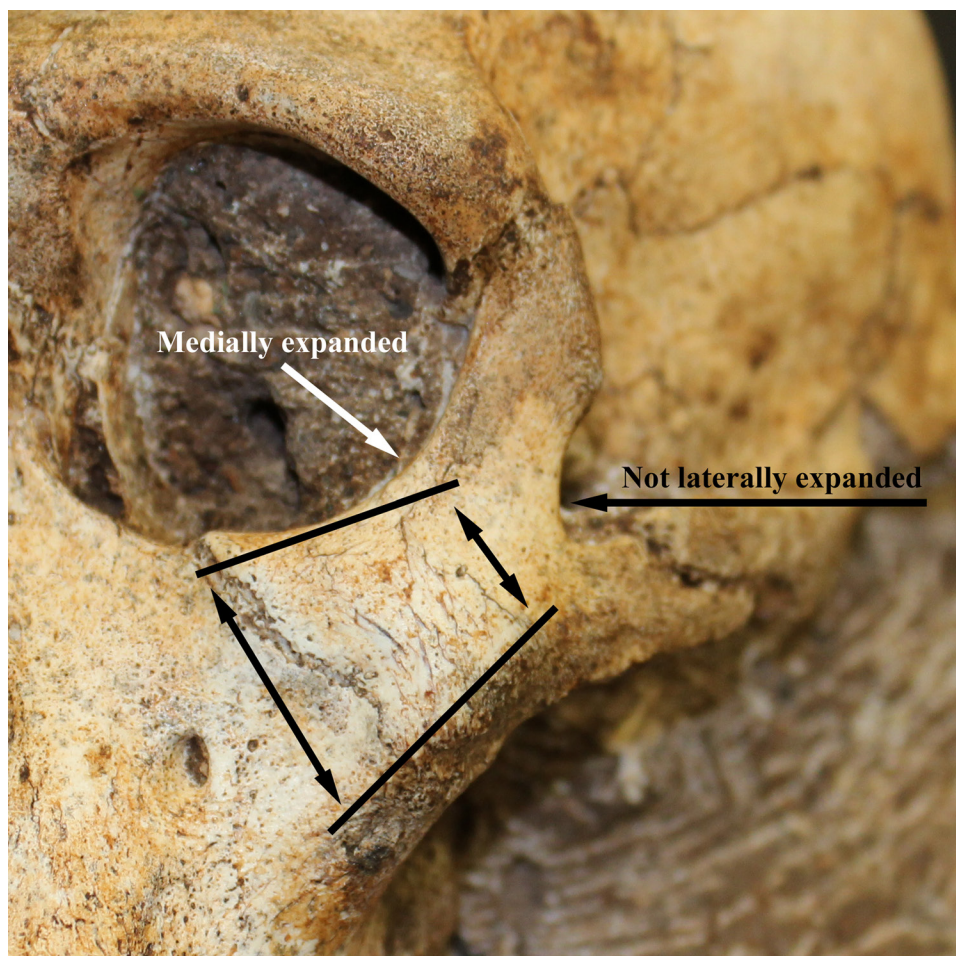


Figure 20. Close up view showing the medial, but not lateral, expansion of the orbit margin and the tapering of the malar region.

rensis and *Au. africanus* is both medially and laterally expanded, a feature Rak (1983) first recognized as diagnostic of the australopiths. This includes StW 53, which is traditionally considered to represent early *Homo*, but which we consider to be better positioned in *Au. africanus*. In contrast, Grine et al. (2013) opined that since StW 53 does not preserve the inferolateral corner of the orbit, i.e., the medially expanded portion, we were perhaps unable to differentiate bone from plaster in our previous report (Berger et al. 2010). Since the original fossil is not encased in plaster, we presume Grine et al. (2013) based their diagnosis on a cast of the reconstructed fossil, whereas we examined the original. As was indicated in the initial description of the morphology of this region (Rak 1983: 15), it is the lateral expansion of the bone that defines the importance of this character, as medial deviation of the frontal process of the zygomatic occurs in all hominins as it widens to form the inferolateral orbital margin. In other words, the lack of preserved bone in the inferolateral corner of the orbit in StW 53 does not influence the diagnosis of this character, as the preserved frontal process of the zygomatic is visibly laterally expanded. The frontal process of the zygomatic in early *Homo* differs from the australopiths in that it is only medially expanded to accommodate the inferolateral orbit-

al margin, and not laterally expanded (Rak 1983). In MH1, the root of the frontal process of the zygomatic is medially, but not laterally, expanded as in early *Homo*, and unlike the arrangement in *Au. africanus* or *Au. afarensis* (Figure 20). As a result, the medial-only expansion of the root of the frontal process of the zygomatic aligns *Au. sediba* with early *Homo*.

The zygomatics of MH1 are moderately robust (see Table 3) and are oriented anterolaterally. There is a weak zygomatic prominence similar to *Au. africanus*, and the anterior face of the bone meets the lateral face at an angle just wider than 90 degrees. The zygomatic arch is thin, with a superior border positioned slightly above the inferior margin of the orbit. The anterior-most projection of the zygomatics is about level with sellion. In all these regards, the zygomatics of MH1 are generally aligned with *Au. africanus* and not early *Homo*, though the zygomatics are not well preserved in *H. habilis* and *H. rudolfensis*. Where MH1 differs from *Au. africanus* is in the lack of flaring of the zygomatics, which more clearly aligns *Au. sediba* with specimens of early *Homo*. While the zygomatics are generally lacking in *H. habilis* and *H. rudolfensis*, there is no indication that they would have been widely flared. In addition, there are multiple representatives of *H. erectus* and *H. naledi* that appear similar to that of *Au. sediba* in being unflared.

Kimbel and Rak (2017) indicated that had it survived into adulthood, the zygomatics of MH1 would likely have become considerably more flared and *Au. africanus*-like, though as noted above, Carlson et al. (2016) concluded that relative zygomatic flaring would likely not have changed substantively had MH1 lived to adulthood. Kimbel and Rak (2017) also note that the zygomatic prominence of MH1 appears similar to that of *Au. africanus*, a point with which we agree. However, although Kimbel and Rak (2017) indicate that the zygomatic prominence in *Au. africanus* does not involve the masseter origin site, the anterior extension of the zygomatic prominence is influenced by the powerful development of the masseter origin in MH1 (see Figure 20).

Zygomaticoalveolar Crest And The Origin Of Masseter

In MH1, the root of the zygomatic is located above the level of P⁴/M¹ (see Figure 1C), overlapping broadly with both australopiths and early *Homo* (see Lockwood and Tobias 1999). Despite the small size of the cranium, the root of the zygomatic is quite thick, which sets MH1 apart from *H. habilis*, though not from other hominins (see Table 3). In *Au. afarensis*, the malar region is either squared in shape (A.L. 444-2) or actually expands laterally (A.L. 333-1) relative to the inferior orbit margin. In contrast, in MH1 (see Figure 20), *Au. africanus*, and some specimens of early *Homo* (e.g., KNM-ER 3773, KNM-WT 15000) there is a distinctly laterally narrowing, tapered shape to the malar region, while other specimens of early *Homo* possess a more square-shaped, non-tapered malar region. The shape of this region is clearly influenced by the steep inclination of the zygomaticoalveolar crest. The zygomaticoalveolar crest in *Au. afarensis* is moderately to markedly curved with a clearly defined malar notch, though a malar tubercle is generally absent. The zygomaticoalveolar crest in *Au. africanus*, on the other hand, is relatively long, straight, and steeply inclined, and a malar notch and tubercle are usually absent. StW 53 departs slightly from this pattern in that it reveals a slight malar tubercle which gives the appearance of a slight malar notch, though these structures are located on an otherwise long, straight, and steeply inclined zygomaticoalveolar crest. In addition, a weak malar tubercle is also evident in Sts 5 and Sts 71 at the anterior extent of the origin of masseter, even if they do not result in a malar notch. In specimens of early *Homo*, the zygomaticoalveolar crest is shorter, more horizontally inclined, with a weak to moderately defined malar notch and tubercle. Interestingly, the D4500 cranium does have a relatively long and straight zygomaticoalveolar crest, though it is more horizontally inclined than is seen in *Au. africanus* specimens. The relatively long, straight, and steeply inclined zygomaticoalveolar crest in MH1 (see Figures 6 and 20), with its high position for the origin of masseter is similar to *Au. africanus*, and unlike *Au. afarensis* and early *Homo*.

Kimbel and Rak (2017) discuss the steeply inclined zygomaticoalveolar crest of MH1, which they consider to be synapomorphic with *Au. africanus*. We agree with their assessment of the similarity between *Au. sediba* and *Au. africanus* in the development of this structure (see also Berger et

al. 2010). However, we are not as confident that this feature is synapomorphic, because chimpanzees and gorillas can likewise exhibit long, steeply inclined zygomaticoalveolar crests, though we do recognize that the relatively shortened appearance of the zygomatic bodies of *Au. sediba* and *Au. africanus* contrasts that of early *Homo*, chimpanzees, and gorillas.

MAXILLOALVEOLAR PROCESS AND PALATE

Size And Shape Of The Maxilloalveolar Process

In both length and breadth of the maxilloalveolar process there is considerable overlap between the australopiths and early *Homo* (see Table 3). The small maxilloalveolar process of MH1 falls only marginally below *Au. africanus* in terms of length, and only marginally above *H. habilis* and *H. erectus*, while it is the same as KNM-ER 62000 of *H. rudolfensis*. In absolute breadth, MH1 tends to be narrower than early *Homo* and most australopith specimens. Converting to a maxilloalveolar index of breadth divided by length, there remains significant overlap between the groups, while MH1 falls slightly below values seen in *H. habilis* and KNM-ER 62000 of *H. rudolfensis*, but otherwise overlaps with the australopiths and *H. erectus* (Table 16, Figure 21). The third molar is unerupted but the crown is formed in the crypt in MH1, thus there would have been some additional growth in the length of the maxilloalveolar process that would make it appear even more australopith-like (i.e., long and narrow) had it grown to adulthood. If we compare maxilloalveolar breadth to superior facial height, MH1 can be distinguished slightly from *H. habilis* and *H. rudolfensis*, but intersects with *Au. afarensis*, *Au. africanus* and *H. erectus*. Comparing maxilloalveolar breadth to bi-orbital breadth, MH1 intersects with *Au. afarensis*, *Au. africanus*, and *H. rudolfensis*, but can be delineated from *H. habilis* and *H. erectus*. And, if we divide maxilloalveolar breadth by bi-maxillary breadth, MH1 overlaps with *Au. africanus* but not with early *Homo*, though there is overlap between these two latter groups. The overall result is that *Au. sediba* generally appears more similar to australopiths than to early *Homo* in terms of maxilloalveolar shape, if not in absolute size, though the separation between australopiths and early *Homo* is not distinct.

Turning to various segments of the dental arcade, although there is overlap between australopiths and early *Homo* in the length of the incisor alveoli, MH1 presents a measure that is slightly higher than that seen in *Au. afarensis*, *Au. africanus*, *H. naledi*, or *H. rudolfensis*, but which intersects with *Au. anamensis*, *H. habilis* and *H. erectus* (see Table 3). Converting to an index of incisor alveolar length divided by maxilloalveolar length, MH1 approaches the values seen in *Au. anamensis* and early *Homo* (see Table 16). The mesiodistal length of the canine alveolus in MH1 intersects with *Au. afarensis*, *Au. africanus*, *H. rudolfensis*, and *H. erectus*, but differs very slightly from *Au. anamensis*, *H. naledi*, and *H. habilis*. Comparing canine alveolus length to maxilloalveolar length, MH1 now intersects with *Au. anamensis*, *Au. afarensis*, *H. rudolfensis*, and *H. erectus*, but not

TABLE 16. MAXILLOALVEOLAR INDICES (W# indications refer to indices provided in Wood [1991]; letters in parentheses refer to values presented in Table 3).

		Maxillo- alveolar breadth / maxillo- alveolar length	Maxillo- alveolar breadth / superior facial height	Maxillo- alveolar breadth / bi- orbital breadth	Maxillo- alveolar breadth / bi- maxillary breadth	I ¹ -I ² alveolar length / maxillo- alveolar length	Canine alveolus length / maxillo- alveolar length	P ³ -P ⁴ alveolar length / maxillo- alveolar length
		W1						
Taxon	Specimen	(ab)/(ac)	(ab)/(k)	(ab)/(m)	(ab)/(o)	(ad)/(ab)	(ae)/(ab)	(af)/(ab)
<i>Au. anamensis</i>	KNM-KP 29283	96				24	13	24
<i>Au. afarensis</i>	Mean	104	82	80		21	13	22
	AL 199-1	115				22	14	20
	AL 200-1	94				21	11	20
	AL 417-1	100	82	73				
	AL 444-2	108	82	86				
<i>Au. africanus</i>	Mean	95	91	85	70	20	10	22
	Sts 5	89	92	81	65	16	8	18
	Sts 17	95		84	68	20	9	23
	Sts 52	100	96	87	79	21	10	25
	Sts 53	94				19	10	19
	Sts 71	95	99	88	72	18	11	20
	StW 13	88	85		68	19	9	22
	StW 53	104	100	80	76	21	10	24
	StW 73	94				23	11	25
	StW 505		77	72	65			
<i>Au. sediba</i>	MH1	100	84	81	75	25	13	29
<i>H. naledi</i>	DH1	80				23	12	25
<i>H. habilis</i>	Mean	106	100	77	71	23	11	25
	KNM-ER 1805	101	101			21	10	23
	KNM-ER 1813	107	98	76	72	26	11	26
	OH 24	110	100	78	70	21	11	26
<i>H. rudolfensis</i>	Mean		89	83				
	KNM-ER 1470		87	77	69			
	KNM-ER 62000	105	92	89		22	13	25
<i>H. erectus</i>	Mean	102	84	68	66	24	12	21
	D2282/211	98		68	69	23	12	20
	D2700/2735	105	93	71	66	23	13	21
	KNM-ER 3733	105	80	62	62	27	11	19
	KNM-WT 15000	100	86	66	66	27	11	23
	Sangiran 4	104						
	SK 847	102	79	73	65	20	11	22

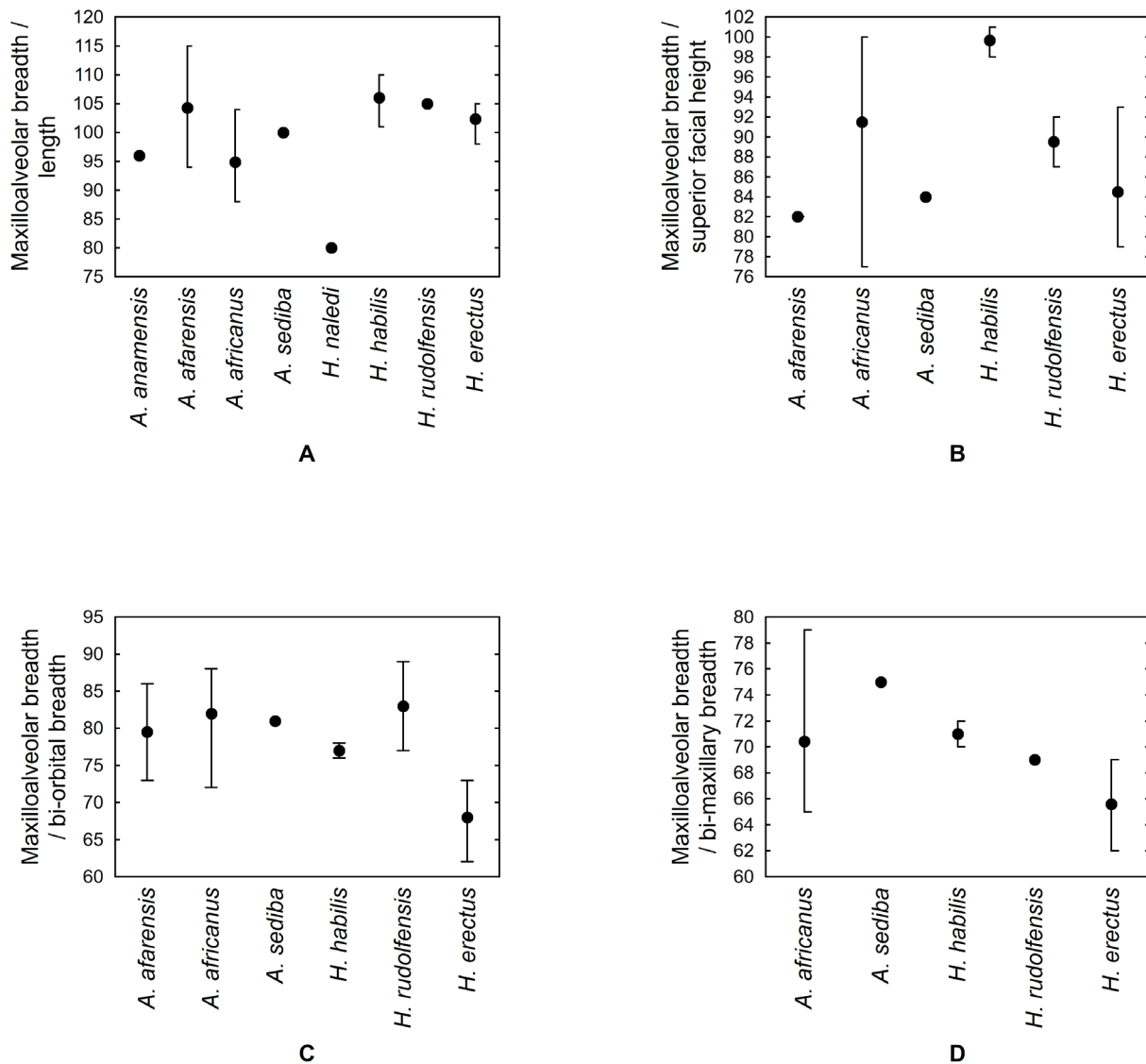


Figure 21. Maxilloalveolar indices: A) maxilloalveolar shape; B) maxilloalveolar breadth relative to superior facial height; C) relative maxilloalveolar breadth I; D) relative maxilloalveolar breadth II. Points represent single values or means, whiskers represent min/max values. Data from Table 16.

with *Au. africanus*, *H. naledi*, or *H. habilis*, though the differences are small. MH1 has a relatively enlarged premolar row that exceeds that of *Au. afarensis* and early *Homo*, but which intersects with *Au. africanus*, in particular Sts 52. In premolar alveolar length relative to maxilloalveolar length, MH1 is uniquely elongated compared to other hominins (Figure 22). In sum, the absolute and relative length of the incisors and the canines do not align *Au. sediba* with any particular group to the exclusion of another, apart from a uniquely elongated premolar row.

Size And Shape Of The Palate

Palate length overlaps considerably across the australopiths and early *Homo* (see Table 3). Palate breadth also shows overlap among these groups, though in general, australopiths are on the narrow end of the spectrum and

early *Homo* is on the wider end. In absolute length, MH1 intersects with *Au. afarensis*, *H. habilis*, *H. rudolfensis*, and *H. erectus*, while falling slightly below the range of *Au. africanus*. In absolute breadth at the M², MH1 falls within the range of *Au. afarensis* exclusively, revealing a narrower palate than other hominins. Dividing palate breadth by palate length, an even clearer pattern emerges. MH1 intersects with *Au. afarensis* and *Au. africanus* alone, and outside the range of early *Homo* (Table 17, Figure 23). Turning to absolute interalveolar distances mesial to the M², MH1 intersects with both australopiths and early *Homo* at the level of the C and P³, though by the level of the P⁴ the similarity with early *Homo* is diminished, again revealing an australopith-like narrow palate (see Table 3). We can express this pattern in the form of two wedging indices, one computed as an angle of tooth row divergence between canine and

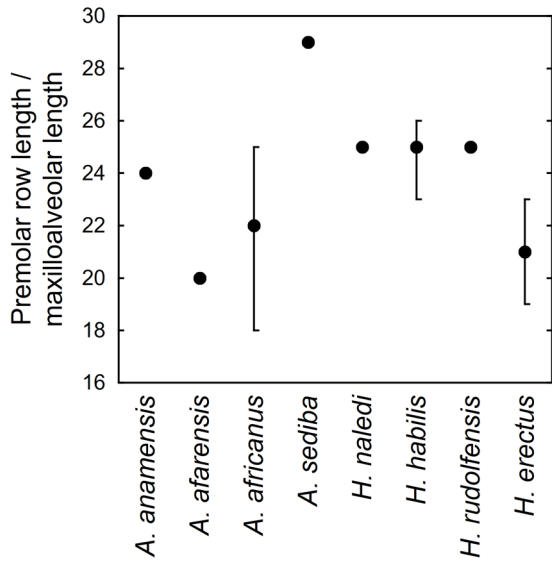


Figure 22. Relative premolar row length. Points represent single values or means, whiskers represent min/max values. Data from Table 16.

M² interalveolar distances (Wedging Index I; see Ward et al. 1999), and the other as an index dividing palate breadth at the M² by palate breadth at the canine (Wedging Index II) (see Table 17, see Figure 23). In the former, *Au. anamensis* has an especially narrow palate that in one case further narrows posteriorly, while *Au. afarensis* and *Au. africanus* both reveal palates that diverge only slightly. Early *Homo* in general reveals moderate wedging, though specimens of *H. naledi*, *H. habilis* and *H. erectus* in particular show especially divergent tooth rows. The narrow palate of MH1 falls closest to specimens of *Au. anamensis* and *Au. afarensis*, approaching only StW 73 within *Au. africanus*. Looking to the index of palate breadth at the M² versus the C, a similar pattern emerges, except that MH1 looks relatively even nar-

rower, mirroring only *Au. anamensis* in its relative lack of widening. Although there is notable overlap between australopiths and *Homo* in both wedging indices, MH1 clearly falls closest to the australopiths, showing a palate that widens only minimally.

MH1 has a moderately deep palate that shallows anteriorly, with a somewhat abrupt transition from the palate to the incisive alveolar margin that occurs at about the level of the incisive fossa (see Table 3). This differs from the shallow palate of *Au. anamensis* and *Au. afarensis*, and is more similar to that of *Au. africanus* and early *Homo*.

Relationship Between Elements Of The Masticatory System

Rak (1983) devised five indices to express the extent to which the dental arcade is retracted beneath the braincase, and the extent to which the masseter muscle is placed anterior to the temporomandibular joint. The protrusion of the palate anterior to sellion is greatest in *Au. afarensis* and *Au. africanus*, and least in early *Homo* (Table 18). There is some overlap, however, with some australopiths (e.g., Sts 52) appearing *Homo*-like, and early *Homo* specimens (e.g., OH 24 and D4500) appearing australopith-like. MH1, like Sts 2, is *Homo*-like, corresponding to both *H. habilis* and *H. erectus*. The protrusion of the palate anterior to the origin of masseter shows considerable overlap across the hominins, and MH1 intersects with both *Au. africanus* and *H. erectus*. The anterior position of the masseter origin relative to the articular eminence is similar across the australopiths, including *Au. sediba*, showing some overlap with *H. habilis* (OH 24), while plotting apart from *H. erectus*. The proximity of the M³ to the articular eminence tends to separate *Au. afarensis* and *Au. africanus* from early *Homo*, though there is some overlap between the groups. Since the M³ is not erupted in MH1, we added its mesiodistal length (determined via synchrotron scan) to the molar row to estimate its distance to the articular eminence. The proximity of the M³ to the articular eminence aligned MH1 exclusively with

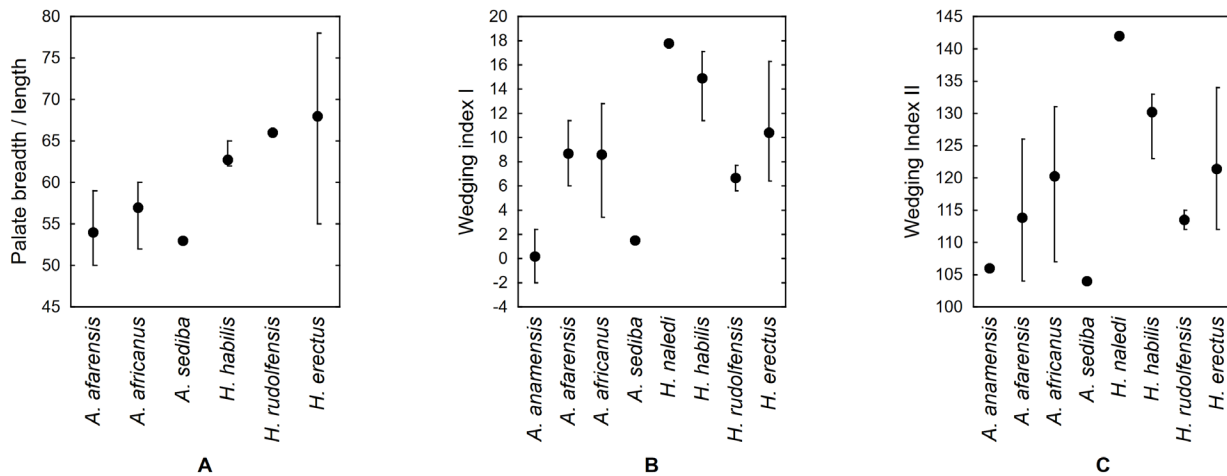


Figure 23. Palatal indices: A) palate shape; B) wedging index I; C) wedging index II. See text for details regarding wedging indices. Points represent single values or means, whiskers represent min/max values. Data from Table 17.

TABLE 17. PALATE INDICES (letters in parentheses refer to values presented in Table 3).

Taxon	Specimen	Palate breadth / palate length	Wedging index ¹	Palate breadth at M2 / Canine interalveolar distance	Palate depth / palate breadth
		(ag)/(ai)	(ah,ai,aj)	(ai)/(ah)	(ak)/(ai)
<i>Au. anamensis</i>	Mean		0.2		
	KNM-ER 30745		-2.0		
	KNM-KP 29283		2.4	106	31
<i>Au. afarensis</i>	Mean	54	8.7	114	34
	AL 199-1	59	8.7	119	38
	AL 200-1	52	6.0	113	26
	AL 417-1	50	11.4	126	48
	AL 427-1			107	34
	AL 442-1			104	
	AL 444-2	55			29
	AL 486-1			114	33
	Mean	57	8.6	120	36
<i>Au. africanus</i>	Sts 5	52	9.3	121	43
	Sts 17		7.3	122	48
	Sts 52		12.2	129	43
	Sts 53	60	8.2	117	35
	Sts 71		12.8	131	26
	StW 13	59	6.0	112	32
	StW 53		9.5	123	28
	StW 73		3.4	107	37
	Mean	53	1.5	104	34
<i>Au. sediba</i>	MH1				
<i>H. naledi</i>	DH1		17.8	142	29
<i>H. habilis</i>	Mean	63	14.9	130	36
	AL 666-1	62	17.1	130	38
	KNM-ER 1805		17.1	133	13
	KNM-ER 1813	62	14.3	132	35
	OH 13	62	11.4	123	49
	OH 24	65	14.7	133	36
	OH 65				44
<i>H. rudolfensis</i>	Mean		6.7	114	41
	KNM-ER 1470		7.7	115	47
	KNM-ER 62000	66	5.6	112	35
<i>H. erectus</i>	Mean	68	10.4	121	38
	D2282/211	72	16.3	134	33
	D2700/2735	67	7.9	116	24
	KNM-ER 3733		6.4	112	53
	KNM-WT 15000	78	9.3	118	28
	Sangiran 4	55			54
	SK 847		12.1	127	36

¹Palate wedging calculated using the formula of Digiovanni et al. (1989) as demonstrated in Ward et al. (1999).

Homo, in particular *H. erectus*. Finally, the index of overlap, which Rak (1983) considered to summarize the “efficiency” of the masticatory system, measures the extent to which dental arcade length overlaps with the distance between the articular eminence and the anterior extent of the origin of masseter. There is again substantial overlap across the hominins, though the value for MH1 is exceeded only by D2700 and KNM-ER 3733. As a result, MH1 appears more *Homo*-like, though it differs not too greatly from Sts 71. Although there is a great deal of overlap in these indices, on the whole *Au. sediba* appears more similar to specimens of early *Homo* than it does to australopiths. This suggests that

although the palate is small and shaped like that of an australopith, in its masticatory adaptations it is beginning to approach the configuration seen in early *Homo*.

MANDIBLE

Lateral Corpus

The alveolar and basal margins of the corpus range from parallel to markedly anteriorly divergent in australopiths (Table 19). In *H. habilis* specimens, the alveolar and basal margins are typically parallel. However, if KNM-ER 1802 does indeed represent *H. habilis* (Spoor et al. 2015), and if

TABLE 18. ELEMENTS OF THE MASTICATORY SYSTEM.

Taxon	Specimen	Palate protrusion anterior to sellion (%)	Palate protrusion anterior to masseter (%)	Position of anterior part of masseter (%)	Proximity of M ³ to articular eminence	Index of overlap
<i>Au. afarensis</i>	Mean	57	54			
	AL 417-1	59	48			
	AL 444-2	55	59	97	57	26
<i>Au. africanus</i>	Mean	49	52	98	47	33
	Sts 5	68	65	103	66	22
	Sts 52	33	54			
	Sts 71	47	43	93	35	40
	StW 53	47	46	97	41	38
<i>Au. sediba</i>	MH1	43	46	95	26	44
<i>H. habilis</i>	Mean	45	54	90	37	35
	KNM-ER 1813	42	56	85	36	32
	OH 24	48	52	95	37	37
<i>H. erectus</i>	Mean	33	47	87	34	40
	D2700/2735	29	42	86	24	48
	D4500/2600	48	62	89	51	25
	KNM-ER 3733	26	42	86	26	46
	KNM-WT 15000	32	47	85	33	39
	SK 847	31	43	89	38	40

UR 501 also represents *H. habilis*, as is likely the case given the evidence for KNM-ER 1802, then divergent margins are known in this taxon. In specimens of *H. rudolfensis* and *H. erectus*, the alveolar and basal margins range from parallel to markedly divergent. In *H. naledi*, the alveolar and basal margins are slightly anteriorly divergent. Villmoare et al. (2015a) considered parallel alveolar and basal margins (from P₃ to M₂) to be one of the characters demonstrating that LD 350-1 represented *Homo* at 2.8 Ma. However, *Au. sediba* also shares parallel alveolar and basal margins, thus combining with the inconstant appearance of this character in early *Homo* fossils to limit the utility of this character (Hawks et al. 2015). Villmoare et al. (2015b) disagreed with Hawks et al.'s (2015) measurement of mandibular corpus height of MH2 at the level of M₂, indicating the latter did not specify their method for measurement. To clarify, the measurement provided by Hawks et al. (2015) was taken on the refit original fossil from the alveolar margin to the basal margin slightly mesial to the MD mid-point of the M₂ (owing to breakage, Figure 24), which demonstrates that the alveolar and basal margins between P₃ (31.0mm) and M₂ (30.5mm) are essentially parallel in MH2, and not 2.5mm to 3.5mm offset as claimed by Villmoare et al. (2015b). In either case, parallel alveolar and basal margins

cannot be considered diagnostic of early *Homo*, since specimens of both *H. habilis* (KNM-ER 1802, UR 501), *H. rudolfensis* (KNM-ER 60000), and *H. erectus* (D2735, SK 45, Sangiran 9, Sangiran 22) show divergent margins.

Both MH1 and MH2 have a small and gracile corpus (see Tables 3 and 19, Figure 25). Although there is overlap with smaller *Au. africanus* individuals such as StW 84, StW 404, and StW 498, these latter specimens retain teeth that are considerably larger than those of *Au. sediba* (Moggi-Cecchi et al. 2006). MH1 and MH2 fall within the range of *Au. anamensis* and *Au. afarensis*, in particular, the smaller *Au. afarensis* individuals. In specimens of *H. habilis*, the corpus tends to be absolutely smaller and relatively more gracile than in the australopiths, though there is overlap between the groups, in particular, owing to KNM-ER 1802 and UR 501. Specimens of *H. rudolfensis* are quite large, sometimes exceeding the corpus size and robusticity seen in australopiths. *H. erectus* has a relatively small, gracile corpus, though there are some tremendously large specimens (e.g., Sangiran 6) that fall within the australopith range. *Homo naledi* possesses an especially gracile mandibular corpus. As a result, *Au. sediba* cannot be clearly distinguished from australopiths or early *Homo* specimens based on corpus robusticity.

TABLE 19. MANDIBULAR CORPUS METRICS FOR AUSTRALOPITHECUS SEDIBA AND COMPARATIVE HOMININ SPECIMENS.

(W# designations refer to measurement descriptions provided in Wood [1991]).

Taxon	Specimen	Corpus height at P ₄	Corpus breadth at P ₄	Corpus area ¹ at P ₄	Corpus height at M ₁	Corpus breadth at M ₁	Corpus area ¹ at M ₁
		W147	W148	W149	W150	W151	W152
<i>Au. anamensis</i>	Mean	38	19	570	29	19	417
	KNM-KP 29281	34	18	481	33	19	503
	KNM-KP 29287	42	20	660		21	
	KNM-KP 31713				29	18	410
	KNM-KP 47956				26	17	347
	Mean	36	19	558	34	20	540
<i>Au. afarensis</i>	AL 128-23		17			19	
	AL 145-35	28	19	418	28	21	462
	AL 188-1						
	AL 198-1	32	16	402	31	16	390
	AL 198-22					22	
	AL 207-13		18		31	18	438
	AL 225-8				31		
	AL 228-2	36	16	452	32	16	402
	AL 266-1	32	21	528	31	22	536
	AL 277-1	39	18	551	37	18	523
	AL 288-1	30	17	401	30	17	401
	AL 311-1		24				
	AL 315-22	33	17	441	30	19	448
	AL 330-5	31	19	463	31	21	511
	AL 333w-1ab	38	19	560	36	19	530
	AL 333w-12	31	17	414	31	18	438
	AL 333w-32-60	40	22	691	39	24	735
	AL 400-1	36	19	537	36	19	537
	AL 417-1	37	18	523	36	18	509
	AL 432-1						
	AL 433-1ab	20			35	20	550
	AL 436-1						
	AL 437-1	44	21	726	40	20	628
	AL 437-2	43	22	743	39	22	674
	AL 438-1	42	25	825	41	25	805
	AL 444-2	44	21	726	41	23	741
	AL 582-1	41	23	741		21	
AL 620-1	38	20	597	36	21	594	
LH 4	36	18	509	32	19	478	
LH 10					22		
MAK 1/2					20		
MAK 1/12	33	18	467	31	19	463	

TABLE 19. MANDIBULAR CORPUS METRICS FOR AUSTRALOPITHECUS SEDIBA AND COMPARATIVE HOMININ SPECIMENS (continued).
(W# designations refer to measurement descriptions provided in Wood [1991]).

Taxon	Specimen	Corpus height at P ₄	Corpus breadth at P ₄	Corpus area ¹ at P ₄	Corpus height at M ₁	Corpus breadth at M ₁	Corpus area ¹ at M ₁
		W147	W148	W149	W150	W151	W152
<i>Au. africanus</i>	Mean	34	21	570	32	21	539
	MLD 2	30	20	471	24	22	415
	MLD 18		21		34	21	561
	MLD 29	35	22	605	37	23	668
	MLD 34				32	20	503
	MLD 40	37	24	697	36	24	679
	Sts 7	41	24	773	42	24	792
	Sts 36	37	19	552	36	20	565
	Sts 52	29	22	501	30	25	589
	StW 84				27	18	382
	StW 404	26	19	388	26	20	408
	StW 498				26	18	368
<i>Au. sediba</i>	Mean	29	17	386	30	18	405
	MH1	27	18	382	28	18	396
	MH2	31	16	390	31	17	414
<i>H. naledi</i>	Mean	25	14	281	26	16	326
	DH1	26	16	327	26	17	347
	DH3				28	16	352
	UW101-001	27	15	318	29	15	342
	UW101-377	21	12	198	20	16	251
	UW101-1142				27	16	339
<i>H. habilis</i>	Mean	33	20	482	31	20	474
	KNM-ER 1501	32	17	427	29	17	387
	KNM-ER 1502				27	17	360
	KNM-ER 1802	40	20	628	38	23	686
	KNM-ER 1805		23		30	21	495
	OH 7		23			24	
	OH 13	26	17	347	27	18	382
	OH 37	31	20	487	32	20	503
	UR 501	35	19	522	34	19	507
<i>H. rudolfensis</i>	Mean	37	22	617	35	22	605
	KNM-ER 1482	33	20	518	31	20	487
	KNM-ER 1483	40	25	785	40	27	848
	KNM-ER 1801	36	19	537	34	20	534
	KNM-ER 60000	38	21	627	35	20	550
<i>H. erectus</i>	Mean	34	19	518	31	19	458
	D 211	27	19	403	26	19	388
	D 2735	26	19	388	23	19	343

TABLE 19. MANDIBULAR CORPUS METRICS FOR AUSTRALOPITHECUS SEDIBA AND COMPARATIVE HOMININ SPECIMENS (continued).
(W# designations refer to measurement descriptions provided in Wood [1991]).

Taxon	Specimen	Corpus height at P ₄	Corpus breadth at P ₄	Corpus area ¹ at P ₄	Corpus height at M ₁	Corpus breadth at M ₁	Corpus area ¹ at M ₁
		W147	W148	W149	W150	W151	W152
<i>H. erectus</i>	Mean	34	19	518	31	19	458
	D 2600	43	22	743	41	21	676
	KGA 10-1	33	21	544	32	22	553
	KNM-BK 67	33	18	467	33	17	441
	KNM-BK 8518	29	19	433	30	21	495
	KNM-ER 730	33	19	492	32	19	478
	KNM-ER 731				27	19	403
	KNM-ER 992	32	21	528	32	20	503
	KNM-WT 15000	28	19	418	24	20	377
	OH 22	29	21	478	29	21	478
	OH 23	32	20	503	33	21	544
	Sangiran 1b	33	16	415	36	17	481
	Sangiran 5	41	19	612	38	20	597
	Sangiran 6	48	28	1056	45	26	919
	Sangiran 8	34	18	481	36	19	537
	Sangiran 9	38	21	627	36	21	594
	Sangiran 22	31	16	390	30	17	401
	Sangiran Bk7905				31	19	463
	Sangiran Ng8503				21	17	280
	SK 15				28	19	418
	SK 45				37	15	436
	Ternifine I	36	19	537	33	19	492
	Ternifine II	35	16	440	32	17	427
	Ternifine III	40	18	565	35	19	522
	Zhoukoudian AII				26	15	306
	Zhoukoudian AN16				27	16	341
	Zhoukoudian FI				26	15	306
	Zhoukoudian GI				33	18	467
	Zhoukoudian HI				25	15	295
	Zhoukoudian K1	28	16	352	26	18	368
	Zhoukoudian Pa86				27	16	339

TABLE 19. MANDIBULAR CORPUS METRICS FOR AUSTRALOPITHECUS SEDIBA AND COMPARATIVE HOMININ SPECIMENS (continued).

(W# designations refer to measurement descriptions provided in Wood [1991]).

Taxon	Specimen	Corpus height at M ₂	Corpus breadth at M ₂	Corpus area at M ₂	Corpus height at M ₃	Corpus breadth at M ₃	Corpus area ¹ at M ₃
		W154	W155	W156	W157	W158	W159
<i>Au. anamensis</i>	Mean						
	KNM-KP 29281						
	KNM-KP 29287		23				
	KNM-KP 31713						
	KNM-KP 47956						
<i>Au. afarensis</i>	Mean	32	22	569	30	24	581
	AL 128-23		23				
	AL 145-35	31	25	609			
	AL 188-1	34	23	614		23	
	AL 198-1	31	18	438	32	21	528
	AL 198-22	34	21	561	33	24	622
	AL 207-13	28	21	462	27		
	AL 225-8	28	21	462		23	
	AL 228-2						
	AL 266-1	28	24	528	29	25	569
	AL 277-1						
	AL 288-1	28	25	550	26		
	AL 311-1						
	AL 315-22	28	20	440		21	
	AL 330-5	28	20	440	27	22	467
	AL 333w-1ab	33	25	638			
	AL 333w-12						
	AL 333w-32-60	36	24	679			
	AL 400-1						
	AL 417-1	33	18	467	32	20	503
	AL 432-1		20			22	
	AL 433-1ab		21			22	
	AL 436-1	26	20	408	24	22	415
	AL 437-1		20			23	
	AL 437-2	37	24	697		27	
	AL 438-1	37	28	814	37	32	930
	AL 444-2	38	31	925			
	AL 582-1						
	AL 620-1	35	23	632			
	LH 4	30	23	542	28		
LH 10							
MAK 1/2	33	21	544	32	24	603	
MAK 1/12	30	21	495	30	25	589	

TABLE 19. MANDIBULAR CORPUS METRICS FOR AUSTRALOPITHECUS SEDIBA AND COMPARATIVE HOMININ SPECIMENS (continued).
(W# designations refer to measurement descriptions provided in Wood [1991]).

Taxon	Specimen	Corpus height at M ₂	Corpus breadth at M ₂	Corpus area at M ₂	Corpus height at M ₃	Corpus breadth at M ₃	Corpus area ¹ at M ₃
		W154	W155	W156	W157	W158	W159
<i>Au. africanus</i>	Mean	30	24	579	32	28	714
	MLD 2	23	23	415			
	MLD 18	32	25	628	32	29	729
	MLD 29						
	MLD 34	33	22	570	23	25	628
	MLD 40	36	27	763	35	30	825
	Sts 7	37	26	756	33		
	Sts 36	38	24	716	33	26	674
	Sts 52	29	28	638	26		
	StW 84	26	22	449			
	StW 404	24	24	452			
	StW 498	23	22	397			
	<i>Au. sediba</i>	Mean	28	21	447		
MH1		25	22	432			
MH2		31	19	463	26	23	470
<i>H. naledi</i>	Mean	25	30	390	28	21	443
	DH1	24	21	396	26	20	408
	DH3	26	20	408	26	20	408
	UW101-001	30	19	448	29	21	478
	UW101-377	18	20	283			
	UW101-1142	28	19	418	29	21	478
<i>H. habilis</i>	Mean	33	24	614	29	24	518
	KNM-ER 1501	30	20	471			
	KNM-ER 1502						
	KNM-ER 1802	38	27	806	33		
	KNM-ER 1805		24		26		
	OH 7		26				
	OH 13	29	23	524	25	23	452
	OH 37	35	24	660	31	24	584
UR 501	31	25	609				
<i>H. rudolfensis</i>	Mean	31	23	548	31	26	633
	KNM-ER 1482	30	22	518	29	24	565
	KNM-ER 1483						
	KNM-ER 1801						
	KNM-ER 60000	32	23	578	33	27	700
<i>H. erectus</i>	Mean	31	20	493	31	22	562
	D 211						
	D 2735	21	24	396	22	23	397

TABLE 19. MANDIBULAR CORPUS METRICS FOR AUSTRALOPITHECUS SEDIBA AND COMPARATIVE HOMININ SPECIMENS (continued).
(W# designations refer to measurement descriptions provided in Wood [1991]).

Taxon	Specimen	Corpus height at M ₂	Corpus breadth at M ₂	Corpus area at M ₂	Corpus height at M ₃	Corpus breadth at M ₃	Corpus area ¹ at M ₃
		W154	W155	W156	W157	W158	W159
<i>H. erectus</i>	Mean	31	20	493	31	22	562
	D 2600						
	KGA 10-1	32	22	553			
	KNM-BK 67	34	19	507	34	21	547
	KNM-BK 8518	32	23	578	33	22	562
	KNM-ER 730	32	19	478	31	19	463
	KNM-ER 731						
	KNM-ER 992	35	24	660	37	25	726
	KNM-WT 15000	25	22	432			
	OH 22	29	21	478	33	22	570
	OH 23	32	20	503			
	Sangiran 1b	33	17	441	31	20	487
	Sangiran 5		21				
	Sangiran 6						
	Sangiran 8						
	Sangiran 9	33	23	596	33	29	752
	Sangiran 22	26	18	368	29		
	Sangiran Bk7905	28	21	462			
	Sangiran Ng8503						
	SK 15				26		
	SK 45						
	Ternifine I	36	19	537	35	23	632
	Ternifine II	35	16	440	32	23	578
	Ternifine III	40	19	597	36	24	679
	Zhoukoudian AII						
	Zhoukoudian AN16						
	Zhoukoudian FI						
	Zhoukoudian GI						
	Zhoukoudian HI						
	Zhoukoudian K1	25	18	353	29	19	433
	Zhoukoudian Pa86						

¹Area calculated as an ellipse, following the formula ($\pi * (\text{corpus height}/2) * (\text{corpus breadth}/2)$).

Villmoare et al. (2015a) suggest that a posteriorly opening mental foramen was the most common condition in early *Homo*, providing support for the claim that LD 350-1 represented early *Homo*. Hawks et al. (2015) countered that the mental foramina in *Au. sediba* also open predominantly laterally with a slight posterior orientation, lessening the utility of this character in diagnosing *Homo*. Villmoare et al. (2015b: 1326c) responded by claiming that Hawks et

al. argued that, “the orientation of the mental foramen in MH2 is lateral, rather than anterior, as we described”. To be precise, what Hawks et al. (2015: 1326-b) actually said is, “the mental foramina in MH1 and MH2 of *Au. sediba* are oriented predominantly laterally (not anteriorly in MH2, as inaccurately reported by Villmoare et al.), similar to nearly all specimens of early *Homo*, with a slight posterior orientation similar if not identical to that of LD 350-1”. The similar



Figure 24. Mandible of MH2 with lines indicating where measures were taken to demonstrate that the alveolar and basal margins are essentially parallel. Note that in this two-dimensional image, the P_3 level measure appears longer, though the convexity of the lateral mandibular corpus means that the chord distance from the alveolar to basal margin is 31mm.

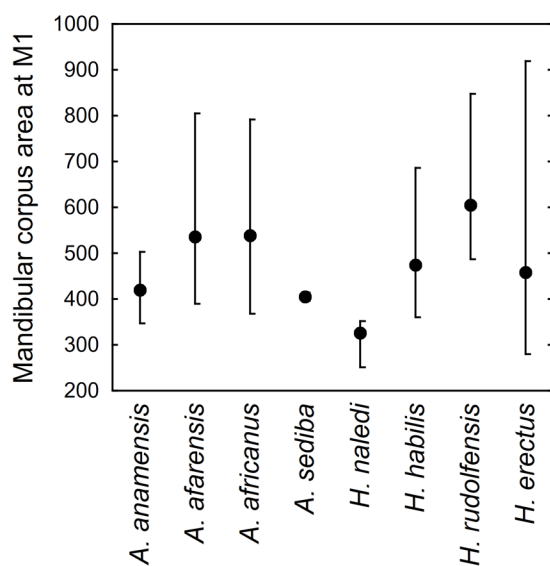


Figure 25. Mandibular corpus area at M1. Area calculated as an ellipse, following the formula ($\pi \times (\text{corpus height}/2) \times (\text{corpus breadth}/2)$). Points represent single values or means, whiskers represent min/max values. Data from Table 19.

orientation of the mental foramina in LD 350-1, MH1, and MH2 again limits the diagnostic utility of this character (Hawks et al. 2015) (Figure 26). In australopiths, the mental foramen tends to be positioned at or below the mid-corpus level, while in early *Homo*, it tends to be positioned at or above the mid-corpus level (Table 20). In *Au. sediba*, the mental foramen is about mid-corpus in height in both MH1 and MH2, while the smaller second foramen on the right side of MH1 is positioned below mid-corpus height, potentially aligning it more closely with australopiths.

The region of the lateral and marginal tori and the intertoral sulcus shows a great deal of variability across hominins. *Au. anamensis* and *Au. afarensis* stand out for the foreshortened appearance of the superior lateral torus, which generally does not approach the mental foramen, and the extent of the marginal torus, which generally turns up to contact the P_3 or canine jugum. Otherwise, the low and broad superior lateral torus and the moderately developed and striated marginal torus of *Au. sediba* define an intertoral sulcus that continues onto the anterior corpus, aligning it with specimens of both *Au. africanus* and early *Homo* (see Figures 2 and 5).

There is considerable overlap in the development and positioning of the anterior and posterior marginal tubercles across all hominin taxa, including *Au. sediba*. The only potential difference is that, in some specimens of early *Homo*, the anterior marginal tubercle is posteriorly positioned relative to the mental foramen, while in the australopiths it is



Figure 26. Close up view of the mental foramen in MH1 (top), and MH2 (bottom), showing that both open predominantly laterally with a slight posterior tilt as in many specimens of early *Homo*. Note the posterosuperiorly directed channel leading away from the mental foramen of MH1; this is not an artifact of preservation or preparation.

positioned almost level with the mental foramen. In MH1, the anterior marginal tubercle is positioned posterior to the mental foramen, similar to what we see in some specimens of *Homo*, while in MH2, the anterior marginal tubercle is positioned almost level with the mental foramen, similar to the australopiths, limiting the utility of this character.

Anterior Corpus

There is substantial overlap in the height and depth of the symphysis across australopiths and early *Homo* (Table 21). MH1 is broken along the midline at an oblique angle that is slightly lateral to the mandibular symphysis on its anterior aspect, though by repositioning U.W. 88-2 and U.W. 88-245

we can reliably measure its height and depth. In both absolute measures MH1 falls near the lower end of the range for both australopiths and early *Homo*. When we calculate the area of the symphysis there is again overlap between the groups, though we can see some indication of separation (see Table 21, Figure 27). The area of the symphysis is similar in *Au. afarensis* and *Au. africanus* and *H. rudolfensis* (KNM-ER 62000). The symphysis in specimens attributed to *H. naledi*, *H. habilis*, and *H. erectus* is smaller on average than those of the australopiths and *H. rudolfensis*, although some especially large individuals of *H. habilis* (e.g., KNM-ER 1802) and *H. erectus* (e.g., D2600, Sangiran 6) fall within the range of the former. MH1 has an especially small symphysis, falling at the low end of the range of *Au. anamensis* and *Au. afarensis*, and intersecting with *H. naledi*, *H. habilis*, and *H. erectus*. The especially small size of the symphysis, therefore, aligns *Au. sediba* somewhat more closely with *H. naledi*, most specimens of *H. habilis*, and *H. erectus* than it does with *H. rudolfensis* or *Au. africanus*.

The mandibular incisure in australopiths tends to be weak and small, though it is only in *Au. africanus* that we see contact between it and the intertoral sulcus. In specimens attributed to *H. habilis* the mandibular incisure is weak, and in direct contact with the intertoral sulcus, while in specimens attributed to *H. rudolfensis*, *H. erectus*, and *H. naledi* the mandibular incisure tends to be clearly defined and moderately developed, and is clearly in direct contact with the well-developed intertoral sulcus (though in some specimens, such as KNM-BK 67, KNM-BK 8518, and Sangiran 6, the mandibular incisure is absent, the entire area being swollen in appearance). In MH1 and MH2 the mandibular incisure is moderately developed. In MH1 it is in direct contact with the intertoral sulcus, while in MH2 the intertoral sulcus does not appear to reach to the mandibular incisure (see Figures 2 and 5). The overall development of the mandibular incisure in *Au. sediba* is reminiscent of specimens of *Homo*, though it does resemble some australopiths such as MLD 18 and Sts 52 in particular.

Although the area is damaged, there is no clear indication that a mental trigon existed in KNM-KP 29281. *Australopithecus afarensis* typically presents an evenly rounded heaping up of bone in the midline in the position of a mental protuberance, sometimes located above the basal margin, other times extending to the basal margin. There are no lateral tubercles, thus a mental trigon proper is not clearly defined (Weidenreich 1936; Tobias 1991). In *Au. africanus*, a low, circular mental protuberance positioned near the basal margin is present, flanked by low, rounded lateral tubercles that combine to form a weak but recognizable mental trigon. Specimens of early *Homo* typically reveal a weak mental protuberance, flanked by distinct lateral tubercles, thus a mental trigon is typically visibly defined. In MH1 the mental protuberance is moderately developed and defined, and is continuous with well-defined lateral tubercles, thus a moderately developed mental trigon is present. The absence of a mental trigon thus separates *Au. anamensis* and *Au. afarensis* from *Au. africanus*, *Au. sediba*, and early *Homo*, the latter which typically express it.

TABLE 20. HEIGHT OF THE MENTAL FORAMEN IN AUSTRALOPITHECUS SEDIBA AND COMPARATIVE HOMININ SPECIMENS

(W# designations refer to measurement descriptions provided in Wood [1991].)

Taxon	Specimen	Height of mental foramen		Corpus height at P ₄	Height of mental foramen from alveolar margin / corpus height at P ₄
		alveolar W162	basal W161		
<i>Au. anamensis</i>	KNM-KP 29281	19	16	34	56
	KNM-KP 29287	23	22	42	55
<i>Au. afarensis</i>	AL 145-35	15	18	28	54
	AL 198-1	19	14	32	59
	AL 266-1	20	14	32	63
	AL 277-1	23	17	39	59
	AL 288-1	20	12	30	67
	AL 333w-1ab	18	20	38	47
	AL 333w-12	19	13	31	61
	AL 333w-32-60	24	17	40	60
	AL 400-1	20	17	36	56
	<i>Au. africanus</i>	MLD 2	16	15	30
MLD 40		21	17	37	57
Sts 7		20	21	41	49
Sts 36		19	17	37	51
Sts 52		16	12	29	55
<i>Au. sediba</i>	MH1	13	17	27	48
	MH2	16	15	31	52
<i>H. naledi</i>	DH1	11	15	26	42
	UW101-001	11	16	27	41
	UW101-377	8		21	38
<i>H. habilis</i>	KNM-ER 1501	15	15	32	47
	OH 13	12	14	26	46
	OH 37	14	17	31	45
	KNM-ER 1802	21	18	40	53
	UR 501	18	15	35	51
<i>H. rudolfensis</i>	KNM-ER 1482	20	13	33	61
	KNM-ER 1483	17	21	40	43
	KNM-ER 1801	17	17	36	47
	KNM-ER 60000	18	18	38	47
<i>H. erectus</i>	D 211	12	12	27	44
	D 2735	13	13	26	50
	D 2600	26	16	43	60
	KNM-BK 67	16	18	33	48
	KNM-BK 8518	10	16	29	34
	KNM-ER 992	14	16	32	44
	KNM-WT 15000	14	14	28	50
	OH 22	13	16	29	45
	OH 23	17	15	32	53
	Sangiran 6	24	24	48	50
	Sangiran 8	17	17	34	50
	Sangiran 9	20	19	38	53
	Ternifine I	16	16	36	44
Ternifine III	22	13	40	55	

TABLE 21. MANDIBULAR SYMPHYSIS METRICS FOR AUSTRALOPITHECUS SEDIBA AND COMPARATIVE HOMININ SPECIMENS

(W# designations refer to measurement descriptions provided in Wood [1991]).

Taxon	Specimen	Symphysis height	Symphysis depth	Symphysis area ¹
		W141	W142	W146
<i>Au. anamensis</i>	Mean	39	20	622
	KNM-KP 29281	42	22	726
	KNM-KP 29287	42	20	660
	KNM-KP 31713	34	18	481
<i>Au. afarensis</i>	Mean	39	20	623
	AL 128-23	34	18	481
	AL 198-1	38	19	567
	AL 266-1	32	20	503
	AL 277-1	42	18	594
	AL 288-1	33	18	467
	AL 315-22		18	
	AL 330-5		18	
	AL 333w-32-60	45	22	778
	AL 400-1	40	19	597
	AL 417-1	38	18	537
	AL 437-1	45	22	778
	AL 437-2	45	22	778
	AL 438-1	40	26	817
	AL 444-2		24	
	AL 620-1		23	
	LH 4	39	19	582
<i>Au. africanus</i>	Mean	37	22	612
	MLD 2	31	22	536
	MLD 40	35	23	632
	Sts 7	46	23	831
	Sts 36	38	18	537
	Sts 52	35	19	522
<i>Au. sediba</i>	MH1	34 ²	18 ²	481
<i>H. naledi</i>	DH1	33	18	467
<i>H. habilis</i>	Mean	33	21	498
	KNM-ER 1805		22	
	OH 7	40		
	OH 13	25	18	353
	OH 37	29	19	433
	KNM-ER 1802	36	25	707
<i>H. rudolfensis</i>	Mean	38	24	781
	KNM-ER 1482	40	25	785
	KNM-ER 1801	32		
	KNM-ER 60000	43	23	777

TABLE 21. MANDIBULAR SYMPHYSIS METRICS FOR AUSTRALOPITHECUS SEDIBA AND COMPARATIVE HOMININ SPECIMENS (continued)
(W# designations refer to measurement descriptions provided in Wood [1991]).

Taxon	Specimen	Symphysis height	Symphysis depth	Symphysis area ¹
		W141	W142	W146
<i>H. erectus</i>	Mean	35	18	519
	D 211	28	17	374
	D 2735	34	16	427
	D 2600	49	21	808
	KNM-BK 67	31	20	487
	KNM-BK 8518	30	22	518
	KNM-ER 730	33	18	467
	KNM-ER 731		20	
	KNM-ER 992	37	21	610
	KNM-ER 1812	32	18	452
	KNM-WT 15000	31	17	414
	OH 22	34	20	534
	Sangiran 1b	32	17	427
	Sangiran 6	47	26	960
	Sangiran 8	29	18	410
	Sangiran 9	41	19	612
	SK 15	31	16	390
	Ternifine I	37	19	552
	Ternifine II	35	18	495
	Ternifine III	40	19	597
	Zhoukoudian GI		14	
	Zhoukoudian HI		14	
	Zhoukoudian K1	33	13	329

¹Area calculated as an ellipse, following the formula (π *(corpus height/2)*(corpus breadth/2)).

²Refitting of the new mandibular fragment UW88-245 resulted in a value that differs from Berger et al. (2010).

The strongly receding symphyseal region of *Au. anamensis*, combined with the absence of a mental trigon, indicates that a mentum osseum is not present in this taxon. In *Au. afarensis*, the weak mandibular incisure combines with the midline heaping up of bone in the position of the mental protuberance to define a rudimentary mentum osseum in some specimens, while others lack such a structure. The weak mandibular incisure of *Au. africanus* combines with the weak mental trigon to define a weak but recognizable mentum osseum. The weak mandibular incisure and clearly defined mental trigon of most specimens of early *Homo* demonstrates the presence of a distinct mentum osseum in these taxa. The moderate mandibular incisure in *Au. sediba*, combined with the mental trigon in MH1 (the area is damaged in MH2), indicates a weak mentum osseum is present in this taxon. The development of this feature in *Au. sediba* is reminiscent of early *Homo*, and somewhat less so of *Au.*

africanus, in that the mandibular incisure and mental trigon tend to be more prominent in *Au. sediba*.

Posterior Corpus

In australopiths, the lingual alveolar plane (a.k.a. alveolar planum, *planum alveolare*, postincisive planum) tends to be elongated and shelf-like, hollowed along both sagittal and transverse axes, and only weakly inclined; it is considerably elongated in *Au. anamensis* and some specimens of *Au. afarensis*. A similar pattern is seen in specimens attributed to *H. habilis* and *H. rudolfensis*, though they are not as elongated as in *Au. anamensis*; the lingual alveolar plane is somewhat elongated and generally shelf-like, typically only weakly to moderately inclined, and hollowed sagittally and transversely. Even the *Homo habilis* specimen OH 13 with its relatively short lingual alveolar plane is only weakly inclined and thus shelf-like. In *H. erectus*, the lin-

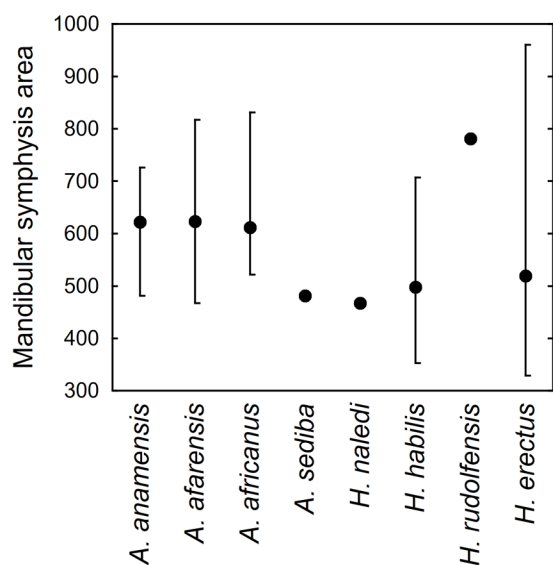


Figure 27. Mandibular symphysis area. Area calculated as an ellipse, following the formula ($\pi \times (\text{corpus height}/2) \times (\text{corpus breadth}/2)$). Points represent single values or means, whiskers represent min/max values. Data from Table 21.

gual alveolar plane is less elongated and not shelf-like, being weakly to moderately inclined. It tends to be hollowed transversely, but less often in the sagittal plane. In *H. naledi* the area of the lingual alveolar plane is steeply inclined and not shelf-like, and is hollowed transversely. MH1 is damaged in the symphyseal region, but enough is preserved to see that the lingual alveolar plane was only weakly developed and steeply inclined, and was likely only slightly hollowed along its transverse axis (see Figure 2). MH2 is too damaged to be certain, but what is preserved corresponds to MH1 (see Figure 5). The steeply angled, non-shelf-like lingual alveolar plane aligns *Au. sediba* with *H. naledi* and *H. erectus* in particular.

The superior transverse torus in *Au. anamensis* is generally well-developed and prominent as the terminal extension of the lingual alveolar plane. The inferior transverse torus is also well-developed and robust, and extends farther posteriorly than the superior transverse torus. In *Au. afarensis*, the superior transverse torus tends to be moderate to large sized and thick, but with low relief. The inferior transverse torus ranges from weak to well-developed, it is positioned low on the corpus, and it typically reaches farther posteriorly than the superior transverse torus. In *Au. africanus*, the superior transverse torus is weakly to moderately developed and generally with limited relief. The inferior transverse torus is generally more robust and more extensive than the superior transverse torus, and tends to be positioned low on the corpus. In specimens attributed to *H. habilis*, the superior transverse torus appears only weakly developed, and we can only clearly see it in KNM-ER 1805 and OH 13. The inferior transverse torus is very weak in KNM-ER 1802, KNM-ER 1805, and OH 13, while Wood (1991) considers KNM-ER 1501 to lack one entirely. In

specimens attributed to *H. rudolfensis*, a superior transverse torus is weakly indicated and not projecting in most specimens, though a moderately developed and overhanging torus is seen in KNM-ER 1482. The inferior transverse torus is only weakly indicated in some specimens (KNM-ER 1801) to entirely absent in others (KNM-ER 62000). On the other hand, it is moderately well-developed and prominent in KNM-ER 1482. In *H. erectus*, the superior transverse torus is low, rounded, and weakly to moderately developed and overhanging. The inferior transverse torus is absent to weakly developed, only occasionally extending farther posteriorly than the superior transverse torus. In *H. naledi*, the superior transverse torus is absent, while a slight, basally positioned inferior transverse torus is present. In MH1, the superior transverse torus is weakly developed, and probably only slightly projecting, and there is no clear indication of an inferior transverse torus. The weakly developed superior transverse torus and absent inferior transverse torus of *Au. sediba* are different from their better developed counterparts in the australopiths, and align it more closely with early *Homo*.

Medial Corpus

In specimens of *Au. anamensis*, *Au. afarensis*, and *Au. africanus*, the alveolar prominence weakly to moderately overhangs the posterior alveolar fossa, which itself is continuous with a weak to absent anterior subalveolar fossa. In all of these species, the alveolar prominence becomes moderately to markedly more vertically extensive anteriorly as it merges with the superior transverse torus. *H. rudolfensis* tends to follow this pattern as well, with a well-developed alveolar prominence that becomes markedly more extensive anteriorly, though it differs from the australopiths in that both anterior and posterior subalveolar fossae are typically present. In specimens of *H. habilis*, *H. erectus*, and *H. naledi*, the alveolar prominence becomes only slightly vertically expanded anteriorly, and moderately to markedly overhangs the continuous anterior and posterior subalveolar fossae. In MH1 and MH2, the alveolar prominence is moderately large and overhanging, becoming only slightly more vertically extensive anteriorly (see Figures 2 and 5). The subalveolar fossa is comprised of continuous anterior and posterior components, both of which are more deeply excavated in MH1 than in MH2. Therefore, in *Au. sediba* the subalveolar fossa is more clearly excavated than is seen in *Au. africanus*, and does not become vertically more extensive anteriorly as in the latter and *Au. afarensis*. In addition, the continuous anterior and posterior subalveolar fossa are more clearly developed in *Au. sediba* than in the australopiths. In this sense *Au. sediba* aligns more closely with early *Homo*.

Basal Corpus

The basal corpus in australopiths tends to be well rounded and thick along its entire extent, with moderate to marked eversion of the basal contour; some specimens of *Au. afarensis* differ in sometimes appearing thinner and more sharpened along the basal corpus. In early *Homo*, the basal margin

is not as thickened or rounded as in australopiths, though in some specimens there is some thinning of the corpus anterior and posterior to the lateral prominence. The eversion of the basal contour is slight to marked in early *Homo*. In MH1 and MH2, the basal corpus is moderately thick and evenly rounded along most of its extent, though there is thinning posterior to the level of the lateral prominence; MH1 is thicker than MH2 (see Figures 2 and 5). The eversion of the basal contour is moderate in both specimens. The thickness of the basal corpus in *Au. africanus* sets it apart from most other hominins examined here, including *Au. sediba*, and in this regard *Au. sediba* aligns more closely with early *Homo* and some specimens of *Au. afarensis*. The marked eversion of the basal margin in most specimens of *Au. afarensis* sets it apart from *Au. sediba*, though there is overlap between the latter and some individuals such as A.L. 288-1.

Occlusal Corpus

In australopiths, the incisors and canines are arranged in a gentle arc. The post-canine tooth rows are generally straight to slightly laterally convex, and are slightly to moderately divergent posteriorly with the exception of the parallel-sided tooth rows of *Au. anamensis*. There is a marked increase in robusticity from the corpus to the symphysis, and a diastema is present in *Au. anamensis*, common in *Au. afarensis*, but absent in *Au. africanus*. In *H. habilis* specimens, the incisors and canines are arranged in a gentle arc, while in *H. rudolfensis* they are arranged in a nearly straight line. The post-canine tooth rows in early *Homo* show a slight lateral convexity, and are slightly posteriorly divergent. There is a slight increase in robusticity from the corpus to the symphysis, and a diastema is absent. In MH1 and MH2, the incisors and canines are arranged in a gentle arc (see Figures 2, 5, and 7), differing mainly from *H. rudolfensis* among early *Homo* material, though some specimens of *H. erectus* also show this arrangement. The tooth rows are moderately convex, and we reconstruct them as being moderately divergent in MH2, but less divergent in MH1 (see Figure 7). The shape and divergence of the tooth rows aligns *Au. sediba*, especially MH1, most closely with the australopiths. The slight gradient in robusticity from the corpus to the symphysis differentiates *Au. sediba* from *Au. africanus*, being related to the development of the lingual alveolar plane and the superior transverse torus. The lack of a diastema distinguishes *Au. sediba* from *Au. anamensis* and *Au. afarensis*.

In australopiths, a weak curve of Spee is evident, and a canine step is indicated, i.e., a topographic step-down from the incisal margin of the incisors and the canine apex to the level of the distal tubercle of the canine and the occlusal surface of the P₃ (see Kimbel and Deleuzene 2009). The incisors and canines in most specimens of *Au. africanus* are either absent or extensively worn to the same level as the post-canine tooth row. Only the young individual Sts 52 retains relatively unworn anterior dentition, and it exhibits a moderate but distinct canine step. In early *Homo*, a moderate curve of Spee tends to be present, though a canine step

is absent, with the possible exception of DH1 of *H. naledi*. A slight curve of Spee is seen in MH1 and MH2. The canine and incisor are worn to the same plane as the post-canine dentition in MH2, thus it would appear a canine step is not present, though attrition is extensive. There is no canine step in MH1. The presence of a canine step in *Au. afarensis* and *Au. africanus* delineates the australopiths from early *Homo*, while the probable absence of a canine step in *Au. sediba* aligns this taxon more closely with *Homo* apart from *H. naledi*.

There is considerable overlap between the australopiths and early *Homo* in the proportions of components of the tooth row (Table 22). *Au. sediba*, in turn, shows substantial overlap with both groups in absolute alveolar proportions. However, morphometric analysis has revealed taxonomic differences in the size and shape of the mandible (de Ruiter et al. 2013b). We summarize the results as follows: the size and shape of the mandibles of *Au. sediba* distinguish them from australopiths, including *Au. africanus*, and where *Au. sediba* mandibles differ from those of *Au. africanus*, they appear most similar to representatives of early *Homo* in both size and shape.

Lateral Ramus

Across hominin taxa there is overlap in the anterior extent of the origin of the ascending ramus. In *Au. anamensis* and *Au. afarensis* the origin is positioned somewhat more anteriorly, while in *Au. africanus* and some specimens of early *Homo* it is positioned more posteriorly. In fact, in many specimens of early *Homo* it is positioned opposite the level of the M₃. Indeed, Villmoare et al. (2015a) used the posterior position of the origin of the ramus to support their conclusion that LD 350-1 represents early *Homo*. Hawks et al. (2015) disagreed with this, however, indicating that in MH2 of *Au. sediba* the origin is at the level of the mesial M₃, while in the juvenile MH1 it is at the level of the M₂. This position in MH2 in particular would suggest that a posterior position for the origin of the ramus is not uniquely diagnostic of *Homo*. Villmoare et al. (2015b) responded by indicating that the point at which the anterior ramus margin becomes independent of the corpus in MH2 is at the level of the M₂/M₃, and provided a photograph of a cast of a segment of the MH2 mandible in support (their Figure 1). We disagree with the orientation of MH2 in their Figure 1, but even when we reorient MH2 into anatomical position, we accept that, according to their description of the trait, the ascending ramus becomes independent of the corpus near the mesial extent of the M₃. However, comparing our Figure 28 to Figure 2 of Villmoare et al. (2015a), the difference between LD 350-1 and MH2 in this regard is not substantive, and difficult to reconcile with a generic level distinction. In addition, there are examples of mandibles attributed to *H. naledi* (DH1), *H. rudolfensis* (KNM-ER 1482), and *H. erectus* (D2735) that share an anteriorly positioned ramal root, thus a posteriorly positioned ramal root cannot be considered uniquely diagnostic of early *Homo* (see Figure 28). There is also a good deal of overlap in the height of the origin of the ramus on the lateral corpus, ranging

TABLE 22. MANDIBULAR TOOTH ROW PROPORTIONS FOR AUSTRALOPITHECUS SEDIBA AND COMPARATIVE HOMININ SPECIMENS

(W# designations refer to measurement descriptions provided in Wood [1991].)

Taxon	Specimen	I ₁ -I ₂ alveolar length	Canine alveolus BL breadth	P ₃ -P ₄ alveolar length	M ₁ -M ₃ alveolar length
		W163	W164	W167	W168
<i>Au. anamensis</i>	KNM-KP 29281	11	10	16	41
<i>Au. afarensis</i>	Mean	11	10	17	41
	AL 128-23		10	16	39
	AL 145-35	9	11	17	
	AL 198-1	12	10	16	36
	AL 266-1	9	9	18	45
	AL 277-1	10	12	18	
	AL 288-1	10	7	13	36
	AL 333w-32-60	12	12	19	44
	AL 400-1	11	9	15	41
	LH 4	11		21	43
<i>Au. africanus</i>	Mean	11	10	18	41
	MLD 2	12			
	MLD 18	11	10	16	40
	MLD 40	11	10	18	45
	Sts 7	9	10	19	42
	Sts 36	9	11	20	42
	Sts 52	11	10	17	41
<i>Au. sediba</i>	Mean	10	9	17	37
	MH1	11	9	18	
	MH2	9	8	16	37
<i>H. naledi</i>	Mean		8	15	37
	DH1	10	9	15	37
	DH3		7	15	
	UW101-001				36
<i>H. habilis</i>	Mean	11	9	18	42
	KNM-ER 1501		7	18	
	KNM-ER 1502	10		17	44
	KNM-ER 1802	10	10	22	
	OH 7	13	9	20	
	OH 13	9	6	17	40
	OH 37		11	16	
	UR 501		9	17	
<i>H. rudolfensis</i>	Mean	13	10	18	43
	KNM-ER 1482	16	8	19	44
	KNM-ER 1483		12	19	
	KNM-ER 1801		9	17	
	KNM-ER 60000	9	9	16	41

TABLE 22. MANDIBULAR TOOTH ROW PROPORTIONS FOR AUSTRALOPITHECUS SEDIBA AND COMPARATIVE HOMININ SPECIMENS (continued)
(W# designations refer to measurement descriptions provided in Wood [1991].)

Taxon	Specimen	I ₁ -I ₂	Canine	P ₃ -P ₄	M ₁ -M ₃
		alveolar length	alveolus BL breadth	alveolar length	alveolar length
		W163	W164	W167	W168
<i>H. erectus</i>	Mean	10	9	18	39
	D 211	9	8	15	35
	D 2735	11	11	16	35
	D 2600	11	11	19	43
	KNM-BK 67	9		18	35
	KNM-BK 8518	8	8	17	38
	KNM-ER 730	10	8	20	38
	KNM-ER 992	13	9	19	40
	KNM-ER 1812		9		
	KNM-WT 15000	11	6	20	
	OH 22	12	9	17	39
	OH 23			15	
	Sangiran 1b		9	18	40
	Sangiran 5			17	
	Sangiran 6			19	
	Sangiran 8			19	
	Sangiran 9	11	9	17	41
	Sangiran 22	9	10	16	37
	Sangiran Bk8606				44
	Sangiran Sb8103				37
	SK 15	9		17	
	Zhoukoudian K1	12	9	18	38

from moderately high to high across the australopiths and *Homo*. *Au. sediba* shares a high origin with both groups. The extramolar sulcus tends to be broad in the australopiths and *H. rudolfensis*, and narrower in *H. habilis*, *H. naledi*, and *Au. sediba*. It is narrow to broad in *H. erectus*, demonstrating overlap between this latter group and the australopiths, and thus limiting the utility of this character.

Rak et al. (2007) describe a pattern of ramal morphology, centered on the area of the mandibular notch, that they consider to clearly characterize *Au. afarensis* and *P. robustus*, and which they suggest casts doubt on the role of *Au. afarensis* as a human ancestor. In gorillas, *Au. afarensis*, and *P. robustus*, the coronoid tends to be higher than the condyle, and the base of the coronoid is broad, resulting in a coronoid tip that has a flat superior contour and a posterior orientation that often forms as a posteriorly directed hook and a narrow mandibular notch, with the deepest point of the notch positioned posteriorly. In humans, chimpanzees, orangutans, and many other primates, the coronoid process tends to be lower than the condyle, and the base

of the coronoid process is reduced, resulting in a tapered point and a spacious mandibular notch, with the deepest point of the notch is positioned anteriorly. These two ramal morphologies are present in MH1 (the *Au. afarensis* / *P. robustus* pattern) and MH2 (the chimpanzee / human pattern) (see Figures 2 and 5). While this might lead one to suggest that these two mandibles are therefore derived from two entirely different taxa, this overlooks several important factors. First, apart from this difference, the mandibles of the two specimens are substantially similar in corpus and dental morphology; second, the associated skeletons of these two individuals are substantially similar in overall morphology; and third, the two skeletons entered the cave at effectively the same time and came to lie almost on top of one another (Dirks et al. 2010). In addition, the right P⁴ of MH1 is developmentally/pathologically maloccluded, being unerupted and impacted in the alveolar bone. This would likely have had an impact on the development of the anterior border of the ramus of MH1. Extraction of the left mandibular ramus of MH1 from its surrounding matrix

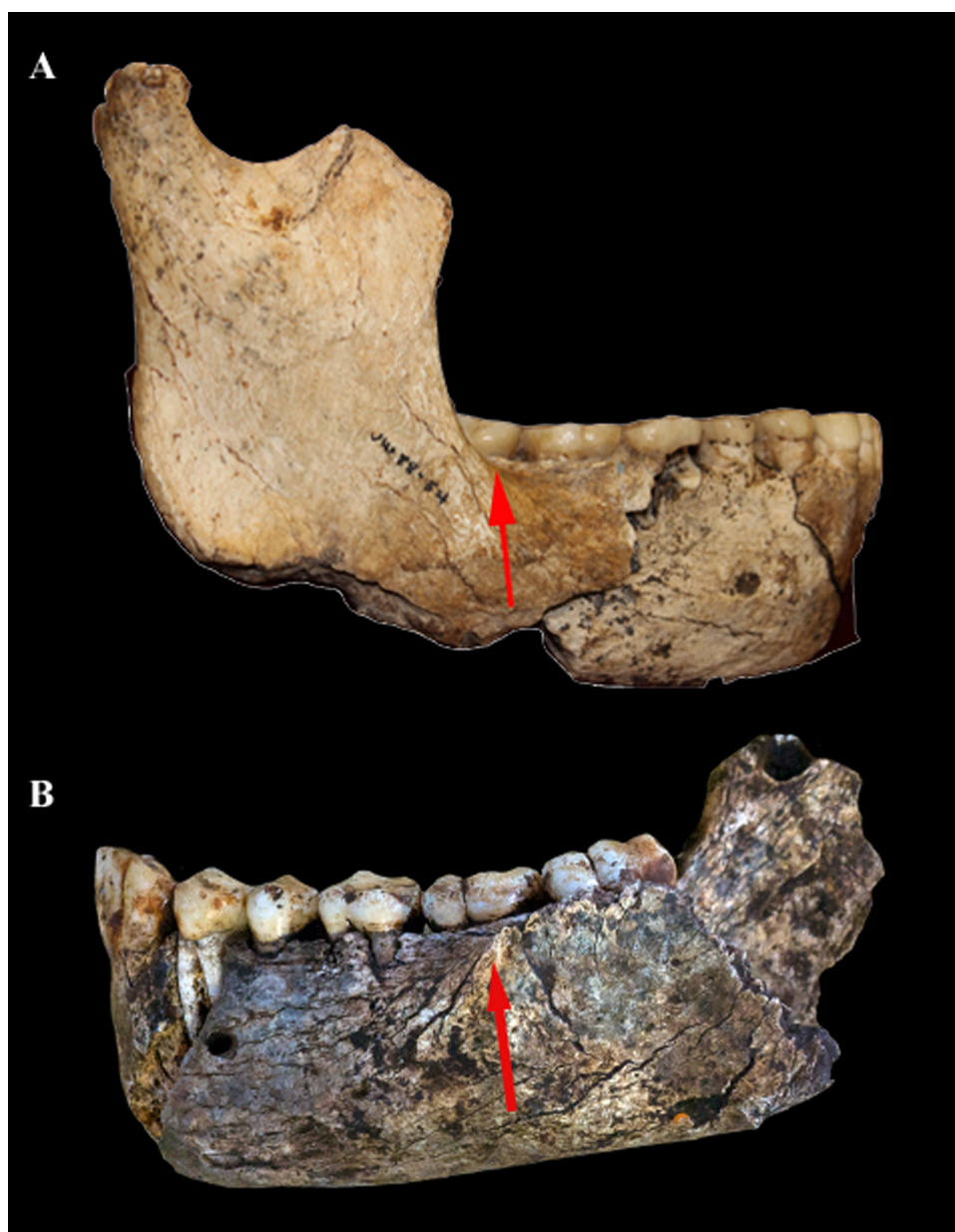


Figure 28. Close up view of the root of the ascending ramus on the corpus in A) MH2; B) DH1 (*H. naledi*). Red arrow indicates point where ascending ramus becomes independent of the corpus. Note that in MH1 this occurs near the mesial extent of the M_2 , while in DH1, type specimen of *Homo naledi*, it occurs at about the midpoint of the M_2 . Compare these to Figure 2 of Villmoare et al. (2015a).

will allow us to determine whether the morphology of the right ramus is bilaterally present.

In A.L. 822-1 of *Au. afarensis*, the ectocoronoid buttress appears well-developed and clearly defined with a superior taper that disappears below the tip of the coronoid. In *Au. africanus*, the ectocoronoid buttress is low, rounded, and weakly developed along the anterior margin of the ramus, disappearing before reaching the tip. The ectocoronoid buttress is a weak ridge along the anterior border of the ramus that starts inferiorly and curves posteroinferiorly along the ramal margin in KNM-ER 62000 of *H. rudolfensis*. In *H. erectus* the ectocoronoid buttress tends to be a weak thickening either along the anterior border or along the midline of the coronoid that does not always reach the tip of the process.

KNM-WT 15000 varies from this pattern in having a relatively robust buttress that does curve all the way to the tip. In MH1, the ectocoronoid buttress is very weak, possibly influenced by the medial deviation of the anterior border; in MH2, the ectocoronoid buttress is damaged. The weak development of the ectocoronoid buttress in *Au. sediba* is more reminiscent of early *Homo*, though sample sizes are too small and available specimens too damaged to make any definitive statements.

Medial Ramus

The mandibular condyle in *Au. afarensis* is highly variable in shape, ranging from a parallelogram in A.L. 288-1 to the kidney-shaped condyles of the Maka specimens. The me-

dial-most extent angles distinctly inferiorly in some, and less distinctly in others. The angle of orientation relative to the coronal plane varies from almost parallel to nearly 45° angle. The mandibular condyle in *Au. africanus* appears small and ovoid in shape, with a marked drop-off at the medial extent. The condyle is oriented slightly oblique to the coronal plane. The condyle in KNM-ER 60000 of *H. rudolfensis* is damaged, but appears to have been relatively anteroposteriorly narrow and oriented parallel to the coronal plane. In *H. erectus*, the condyle tends to be moderately large and narrow, with a highly variable shape ranging from ovoid to kidney-shaped. There is a distinct drop-off at the medial extent, and the condyle is oriented parallel to or just slightly oblique to the coronal plane. In MH1, the condyle is anteroposteriorly narrow and elongated, while in MH2, it is more anteroposteriorly broad (see Figure 7). The shape in both specimens is of a parallelogram, with a distinct medial drop-off in MH1 (damaged in MH2). In both specimens, the orientation of the condyle is slightly oblique to the coronal plane. In terms of absolute dimensions, there is considerable overlap across australopiths and early *Homo*. The main stand out is the anteroposteriorly narrow condyle in MH1. Otherwise, there is little in this feature to distinguish the different groups.

The endocoronoid buttress in australopiths varies from low and rounded with limited relief to robust and rugose with marked relief. The endocondyloid buttress is weak to strong, but generally low and rounded, providing contact between the condyle and the triangular torus. In early *Homo*, the endocoronoid buttress ranges from low and rounded to high and sharp, reaching almost to the tip of the coronoid. The endocondyloid buttress tends to be low and rounded, and usually, but not always, reaches the condyle (e.g., in KNM-BK 67 and D2735 it does not). The endocoronoid buttress is low, rounded and weak in MH1, and higher and sharper in MH2. In MH1, the endocondyloid buttress is effectively absent, while in MH2, it is weakly developed and fades before reaching the condyle. The most striking difference in *Au. sediba* therefore lies in the absence or weak development of the endocondyloid buttress, and the fact that it does not provide a link between the triangular torus and the condyle. This is seen in some, but not all, early *Homo* specimens, but not in any australopith.

In MH1 and MH2 the mandibular foramen is moderate sized, oval-shaped, and shallow. The mylohyoid groove is shallow but clearly defined. The lingula on MH1 is small and triangular, while in MH2, it is only faintly indicated as a slight thickening of the anterior border of the mandibular foramen. The development of the mandibular foramen and mylohyoid groove in *Au. sediba* therefore broadly overlaps with that of *Au. africanus* and early *Homo*.

TEETH

Maxillary Dentition

In MH1, the lingual face of the I¹ is slightly concave with a weak median ridge as is seen in the australopiths. Conversely, the lingual cervical prominence of the I¹ is broad

and uninflated, as is seen in early *Homo*. In the I² of MH1, the lingual mesial marginal ridge and distal marginal ridge are moderately developed, and they merge on the cervical prominence as is seen in australopiths. The maxillary canine of MH1 reveals a narrow and uninflated lingual cervical prominence as in australopiths, while the lingual median ridge is broad and weakly prominent as in early *Homo*. The cusp apices of the maxillary premolars (and molars, see below) are moderately closely spaced in australopiths, including *Au. sediba*, being inset relative to the lingual and buccal margins of the crown; in early *Homo*, the cusp apices are set more widely apart, near to or at the lingual and buccal margins. The buccal grooves of the maxillary premolars are weakly developed, and the lingual and buccal cervical prominences are weakly developed, as in early *Homo*. In the maxillary molars of MH1, the cusp apices are moderately closely spaced and the anterior fovea is small and buccally directed and is not bounded posteriorly by a well-developed epicrista as is seen in australopiths. In contrast, the lingual and buccal cervical eminences are weakly developed as in early *Homo*.

Mandibular Dentition

The mandibular incisors of MH2 are too worn to be useful for comparative purposes. The mandibular canine reveals a crown outline that is markedly asymmetrical with the apex set distal to the crown midline as is seen in australopiths. Conversely, in the mandibular canine of MH1, the labial buccal grooves are very weakly expressed, the mesial marginal ridge and distal marginal ridge are equally developed, and the lingual median ridge is weakly developed and not prominent, all as is seen in early *Homo*. The cusp apices in the mandibular premolars are closely spaced, and the mesial marginal ridge and distal marginal ridge are well-developed and thick, in particular in the P₃, as is shared with australopiths. Buccal grooves are present on the premolars of *Au. sediba* as in *Au. africanus*, though the distal groove is more strongly developed, unlike the more strongly developed mesial groove that is typical of *Au. africanus*. On the other hand, the cervical prominence is weakly developed on the lingual and buccal faces as is shared with early *Homo*. Turning to the mandibular molars, the cusp apices are moderately closely spaced as in australopiths. However, the protoconid is positioned slightly mesial to the metaconid, and the cervical prominence is weakly developed as in early *Homo*.

DISCUSSION AND CONCLUSIONS

The species *Au. sediba* is characterized by a mosaic of both australopith-like and *Homo*-like traits across both the cranium and postcranium (Berger et al. 2010; Carlson et al. 2011; Churchill et al. 2013; de Ruiter et al. 2013a, b; DeSilva et al. 2013; Irish et al. 2013; Kibii et al. 2011; Kivell et al. 2011; Schmid et al. 2013; Williams et al. 2013; Zipfel et al. 2011). We discuss these similarities below, beginning with features shared only with australopiths to the exclusion of *Homo*, then turning to characters that are australopith-like in *Au. sediba* but for which there is overlap between aus-

tralopiths and *Homo*. Following this, we examine features that are *Homo*-like in *Au. sediba*, but for which again there is overlap between australopiths and *Homo*. Finally, we focus on those features that *Au. sediba* shares with *Homo* to the exclusion of other australopiths.

Australopithecus sediba shares several characters with other australopiths to the exclusion of early *Homo*. The brain is relatively small, with correspondingly small relative cranial height and breadth. There is a patent premaxillary suture, otherwise only encountered in australopiths. The zygomatic bone is relatively robust. The entrance to the nasal cavity is vertically offset from the nasal sill, resulting in a 'continuous-discrete' appearance (see McCollum 2000). The I¹ has a weak lingual median ridge, the I² mesial marginal ridge and distal marginal ridge merge onto the cervical prominence, the C¹ has an uninflated cervical prominence, the anterior fovea of the P³⁻⁴ are not bounded by a distinct epicrista, the C₁ has a markedly asymmetrical crown shape, the P₃₋₄ have mesial and distal buccal grooves and thick mesial marginal ridge and distal marginal ridge, and the cusp apices of the maxillary and mandibular premolars and molars are relatively closely spaced.

In addition to these characters are a suite of traits in which the morphology of *Au. sediba* most closely resembles that of the australopiths, but for which there is also overlap between australopiths and specimens of early *Homo*. The mandibular fossa is roughly half as long as it is broad, a condition encountered in most, but not all, australopiths, while in early *Homo* mandibular fossa length tends to be more than half of fossa breadth. The root of the zygomatic process is parallel to the FH and not angled some 30 degrees downward as in many, though not all, early *Homo* specimens. Total facial height relative to bi-orbital breadth highlights the narrow upper face of MH1, which is more characteristic of australopiths. In terms of overall facial prognathism, the value for MH1 falls on the mean for *Au. africanus*, while it is smaller than that seen in any early *Homo* specimen with the exception of OH 24, though damage to this latter specimen is likely influencing this result. Likewise, the angle of the nasal aperture is similar to australopith specimens, and unlike values encountered in early *Homo*. The only early *Homo* value that approaches MH1 is again OH 24, and once again the damage to this specimen is likely a contributing factor. Although there is a slight midline glabellar depression as is typically encountered in early *Homo*, the prominent glabellar block of MH1 is most closely matched in Sts 71. Nasal aperture height in MH1 is roughly half of the total nasal height as in the australopiths, while in early *Homo* the nasal aperture tends to be more than half of the total nasal height. OH 24, and to a lesser extent SK 847, are close to the value for MH1, though damage to these specimens, in particular OH 24, is likely affecting this result. Both the palate and the mandible of MH1 are notably narrow, with tooth rows that diverge only slightly. Although there are specimens of early *Homo* with narrow or not overly wedged palates, in this regard MH1 appears especially australopith-like, being narrower than most specimens of *Au. afarensis* and *Au. africanus* and approaching values encountered in *Au.*

anamensis. Although the position of the anterior marginal tubercle is variable across the hominins, in *Au. sediba* it is located almost level with the mental foramen in the adult MH2, while in many early *Homo* specimens (and the juvenile MH1) it is positioned posterior to the mental foramen. And, while the mental foramina of MH1 and MH2 are positioned near mid-corpus height, the secondary mental foramen of MH1 is positioned slightly below mid-corpus, thus it bears a greater similarity to australopiths in this regard.

Australopithecus sediba also shows a suite of traits more closely aligned with that of early *Homo*, but for which there is again overlap between the australopiths and specimens of early *Homo*. Despite the small cranial size, the vertically oriented cranial walls appear more *Homo*-like in the sharp angulation between the lateral and superior parietal aspects, though specimens such as MLD 37/38 mirror this appearance. Although bi-orbital breadth is relatively narrow as in australopiths, the relative proportions of other segments of the face in MH1 are more *Homo*-like, including relative facial height, bi-maxillary breadth, and bi-zygomatic breadth, revealing a mid-face that is narrowed as in early *Homo* owing to the lack of flaring of the zygomatics. This results in an upper face in *Au. sediba* and early *Homo* that is squared in appearance, unlike the more tapered upper face that is seen in australopiths. The only overlap that occurs between the australopiths and early *Homo* in zygomatic flaring rests with D4500, otherwise this lack of zygomatic flaring would align *Au. sediba* exclusively with early *Homo*. The interorbital region is relatively broad. The nasal bones are short relative to inferior nasal breadth. The nasal bridge is slightly prominent relative to the facial plane, more so than is seen in australopiths, though some early *Homo* specimens such as KNM-ER 1470 and OH 24 are only weakly prominent like australopiths. MH1 lacks anterior pillars that are typical, but not universal, in *Au. africanus*, but which are also encountered in some early *Homo* specimens. The nasoalveolar clivus is more vertically projecting than it is horizontally projecting in MH1, in conjunction with the majority of early *Homo* specimens. The mandibular symphysis is relatively gracile in *Au. sediba*, and while there are some especially large mandibles of both *H. rudolfensis* and *H. erectus* that overlap with the australopiths, the decidedly non-robust symphysis of *Au. sediba* aligns more closely with early *Homo*. The mandibular incisure and mental trigon tend to be more prominent in *Au. sediba* than they are in australopiths, though this character is variable in early *Homo*. There is no canine step in *Au. sediba*, the topographical step-down from the incisors and canine to the premolar row that is encountered in *Au. afarensis* and Sts 52 (the only *Au. africanus* mandible with canines *in situ* and unworn enough to make a determination), but which is also encountered in *H. naledi*.

There are a number of characters that *Au. sediba* shares with early *Homo* to the exclusion of other australopiths. Postorbital constriction is minimal, with correspondingly small temporal foramina. The temporal lines encroach only slightly on (the posterior face of) the supraorbital torus, are coplanar with the medial wall of the temporal fora-

men, and remain widely spaced along their entire extent; KNM-ER 1805 is the only *Homo* specimen to show a sagittal crest. The root of the zygomatic process expands laterally in a relatively anterior position above the mandibular fossa, instead of above the EAM as in australopiths. The mandibular fossa is positioned almost entirely medial to the parasagittal plane of the lateral wall of the cranium. The infraorbital region is coplanar with the orbital plane. The supraorbital torus is moderately developed and anteriorly projecting, and is defined by a shallow supratoral sulcus. Laterally, the supraorbital torus forms as a distinctly expanded, triangular shaped supraorbital trigon. The lateral orbital margin is gently curved and not folded as in *Au. africanus*, and is anterolaterally, rather than anteriorly, oriented. The root of the frontal process of the zygomatic (i.e., the root of the lateral orbital margin) is medially but not laterally expanded, unlike the medially and laterally expanded root in other australopiths. Although there are no specimens of early *Homo* preserving the requisite area, the superior orbital fissure of MH1 is comma-shaped, unlike the round shape of other australopiths. The intermaxillary suture forms as a raised ridge instead of an excavated channel on the nasoalveolar clivus. The anterior nasal tubercle is positioned slightly anterior to the lateral nasal aperture margins. Turning to the mandible, the lingual alveolar plane is steeply inclined and not-shelf-like, and in this regard looks like specimens of *H. erectus* and *H. naledi*, but not australopiths, *H. habilis* or *H. rudolfensis*. The weak superior transverse torus and absent inferior transverse torus are dissimilar to those seen in other australopiths. The alveolar prominence reveals considerable relief relative to the subalveolar fossa in *Au. sediba*, while *Au. africanus* presents a considerably inflated subalveolar fossa and thus limited relief relative to the alveolar prominence. The endocondyloid buttress is weakly developed to absent, and does not contact the condyle directly, unlike the stronger development encountered in australopiths. The mandible of *Au. sediba* differs from that of *Au. africanus* in having a relatively smaller and deeper corpus, a relatively elongated premolar row, and mandibular premolars that differ in occlusal outline shape (de Ruiter et al. 2013b). The I¹ lingual cervical prominence is broad and uninflated, the C¹ has a weak lingual median ridge, the C₁ mesial marginal ridge and distal marginal ridge are equally developed, the C₁ has a weak lingual median ridge, the mandibular M₁₋₃ reveal a protoconid that is positioned slightly mesial to the metaconid, and the maxillary and mandibular premolars and molars have uninflated cervical eminences.

Among the above mentioned traits, *Au. sediba* shares a small number with *Au. africanus* to the exclusion of *Au. anamensis*, *Au. afarensis*, or early *Homo*. These include the pronounced glabellar block, the zygomatic prominence, the long and steeply inclined zygomaticoalveolar crest, and the insertion of vomer below the nasal sill in the incisive fossa. There are also a small number of discrete dental characters that link *Au. africanus* and *Au. sediba* (Irish et al. 2013). Berger et al. (2010) initially hypothesized that *Au. sediba* was derived from *Au. africanus* via cladogenesis. However,

given the small number of traits shared exclusively between these taxa it is unclear whether, on present evidence, we can support the hypothesis that *Au. sediba* is descended from *Au. africanus* via cladogenesis. *Au. africanus* shares a suite of derived characters with *P. robustus*, mostly relating to the generation and transmission of masticatory forces, prompting some to propose an exclusive phylogenetic link between the two (Johanson and White 1979; Kimbel et al. 1984; Rak 1983; White et al. 1981). In particular, buttressing of the face, robusticity of the mandible, increased size of the dentition, and molarization of the premolars align *Au. africanus* and *P. robustus*. *Au. sediba* does not share these characters, reflecting a less specialized morphology than is seen in the other South African australopiths. It is possible that *Au. africanus* and *Au. sediba* share a common ancestry that predates the samples of these taxa from Taung, Makapansgat, Sterkfontein, and Malapa. The hypothesized position of *Au. africanus* as the ancestor of *Au. sediba* was predicated, at least in part, on the greater age of the Sterkfontein and Makapansgat fossils relative to the younger Malapa material. However, while the age of Malapa is 1.977 Ma, the age of *Au. sediba* as a species unknown (Berger et al. 2010; Pickering et al. 2011). MH1 and MH2 sample a species—*Au. sediba*—which had a broader temporal and geographic span than is currently known from the single locality of Malapa (Robinson et al. 2018). While Sterkfontein and Makapansgat predate Malapa, that does not mean that *Au. africanus* necessarily predates *Au. sediba*. We therefore hypothesize that *Au. africanus* and *Au. sediba* share a common ancestry, but the nature of that ancestry is, at present, unresolved. This conclusion is in line with the results of Dembo et al. (2015), who, using cranial data provided in Berger et al. (2010), were able to explicitly reject a phylogenetic model of *Au. sediba* as a descendent of *Au. africanus*.

Kimbel and Rak (2017) have challenged our interpretation of some of the *Homo*-like features of *Au. sediba*, instead concluding that had MH1 survived into adulthood it would have grown to resemble *Au. africanus* in cranial morphology. We would again point out that the conclusions of Kimbel and Rak (2017) are at odds with those of Carlson et al. (2016), the latter whom concluded that additional growth in MH1 would not have substantially altered the morphology of the specimen (see above for additional detail). Support for this is found in a recent study which demonstrated MH1 shared a maturation schedule with the similarly-ontogenetically-aged KNM-WT 15000 skeleton (Cameron et al. 2017). The skull of KNM-WT 15000 is morphologically similar to adult specimens of *H. erectus*, thus the amount of growth that would have occurred by adulthood would be limited, suggesting that MH1 would likewise have undergone only limited additional growth (a la Carlson et al. 2016; contra Kimbel and Rak 2017). Many of the characters that Kimbel and Rak (2017) discuss are related to the zygomatic region in some capacity, and indeed, in several instances the zygomatic region of MH1 appears more australopith-like than *Homo*-like. Kimbel and Rak (2017) consider this to indicate a unique relationship between *Au. sediba* and *Au. africanus*, a conclusion that we

do not necessarily disagree with. However, we also note that there are a large number of characters that align *Au. sediba* with early *Homo*, which prompted us to hypothesize a unique relationship between these latter taxa, in addition to *Au. africanus* (Berger et al. 2010; Pickering et al. 2011). While the morphologies that Kimbel and Rak (2017) discuss do challenge our understanding of the nature of the relationship between *Au. sediba* and *Homo*, we maintain our hypothesis that *Au. sediba* represents a viable candidate ancestor for the genus *Homo*, or a close sister group to that ancestor. Ultimate resolution of this question must await recovery of an adult cranium of *Au. sediba*. When such a cranium is finally recovered, if it reveals adult morphology that is largely reminiscent of the preserved juvenile morphology of MH1 (e.g., Carlson et al. 2016), this would lend support to our hypothesis. If, on the other hand, the cranium appears *Au. africanus*-like as Kimbel and Rak (2017) contend it will, this would weaken our hypothesis and we would have to significantly revise our understanding of the morphologies shared between *Au. sediba* and early *Homo* across the skull and skeleton.

For the present, the similarities shared between *Au. sediba* and early *Homo* species are numerous, which when combined with postcranial evidence, encompass distinct functional systems including mastication, locomotion, manipulation, and reproduction. *Australopithecus sediba* lacks the powerful masticatory apparatus that typifies other australopiths (Berger et al. 2010; de Ruiter et al. 2013b; Ledogar et al. 2016; but see Daegling et al. 2016), and possesses a highly flexible spine alongside pelvic and lower limb segments similar to that seen in *Homo* (DeSilva et al. 2013; Kibii et al. 2011; Williams et al. 2013; Zipfel et al. 2011), a hand with a long thumb and short fingers that are associated with precision grip (Kivell et al. 2011), and a *Homo*-like pelvic arrangement in a small-brained species that indicates birthing large-brained babies was not driving pelvic evolution at the time (Carlson et al. 2011; Kibii et al. 2011). While it is possible that the characters shared between *Au. sediba* and early *Homo* reflect considerable levels of homoplasy, we think it is more parsimonious to suggest that some or even most of these characters truly do align *Au. sediba* more closely with early *Homo* than any australopith yet discovered (de Ruiter et al. 2017). We hypothesize that these shared characters demonstrate a close affinity between the groups. On present evidence, *Au. sediba* represents a candidate australopith ancestor for the genus *Homo*, or a close sister-group to that ancestor, closer than any other australopith known in the fossil record. This conclusion is in line with that of Dembo et al. (2015), wherein their best supported phylogenetic hypothesis (which was based, in part, on data gathered from Berger et al. [2010]), placed *Au. sediba* as the sister taxon to a clade comprising all early *Homo* species, consistent with the hypothesis of Berger et al. (2010) that *Au. sediba* might represent the ancestor of *Homo*, or a close sister-group to that ancestor.

Notwithstanding these similarities with early *Homo*, we maintain that *Au. sediba* presents an overall body plan that is at an australopith adaptive grade. This is based on the

possession of such features as small brain and body size, narrow palate and mandible, a high origin for masseter, australopith-like postcanine tooth cusps, a relatively long forelimb with a high brachial index, upper limb joint dimensions that are large relative to those of the lower limb, and a relatively primitive calcaneus. On a philosophical level we agree with the arguments of Wood and Collard (1999) regarding the conditions necessary to attribute a fossil to the genus *Homo*. *Australopithecus sediba* clearly fails two of their six criteria (both body mass and body proportions should be more similar to humans than australopiths) and quite probably fails on a third (should show obligate bipedalism with limited climbing ability [Churchill et al. 2013; Rein et al. 2017]). It also fails on the fourth criterion (should show extended ontogenetic development), as MH1 reveals a more rapid developmental pattern than modern humans (Le Cabec et al. 2014). The fifth criterion (teeth and jaws similar in relative size to humans) appears to position the Malapa hominins within *Homo*, though we would note that the small posterior teeth from Malapa retain an australopith-like cuspal arrangement and molar size gradient. The remaining criterion (should be more closely related to humans than to australopiths) is more difficult to assess, because we presently do not fully understand the relationship of *Au. sediba* relative to the australopiths and early *Homo*.

Derived characters shared between *Au. africanus* and *Au. (P.) robustus* on the one hand, alongside the derived characters shared between *Au. sediba* and *Homo* on the other, appear to reflect the emergence of two distinct adaptive strategies. In *Au. africanus* and *Au. (P.) robustus*, the emphasis is on increasing occlusal forces along the postcanine tooth row, reflecting a dietary adaptation for tough or hard and brittle items (Scott et al. 2005), or mechanically protected items like large nuts and seeds that required initial premolar preparation (Strait et al. 2009). The diet of *Au. sediba* differed from that of other australopiths, though a wide variety of foods is indicated (Henry et al. 2012). *Au. sediba* was capable of consuming tough or hard foods similar to other australopiths, though hard object feeding and/or prolonged mastication were not likely to have been major factors in its subsistence strategy (Ledogar et al. 2016). The diet of early *Homo* has been described as being based on flexible, versatile subsistence strategies (Ungar et al. 2006), a description that could equally apply to *Au. sediba* (Henry et al. 2012). Many of the characters shared by *Au. sediba* and early *Homo* that are clustered around the temporal lines, the supramastoid crest, the position of the mandibular fossa, the development of the zygomatics, the nasal aperture margins, the clivus, the palate, the mandibular corpus and symphysis, and the alveolar proportions, relate to mastication in some manner. Indeed it is possible that some component of the unique facial anatomy of *Au. sediba* was directly linked to changes in masticatory system loading (Lacruz et al. 2015). This implies that diet driven adaptations were playing a major role in the early evolution of the genus *Homo*, though the shift from an australopith dietary adaption to that of early *Homo* in the highly variable paleoenvironments of the Pleistocene of Africa would not be a straightforward transi-

tion (Antón et al. 2014; Potts 2012; Ungar et al. 2006). Other characters shared between *Au. sediba* and early *Homo* that are grouped around the reorganization of the brain, post-orbital constriction, the shape of the cranium, the supra-orbital torus, the orbits and orbital margins, the infraorbital plane, the nasal bones, the anterior nasal tubercle, and the mentum osseum do not appear to relate directly to mastication, thus diet alone does not explain the transition to early *Homo*. Natural selection can be detected operating on all regions of the skull of early hominins (Schroeder et al. 2015), though not all of the affected cranio-mandibular morphologies appear to be diet related. In addition, the role of genetic drift, i.e., random evolutionary processes, in the development of cranial shape in the transition from australopithecine to early *Homo* has previously been underestimated (Schroeder et al. 2015). These combined factors indicate that a more complex and multifaceted set of adaptive and non-adaptive processes were in operation in the transition from australopithecine to early *Homo* (a transition that likely occurred piecemeal, over long spans of time [Kimbel and Villmoare, 2016]) than are currently understood, and that, although clearly important, diet alone was not the singular driving factor in the appearance of our genus.

ACKNOWLEDGEMENTS

We thank the South African Heritage Resource agency for the permits to work on the Malapa site, and the Nash family for granting access to the Malapa site and continued support of research on their reserve. The South African Department of Science and Technology, the South African National Research Foundation, the Institute for Human Evolution (IHE), the Palaeontological Scientific Trust (PAST), the Andrew W. Mellon Foundation, the United States Diplomatic Mission to South Africa, the French Embassy in South Africa, the National Geographic Society, the A. H. Schultz Foundation, the Oppenheimer and Ackerman families, Sir Richard Branson, the Texas A&M University Program to Enhance Scholarly and Creative Activities, and the Texas A&M University College of Liberal Arts Seed Grant all provided funding for this research. DJD holds a Cornerstone Faculty Fellowship in the College of Liberal Arts at Texas A&M University, which provided additional funding. The University of the Witwatersrand's Schools of Geosciences and Anatomical Sciences and the Bernard Price Institute for Palaeontology provided support and facilities. We thank E. Mbua, P. Kiura, V. Iminjili, and the National Museums of Kenya, Dr. P. Msemwa and the National Museum and House of Culture of Tanzania, and Ms. S. Potze for access to comparative fossil materials in their care. We thank Paul Tafforeau, the ESRF ID17 beamline team, and the ESRF for granting beamtime under proposal EC521. Numerous individuals have been involved in the ongoing preparation and excavation of these fossils including C. Dube, B. Eloff, C. Kemp, M. Kgasi, M. Languza, J. Malaza, G. Mokoma, P. Mukanela, T. Nemvundi, M. Ngcamphalala, S. Jirah, S. Tshabalala, and C. Yates. Other individuals who have given significant support to this project include B. de Klerk, C. Steininger, B. Kuhn, L. Pollarolo, B. Zipfel, J. Kretzen, D.

Conforti, J. McCaffery, C. Dlamini, H. Visser, R. McCrae-Samuel, B. Nkosi, B. Louw, L. Backwell, F. Thackeray, and M. Peltier. All of the specimens of *Au. sediba* described in this paper are curated at the Evolutionary Studies Institute at the University of the Witwatersrand, and are available to all bona fide researchers. Laser surface scan generated surface models of the cranial material described above are available for download on Morphosource.org.

REFERENCES

- Aiello, L. and Dean, C. 1990. *An Introduction to Human Evolutionary Anatomy*. Elsevier, Amsterdam.
- Antón, S.C., Potts, R., and Aiello, L.C. 2014. Evolution of early *Homo*: an integrated biological perspective. *Science* 345, 1236828.
- Asfaw, B., White, T.D., Lovejoy, O., Latimer, B., Simpson, S., and Suwa, G. 1999. *Australopithecus garhi*: a new species of early hominid from Ethiopia. *Science* 284, 629–635.
- Balter, M. 2010. Candidate human ancestor from South Africa sparks praise and debate. *Science* 328, 154–155.
- Berger, L.R., de Ruiter, D.J., Churchill, S.E., Schmid, P., Carlson, K.J., Dirks, P.H.G.M., and Kibii, J.M. 2010. *Australopithecus sediba*: a new species of *Homo*-like australopithecine from South Africa. *Science* 328, 195–204.
- Berger, L.R., Hawks, J., de Ruiter, D.J., Churchill, S.E., Schmid, P., Deleuzene, L.K., Kivell, T.L., Garvin, H.M., Williams, S.A., DeSilva, J.M., Skinner, M., Musiba, C.M., Cameron, N., Holliday, T.W., Harcourt-Smith, W., Ackermann, R.R., Bastir, M., Bogin, B., Bolter, D., Brophy, J.K., Cofran, Z.D., Congdon, K.A., Deane, A.S., Dembo, M., Drapeau, M., Elliott, M., Feuerriegel, E.M., Garcia-Martinez, D., Green, D.J., Gurtov, A., Irish, J.D., Kruger, A., Laird, M.F., Marchi, D., Meyer, M.R., Nalla, S., Negash, E.W., Orr, C., Radović, D., Schroeder, L., Scott, J.E., Throckmorton, Z., Tocheri, M., VanSickle, C., Walker, C.S., Wei, P., and Zipfel, B. 2015. *Homo naledi*, a new species of the genus *Homo* from the Dinaledi Chamber, South Africa. *eLIFE* 4, e09560.
- Brunet, M., Beauvillain, A., Coppens, Y., Heintz, E., Moutaye, A.H.E., and Pilbeam, D. 1995. The first australopithecine 2,500 kilometres west of the Rift Valley, Chad. *Nature* 378, 273–275.
- Cameron, N., Bogin, B., Bolter, D., and Berger, L.R. 2017. The postcranial skeletal maturation of *Australopithecus sediba*. *American Journal of Physical Anthropology* 163, 633–640.
- Carlson, K.B. 2014. *Developmental Simulation of the Adult Cranial Morphology of Australopithecus sediba*. Ph.D. Dissertation, Texas A&M University, College Station.
- Carlson, K.B., de Ruiter, D.J., DeWitt, T.J., McNulty, K.P., Carlson, K.J., Tafforeau, P., and Berger, L.R. 2016. Developmental simulation of the adult cranial morphology of *Australopithecus sediba*. *South African Journal of Science* 112, 84–92.
- Carlson, K.J., Stout, D., Jashashvili, T., de Ruiter, D.J., Tafforeau, P., Carlson, K.B., and Berger, L.R. 2011. The endocast of MH1, *Australopithecus sediba*. *Science* 333, 1402–1407.

- Channell, J.E.T., Mazaud, M., Sullivan, P., Turner, S., and Raymo, M.E. 2002. Geomagnetic excursions and paleointensities in the Matuyama Chron at Ocean Drilling Program Sites 983 and 984 (Iceland Basin). *Journal of Geophysical Research-Solid Earth* 107, 2114–2127.
- Cherry, M. 2010. Claim over 'human ancestor' sparks furor. *Nature* doi:10.1038/news.2010.171.
- Churchill, S.E., Holliday, T.W., Carlson, K.J., Jashashvili, T., Macias, M.E., Mathews, S., Sparling, T.L., Schmid, P., de Ruiter, D.J., and Berger, L.R. 2013. The upper limb of *Australopithecus sediba*. *Science* 340, 1233477.
- Clarke, R.J. 1977. *The Cranium of the Swartkrans Hominid, SK 847 and Its Relevance to Human Origins*. Ph.D. Thesis, University of the Witwatersrand, Johannesburg.
- Clarke, R.J. 1985. *Australopithecus* and early *Homo* in southern Africa. In *Ancestors: The Hard Evidence*, Delson, E. (ed.). Alan R. Liss, New York, pp. 171–177.
- Clarke, R.J. 1988. A new *Australopithecus* cranium from Sterkfontein and its bearing on the ancestry of *Paranthropus*. In *Evolutionary History of the "Robust" Australopithecines*, Grine, F.E. (ed.). Aldine, New Brunswick, pp. 285–292.
- Clarke, R.J. 1994. Advances in understanding the craniofacial anatomy of South African early hominids. In *Integrative Paths to the Past*, Corruccini, R.S. and Ciochon, R.L. (eds.). Prentice Hall, Englewood Cliffs NJ, pp. 205–222.
- Clarke, R.J. 2008. Latest information on Sterkfontein's *Australopithecus* skeleton and a new look at *Australopithecus*. *South African Journal of Science* 104, 443–449.
- Clarke, R.J. 2013. *Australopithecus* from Sterkfontein caves, South Africa. In *The Paleobiology of Australopithecus*, Reed, K.E., Fleagle, J.G., and Leakey, R.E. (eds.). Springer, Dordrecht, pp. 105–123.
- Curnoe, D. and Tobias, P.V. 2006. Description, new reconstruction, comparative anatomy, and classification of the Sterkfontein StW 53 cranium, with discussions about the taxonomy of other southern African early *Homo* remains. *Journal of Human Evolution* 50, 36–77.
- Daegling, D.J., Carlson, K.J., Tafforeau, P., de Ruiter, D.J., and Berger, L.R. 2016. Comparative biomechanics of *Australopithecus sediba* mandibles. *Journal of Human Evolution* 100, 73–86.
- Dart, R.A. 1948. The Makapansgat proto-human *Australopithecus prometheus*. *American Journal of Physical Anthropology* 6, 259–284.
- Dart, R.A. 1954. The second, or adult, female mandible of *Australopithecus prometheus*. *American Journal of Physical Anthropology* 12, 313–344.
- Dembo, M., Matzke, N.J., Mooers, A.Ø., and Collard, M. 2015. Bayesian analysis of a morphological supermatrix sheds light on controversial fossil hominin relationships. *Proceedings of the Royal Society of London B* 282, 20150943.
- de Ruiter, D.J., Churchill, S.E., and Berger, L.R. 2013a. *Australopithecus sediba* from Malapa, South Africa. In *The Paleobiology of Australopithecus*, Reed, K.E., Fleagle, J.G., and Leakey, R.E. (eds.), Springer, Dordrecht, pp. 147–160.
- de Ruiter, D.J., Churchill, S.E., Hawks, J., and Berger, L.R. 2017. Late australopiths and the emergence of *Homo*. *Annual Review of Anthropology* 46, 99–115.
- de Ruiter, D.J., DeWitt, T.J., Carlson, K.B., Brophy, J.K., Schroeder, L., Ackermann, R.R., Churchill, S.E., and Berger, L.R. 2013b. Mandibular remains support taxonomic validity of *Australopithecus sediba*. *Science* 340: 1232997.
- DeSilva, J.M., Holt, K.G., Churchill, S.E., Carlson, K.J., Walker, C.S., Zipfel, B., and Berger, L.R. 2013. The lower limb and mechanics of walking in *Australopithecus sediba*. *Science* 340, 1232999.
- Digiovanni, B.F., Scoles, P.V., and Latimer, B.M. 1989. Anterior extension of thoracic vertebral bodies in Scheuermann's kyphosis, an anatomic study. *Spine* 14, 712–716.
- Dirks, P.H.G.M., Kibii, J.M., Kuhn, B.F., Steininger, C., Churchill, S.E., Kramers, J.D., Pickering, R., Farber, D.L., Meriaux, A.S., Herries, A.I.R., King, G.C.P., and Berger, L.R. 2010. Geological setting and age of *Australopithecus sediba* from South Africa. *Science* 328, 205–208.
- Dirks, P.H.G.M., and Berger, L.R. 2013. Hominin-bearing caves and landscape dynamics in the Cradle of Humankind, South Africa. *Journal of African Earth Sciences* 78, 109–131.
- Eckhardt, R.B. 1987. Hominoid nasal region polymorphism and its phylogenetic significance. *Nature* 328, 333–335.
- Falk, D., Redmond, J.C., Guyer, J., Conroy, G.C., Recheis, W., Weber, G.W., and Seidler, H. 2000. Early hominid brain evolution: a new look at old endocasts. *Journal of Human Evolution* 38, 695–717.
- Gorjanovic-Kramberger, K. 1909. Der vordere unterkieferabschnitt des altdiluvian menschen in sienem genetischen verhältnis zum unterkiefer des recenten menschen und dem der Anthropoiden. *Zeitschrift für Induktive Abstammungs und Vererbungslehre* 1, 411–439.
- Gower, C.D. 1923. A contribution to the morphology of the apertura piriformis. *American Journal of Physical Anthropology* 6, 27–36.
- Grine, F.E. 1984. *The Deciduous Dentition of the Kalahari San, the South African Negro and the South African Plio-Pleistocene Hominids*. Ph.D. dissertation, University of the Witwatersrand, Johannesburg.
- Grine, F.E. 1989. New hominid fossils from the Swartkrans Formation (1979–1986 excavations): craniodental specimens. *American Journal of Physical Anthropology* 79, 409–449.
- Grine, F.E. 2013. The alpha taxonomy of *Australopithecus africanus*. In *The Paleobiology of Australopithecus*, Reed, K.E., Fleagle, J.G., and Leakey, R.E. (eds.). Springer, Dordrecht, pp. 73–104.
- Grine, F.E., Delanty, M.M., and Wood, B.A. 2013. Variation in mandibular postcanine dental morphology and hominin species in Member 4, Sterkfontein, South Africa. In *The Paleobiology of Australopithecus*, Reed, K.E., Fleagle, J.G., and Leakey, R.E. (eds.). Springer, Dordrecht, pp. 125–146.
- Hawks, J., de Ruiter, D.J., Berger, L.R., 2015. Technical com-

- ment on “Early *Homo* at 2.8 Ma from Ledi-Geraru, Afar, Ethiopia”. *Science* 348, 1326.
- Henry, A.G., Ungar, P.S., Passey, B.H., Sponheimer, M., Rossouw, L., Bamford, M., Sandberg, P., de Ruiter, D.J., and Berger, L.R. 2012. Diet of *Australopithecus sediba*. *Nature* 487, 90–93.
- Hlusko, L.J. 2004. Protostylid variation in *Australopithecus*. *Journal of Human Evolution* 46, 579–594.
- Holliday, T.W., Churchill, S.E., Carlson, K.J., DeSilva, J.M., Schmid, P., Walker, C.S., and Berger, L.R. 2018 (this volume). Body size and proportions of *Australopithecus sediba*. *PaleoAnthropology* 2018, 406–422.
- Holloway, R. 1988. Robust australopithecine brain endocasts: some preliminary observations. In *Evolutionary History of the “Robust” Australopithecines*, Grine, F.E. (ed.). Aldine, New Brunswick, pp. 97–105.
- Holloway, R., Broadfield, D.C., and Yuan, M.S. 2004. *The Human Fossil Record Volume 3: Brain Endocasts: the Paleoneurological Evidence*. Wiley and Sons, New York.
- Hughes, A.R. and Tobias, P.V. 1977. A fossil skull probably of the genus *Homo* from Sterkfontein, Transvaal. *Nature* 265, 310–312.
- Irish, J.D., Guatelli-Steinberg, D., Legge, S., Berger, L.R., and de Ruiter, D.J. 2013. Dental morphology and the phylogenetic ‘place’ of *Australopithecus sediba*. *Science* 340, 1233062.
- Johanson, D.C. and White, T.D. 1979. A systematic assessment of early African hominids. *Science* 203, 321–330.
- Johanson, D.C., Lovejoy, C.O., Kimbel, W.H., White, T.D., Ward, S.C., Bush, M.E., Latimer, B.M., and Coppens, Y. 1982. Morphology of the Pliocene partial hominid skeleton (A.L. 288-1) from the Hadar Formation, Ethiopia. *American Journal of Physical Anthropology* 57, 403–451.
- Kibii, J.M., Churchill, S.E., Schmid, P., Carlson, K.J., Reed, N.D., de Ruiter, D.J., and Berger, L.R. 2011. A partial pelvis of *Australopithecus sediba*. *Science* 333, 1407–1411.
- Kimbel, W.H. 2013. Hesitation on hominin history. *Nature* 497, 573–574.
- Kimbel, W.H. and Deleuzene, L.K. 2009. “Lucy” redux: a review of research on *Australopithecus afarensis*. *Yearbook of Physical Anthropology* 52, 2–48.
- Kimbel, W.K. and Rak, Y. 2017. *Australopithecus sediba* and the emergence of *Homo*: questionable evidence from the cranium of the juvenile holotype MH 1. *Journal of Human Evolution* 107, 94–106.
- Kimbel, W.K. and Villmoare, B. 2016. From *Australopithecus* to *Homo*: the transition that wasn’t. *Philosophical Transactions of the Royal Society B* 371, 2015248.
- Kimbel, W.H., Johanson, D.C., and Rak, Y. 1997. Systematic assessment of a maxilla of *Homo* from Hadar, Ethiopia. *American Journal of Physical Anthropology* 103, 235–262.
- Kimbel, W.H., Walter, R.C., Johanson, D.C., Reed, K.E., Aronson, J.L., Assefa, Z., Marean, C.W., Eck, G.G., Bobe, R., Hovers, E., Rak, Y., Vondra, C., Yemane, T., York, D., Chen, Y., Evensen, N.M., and Smith P.E. 1996. Late Pliocene *Homo* and Oldowan tools from the Hadar Formation (Kada Hadar Member), Ethiopia. *Journal of Human Evolution* 31, 549–561.
- Kimbel, W.H., White, T.D., and Johanson, D.C. 1984. Cranial morphology of *Australopithecus afarensis*: a comparative study based on a composite reconstruction of the adult skull. *American Journal of Physical Anthropology* 64, 337–388.
- Kimbel, W.K., Rak, Y., and Johanson, D.C. 2004. *The Skull of Australopithecus afarensis*. Oxford University Press, Oxford.
- Kivell, T.L., Churchill, S.E., Kibii, J.M., Schmid, P., and Berger, L.R. 2018 (this volume). The hand of *Australopithecus sediba*. *PaleoAnthropology* 2018, 281–332.
- Kivell, T.L., Kibii, J.M., Churchill, S.E., Schmid, P., and Berger, L.R. 2011. *Australopithecus sediba* hand demonstrates mosaic evolution of locomotor and manipulative abilities. *Science* 333, 1411–1417.
- Klaatsch, H. and Hauser, O. 1910. *Homo aurignacensis* Hausseri. *Praehistorische Zeitschrift* 1, 372–338.
- Lacruz, R.S., Bromage, T.G., O’Higgins, P., Toro-Ibacache, V., Warshaw, J., and Berger, L.R. 2015. Distinct growth of the nasomaxillary complex in *A. sediba*. *Nature Scientific Reports* 5: 15175.
- Laird, M.F., Schroeder, L., Garvin, H.M., Scott, J.E., Dembo, M., Radovic, D., Musiba, C.M., Ackermann, R.R., Schmid, P., Hawks, J., Berger, L.R., and de Ruiter, D.J. 2017. The skull of *Homo naledi*. *Journal of Human Evolution* 104, 100–123.
- Leakey, L.S.B., Tobias, P.V., and Napier, J.R. 1964. A new species of the genus *Homo* from Olduvai Gorge. *Nature* 202, 7–9.
- Leakey, M.G., Spoor, F., Brown, F.H., Gathogo, P.N., Kiarie, C., Leakey, L.N., and McDougall, I. 2001. New hominin genus from eastern Africa shows diverse middle Pleistocene lineages. *Nature* 410, 433–440.
- Leakey, M.G., Spoor, F., Dean, M.C., Feibel, C.S., Antón, S.C., Kiarie, C., and Leakey, L.N. 2012. New fossils from Koobi Fora in northern Kenya confirm taxonomic diversity in early *Homo*. *Nature* 488, 201–204.
- Le Cabec, A., Tafforeau, P., Smith, T.M., Carlson, K.J., and Berger, L.R. 2014. Dental development of the *Australopithecus sediba* juvenile MH1 determined from synchrotron virtual paleohistology. *American Journal of Physical Anthropology* (abstracts) 153 (S58), 166.
- Ledogar, J.A., Smith, A.L., Benazzi, S., Weber, G.W., Spencer, M.A., Carlson, K.B., McNulty, K.P., Dechow, P.C., Grosse, I.R., Ross, C.F., Richmond, B.G., Wright, B.W., Wang, Q., Byron, C., Slice, D.E., Carlson, K.J., de Ruiter, D.J., Berger, L.R., Tamvada, K., Pryor Smith, L.C., Berthaume, M.A., and Strait, D.S. 2016. Mechanical evidence that *Australopithecus sediba* was limited in its ability to eat hard foods. *Nature Communications* 7, 10596.
- Lockwood, C.A. and Tobias, P.V. 1999. A large male hominin cranium from Sterkfontein, South Africa, and the status of *Australopithecus africanus*. *Journal of Human Evolution* 36, 637–685.
- Lockwood, C.A. and Tobias, P.V. 2002. Morphology and affinities of new hominin cranial remains from Member 4 of the Sterkfontein Formation, Gauteng Province, South Africa. *Journal of Human Evolution* 42, 389–450.

- Lordkipanidze, D., Ponce de Leon, M.S., Margvelashvili, A., Rak, Y., Rightmire, J.P., Vekua, A., and Zollikofer, C.P. 2013. A complete skull from Dmanisi, Georgia, and the evolutionary biology of *Homo*. *Science* 342, 326–331.
- Maureille, B. and Braga, J. 2002. Between the incisive bone and premaxilla: from African apes to *Homo sapiens*. In *Human Evolution through Developmental Change*, Minugh-Purvis, N. and McNamara, K.J. (eds.). The Johns Hopkins University Press, Baltimore, pp. 464–478.
- McCollum, M.A. 2000. Subnasal morphological variation in fossil hominids: a reassessment based on new observations and recent developmental findings. *American Journal of Physical Anthropology* 112, 275–283.
- McCollum, M.A., Grine, F.E., Ward, S.C., and Kimbel, W.H. 1993. Subnasal morphological variation in extant hominoids and fossil hominids. *Journal of Human Evolution* 24, 87–111.
- Moggi-Cecchi, J., Grine, F.E., and Tobias, P.V. 2006. Early hominid dental remains from Members 4 and 5 of the Sterkfontein Formation (1966–1996 excavations): catalogue, individual associations, morphological descriptions and initial metrical analysis. *Journal of Human Evolution* 50, 239–328.
- Olson, T.R. 1978. Hominid phylogenetics and the existence of *Homo* in Member 1 of the Swartkrans Formation, South Africa. *Journal of Human Evolution* 7, 159–178.
- Olson, T.R. 1985. Taxonomic affinities of the immature hominid crania from Hadar and Taung. *Nature* 316, 539–540.
- Oschinsky, L. 1962. Facial flatness and cheekbone morphology in Arctic Mongoloids. *Anthropologica* n.s. 4, 349–377.
- Pickering, R., Dirks, P.H.G.M., Jinnah, Z., de Ruiter, D.J., Churchill, S.E., Herries, A.I.R., Woodhead, J.D., Hellstrom, J.C., and Berger, L.R. 2011. *Australopithecus sediba* at 1.977 Ma and implications for the origins of the genus *Homo*. *Science* 333, 1421–1423.
- Potts, R. 2012. Environmental and behavioral evidence pertaining to the evolution of early *Homo*. *Current Anthropology* Supplement 53, S299–S317
- Rak, Y. 1983. *The Australopithecine Face*. Academic Press, New York.
- Rak, Y., Ginzburg, A., and Geffen, E. 2007. Gorilla-like anatomy on *Australopithecus afarensis* mandibles suggests *A. afarensis* link to robust australopiths. *Proceedings of the National Academy of Sciences USA* 104, 6568–6572.
- Rak, Y., Kimbel, W.H., and Johanson, D.C. 1996. The crescent of foramina in *Australopithecus afarensis* and other early hominids. *American Journal of Physical Anthropology* 101, 93–99.
- Rein, T.R., Harrison, T., Carlson, K.J., Harvati, K. 2017. Adaptation to suspensory locomotion in *Australopithecus sediba*. *Journal of Human Evolution* 104, 1–12.
- Rightmire, G.P., Lordkipanidze, D., and Vekua, A. 2006. Anatomical descriptions, comparative studies and evolutionary significance of the hominin skulls from Dmanisi, Republic of Georgia. *Journal of Human Evolution* 50, 115–141.
- Robinson, C., Campbell, T.L., Cote, S., and de Ruiter, D.J. 2018. Temporal ranges and ancestry in the hominin fossil record: the case of *Australopithecus sediba*. *South African Journal of Science* 114, 92–98.
- Robinson, J.T. 1956. *The Dentition of the Australopithecinae*. Transvaal Museum Memoir No. 9, Transvaal Museum, Pretoria.
- Robinson, J.T. 1958. Cranial cresting patterns and their significance in the Hominoidea. *American Journal of Physical Anthropology* 16, 397–428.
- Schmid, P., Churchill, S.E., Nalla, S., Weissen, E., Carlson, K.J., de Ruiter, D.J., and Berger, L.R. 2013. Mosaic morphology in the thorax of *Australopithecus sediba*. *Science* 340, 1234598.
- Schroeder, L., Roseman, C.C., Cheverud, J.M., and Ackerman R.R. 2014. Characterizing the evolutionary path(s) to early *Homo*. *PLoS One* 9, e114307.
- Schwalbe, G. 1906. Das schadelfragment von Brux und verwandte schadelforamen. *Zeitschrift für Morphologie und Anthropologie* Special Issue (May), 82–182.
- Spoor, F. 2011. Malapa and the genus *Homo*. *Nature* 478, 44–45.
- Spoor, F., Gunz, P., Neubauer, S., Stelzer, S., Scott, N., Kwekason, A., and Dean, M.C. 2015. Reconstructed *Homo habilis* type OH 7 suggests deep-rooted species diversity in early *Homo*. *Nature* 519, 83–86.
- Strait, D.S., Grine, F.E., and Moniz, M.A. 1997. A reappraisal of early hominid phylogeny. *Journal of Human Evolution* 32, 17–82.
- Strait, D.S., Weber, W.G., Neubauer, S., Chalk, J., Richmond, B.G., Lucas, P.W., Spencer, M.A., Shreiner, C., Dechow, P.C., Ross, C.F., Grosse, I.R., Wright, B.W., Constantino, P., Wood, B.A., Lawn, B., Hylander, W.L., Wang, Q., Byron, C., Slice, D.E., and Smith, A.L. 2009. The feeding biomechanics and dietary ecology of *Australopithecus africanus*. *Proceedings of the National Academy of Sciences USA* 106, 2124–2129.
- Stringer, C. 1986. The credibility of *Homo habilis*. In *Major Topics in Primate and Human Evolution*, Wood, B.A., Martin, R., and Andrews, P. (eds.). Cambridge University Press, Cambridge, pp. 266–298.
- Tobias, P.V. 1967. *Olduvai Gorge* Volume 2. *The Cranium of Australopithecus (Zinjanthropus) boisei*. Cambridge University Press, Cambridge.
- Tobias, P.V. 1971. *The Brain in Hominid Evolution*. Columbia University Press, New York.
- Tobias, P.V. 1991. *Olduvai Gorge* Volume 4. *The Skulls, Endocasts and Teeth of Homo habilis*. Cambridge University Press, Cambridge.
- Ungar, P.S., Grine, F.E., and Teaford, M.F. 2006. Diet in early *Homo*: a review of the evidence and a new model of adaptive versatility. *Annual Review of Anthropology* 35, 209–228.
- Villmoare, B., Kimbel, W.H., Seyoum, C., Campisano, C.J., DiMaggio, E.N., Rowan, J., Braun, D.R., Arrowsmith, J.R., and Reed, K.E. 2015a. Early *Homo* at 2.8 Ma from Ledi-Geraru, Afar, Ethiopia. *Science* 347, 1352–1355.

- Villmoare, B., Kimbel, W.H., Seyoum, C., Campisano, C.J., DiMaggio, E.N., Rowan, J., Braun, D.R., Arrowsmith, J.R., and Reed, K.E. 2015b. Response to comment on “Early *Homo* at 2.8 Ma from Ledi-Geraru, Afar, Ethiopia.” *Science* 348, 1326.
- Ward, C.V., Leakey, M.G., and Walker, A. 1999. The new hominid species *Australopithecus anamensis*. *Evolutionary Anthropology* 7, 197–205.
- Ward, C.V., Leakey, M.G., and Walker, A. 2001. Morphology of *Australopithecus anamensis* from Kanapoi and Allia Bay, Kenya. *J. Hum. Evol.* 41, 255–368.
- Weidenreich, F. 1936. The mandibles of *Sinanthropus pekinensis*. *Palaeontologia Sinica* Series D 7, 1–163.
- Weidenreich, F. 1937. The dentition of *Sinanthropus pekinensis*. *Palaeontologia Sinica*, New Series D 1, 1–121.
- Weidenreich, F. 1943. The skull of *Sinanthropus pekinensis*. *Palaeontologia Sinica* New Series D 10, 1–485.
- White, T.D. 2013. Paleoanthropology: five’s a crowd in our family tree. *Current Biology* 23, R112–R115.
- White, T.D. and Johanson, D.C. 1982. Pliocene hominid mandibles from the Hadar Formation, Ethiopia: 1974–1977 collections. *American Journal of Physical Anthropology* 57, 501–544.
- White, T.D., Johanson, D.C., and Kimbel, W.H. 1981. *Australopithecus africanus*: its phyletic position reconsidered. *South African Journal of Science* 77, 445–470.
- Williams, S.A., Meyer, M.R., Nalla, S., García-Martínez, D., Nalley, T.K., Eyre, J., Prang, T.C., Bastir, M., Schmid, P., Churchill, S.E., and Berger, L.R. 2018 (this volume). The vertebrae, ribs, and sternum of *Australopithecus sediba*. *PaleoAnthropology* 2018, 156–233.